

Supplementary figures and tables to accompany:

A human Tau expressing zebrafish model of progressive supranuclear palsy identifies Brd4 as a regulator of microglial synaptic elimination

Qing Bai, Enhua Shao, Denglei Ma, Binxuan Jiao, Seth D. Scheetz, Karen A. Hartnett-Scott, Vladimir A. Ilin, Elias Aizenman, Julia Kofler, Edward A. Burton

Nature Communications (2024)

Contents

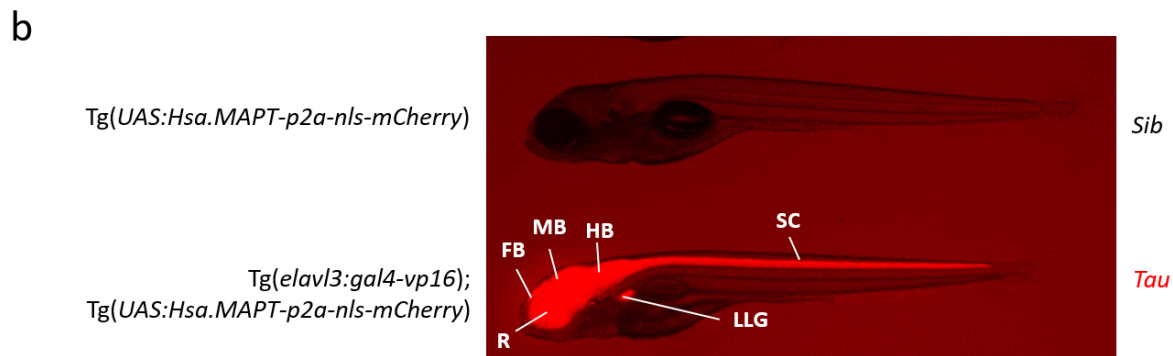
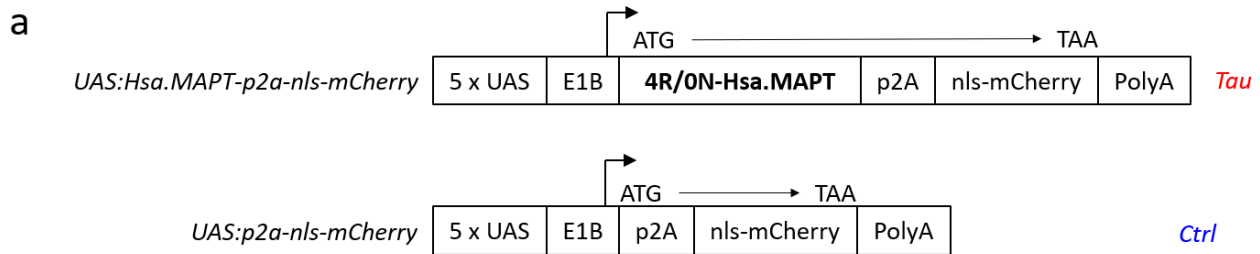
Supplementary Figure S1 – Transgene constructs and expression	5
Supplementary Table 1 – Primer sequences for quantitative real-time PCR analysis of gene expression	6
Supplementary Figure S2 – Verification of gene primers for reverse transcription PCR	6
Supplementary Figure S3 – Verification of reference gene primers for real-time quantitative RT-PCR.....	7
Supplementary Figure S4 – Verification of human and zebrafish Tau primers for real-time quantitative RT-PCR.....	8
Supplementary Table 2 – Amplification efficiency of each primer pair	9
Supplementary Figure S5 – Expression of human Tau transgene relative to the endogenous zebrafish Tau paralogues <i>mapta</i> and <i>maptb</i>	10
Supplementary Table 3 – Abbreviations and genotypes of zebrafish lines used in this study.....	11
Supplementary Table 4 – Statistical analysis of survival in Tau zebrafish	12
Supplementary Figure S6 - Survival of [GFP + mCherry] and [α -Synuclein + mCherry] zebrafish	13
Supplementary Table 5 – Statistical analysis of survival in [GFP + mCherry] and [α -Synuclein + mCherry] zebrafish.....	14
Supplementary Table 6 – ANOVA summary for Figure 2d (Acridine Orange labeling)	15
Supplementary Table 7 – ANOVA summary for Figure 2e (TUNEL labeling)	16
Supplementary Table 8 – ANOVA summary for Figure 2f (activated Caspase-3 labeling)	17
Supplementary Figure S7 – Caspase 3 cleavage by Western blot in Tau zebrafish at 3 – 5 dpf.....	18
Supplementary Figure S8 – Quantification of labeled CNS cells in zebrafish larval sections	19
Supplementary Table 9 – Exact <i>p</i> -values for Figure 2g.....	20
Supplementary Table 10 – ANOVA summary for Figure 2i (7.4.C4 ⁺ microglia)	21
Supplementary Figure S9 – No evidence that human Tau is transferred to cells not expressing the transgene.....	22
Supplementary Figure S10 – Serial extraction of Tau zebrafish in RIPA then DIGE.....	23
Supplementary Figure S11 – Relative expression of human MAPT mRNA during development in transgenic Tau zebrafish	24
Supplementary Table 11 – Šidák multiple comparisons test for Figure 5b	25
Supplementary Figure S12 – Biological replicate motor activity assays comparing Tau and Ctrl zebrafish	26
Supplementary Table 12 – ANOVA summary for Supplementary Figure S12	27
Supplementary Figure S13 – Three different control groups behave similarly in motor activity assays	28
Supplementary Figure S14 – Heterologous protein over-expression does not alone cause motor phenotypes.....	29
Supplementary Figure S15 – Methodology and abnormalities of ocular movement in Tau zebrafish	30
Supplementary Figure S16 – Abnormalities of the visual motor response in Tau zebrafish.....	31
Supplementary Table 13 – Šidák multiple comparisons table for Supplementary Figure S16b.....	32
Supplementary Table 14 – Small molecule screening data	33
Supplementary Figure S17 – Small molecule screen part 1: Determination of maximum tolerated concentration	34

Supplementary Figure S18 – Small molecule screen part 2: Rescue of motor phenotype in Tau zebrafish	35
Supplementary Figure S19 – Algorithm logic for analysis of video tracking data from rescue screening assays	36
Supplementary Figure S20 – Example outputs from screening assay	37
Supplementary Table 15 – Summary of data from the small molecule screen in Figure 7d	38
Supplementary Figure S21 – Hits recovered from epigenetic library screen	42
Supplementary Table 16 – Data summary by target	43
Supplementary Figure S22 – Ranked phenotypic rescue activity by target	44
Supplementary Table 17 – Properties of compounds categorized as ‘other’ in Figure 7e	45
Supplementary Figure S23 – Verification of hits by analysis of repurchased compound	46
Supplementary Figure S24 – Concentration-dependent rescue of motor function in Tau zebrafish by (+)JQ1	47
Supplementary Table 18 - Exact <i>p</i> -values for Figure 8b, 8d – 8i	48
Supplementary Figure S25 – Specificity controls for (+)JQ1 rescue of motor function in Tau zebrafish	49
Supplementary Figure S26 – (+)JQ1 does not silence transgene expression in Tau zebrafish	50
Supplementary Table 19 – Statistical analysis of Tau zebrafish survival in presence or absence of (+)JQ1	51
Supplementary Table 20 – Statistical analysis of Ctrl zebrafish survival in presence or absence of (+)JQ1	51
Supplementary Figure S27 – (+)JQ1 does not rescue OKR deficits in Tau zebrafish	52
Supplementary Figure S28 – Volumetric imaging of synapse abundance in zebrafish larval brain	53
Supplementary Table 21 – Exact <i>p</i> -values for Figure 9b, 9c, 9e, 9g	54
Supplementary Figure S29 – Quantification of PSD95-immunoreactive synaptic material inside zebrafish microglia	55
Supplementary Figure S30 – (+)JQ1 mitigates microglial accumulation of PSD95-immunoreactive synaptic material in Tau zebrafish	56
Supplementary Figure S31 – Rat primary co-culture system to test the activity of (+)JQ1 in mammalian microglia	57
Supplementary Figure S32 – Quantification of PSD95-immunoreactive puncta inside rat microglia	58
Supplementary Figure S33 – (+)JQ1 mitigates accumulation of PSD95-immunoreactive puncta within rat microglia co-cultured with neurons transfected to express human 0N/4R-Tau	59
Supplementary Figure S34 – Transient knockdown of <i>Brd4</i> in Tau zebrafish mitigates microgliosis at 4dpf	60
Supplementary Figure S35 – Generation of a stable <i>brd4</i> null allele using Cas9/CRISPR	61
Supplementary Figure S36 – Developmental phenotypes in <i>brd4</i> ^{-/-} zebrafish	62
Supplementary Figure S37 – Motor activity abnormalities in <i>brd4</i> ^{-/-} zebrafish	63
Supplementary Figure S38 – Heterozygous <i>brd4</i> ^{+/-} mutations partially rescue motor phenotypes in Tau zebrafish	64
Supplementary Table 22 – Exact <i>p</i> -values for Figure 10d – 10i	65
Supplementary Figure S39 – Heterozygous <i>brd4</i> ^{+/-} mutation does not rescue OKR deficits in Tau zebrafish	66
Supplementary Figure S40 – Rescue of synaptic puncta in Tau zebrafish with heterozygous <i>brd4</i> ^{+/-} mutations	67
Supplementary Figure S41 – <i>Brd4</i> expression in the nuclei of human substantia nigra microglia	68

Supplementary Figure S42 – Brd4 expression in microglia from multiple control and PSP cases 69

References 70

Supplementary Figure S1 – Transgene constructs and expression



a: Schematic maps (not to scale) of the transgene constructs used to make Tau and Ctrl zebrafish. Key: UAS, upstream activating sequence; E1B, minimal promoter; p2A, self-cleaving viral 2A peptide; ON/4R-Hsa.MAPT, human Tau cDNA lacking exons 2 and 3 but including exon 10, encoding human ON/4R-Tau; nls-mCherry, mCherry fluorescent protein fused to a nuclear localization signal; PolyA, polyadenylation signal. Positions of the open reading frames are indicated, illustrating the bicistronic cassette in the Tau-2A-nls-mCherry construct.

b: Widefield epifluorescence image of a *Tg(elavl3:gal4-vp16); Tg(UAS:Hsa.MAPT-2a-nls-mCherry)* 'Tau' zebrafish and its *Tg(UAS:hsa.MAPT-2a-nls-mCherry)* sibling at 5 dpf, illustrating robust transactivation of the transgene in the forebrain (FB), midbrain (MB), hindbrain (HB), retina (R), spinal cord (SC) and lateral line ganglion (LLG) by the pan-neuronal *Tg(elavl3:gal4-vp16)* driver.

Supplementary Table 1 – Primer sequences for quantitative real-time PCR analysis of gene expression

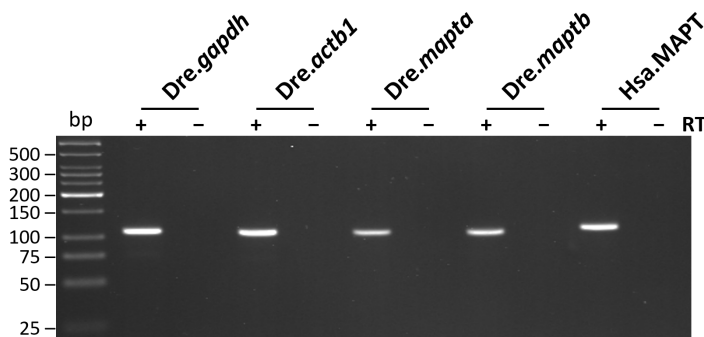
Species*	Gene	5' Primer sequence	3' Primer sequence	Product	Type [§]
Dre	<i>bact1</i>	ACCGAGCGTGGCTACAGCTT	TCCCATCTCCTGCTCGAAGTC	105bp	R
Dre	<i>gapdh</i>	AGATCGTGGCCATCAATGACC	CGCCTTCTGCCTTAACCTCAC	108bp	R
Dre	<i>mapta</i>	AGCAGCCCTGGCACTCCTAA	AGGGGTCTGAGCGAATCACTG	105bp	E
Dre	<i>maptb</i>	CTAAAACCCAGACCGCAGTG	TGATTTGGGTGGGGTGCCTA	104bp	E
Hsa	MAPT	AAAACGAAGATCGCCACACCG	TGGGTGGTGTCTTTGGAGCG	109bp	T
Dre	18S rRNA	TGTTCAAAGCAGGCCGCCCA	AATCATGGCCCCGGTTCCA	104bp	R

*Species: Dre = *Danio rerio* (zebrafish); Hsa = *Homo sapiens* (human)

§Type: R = reference gene; E = endogenous Tau paralogue; T = human Tau transgene

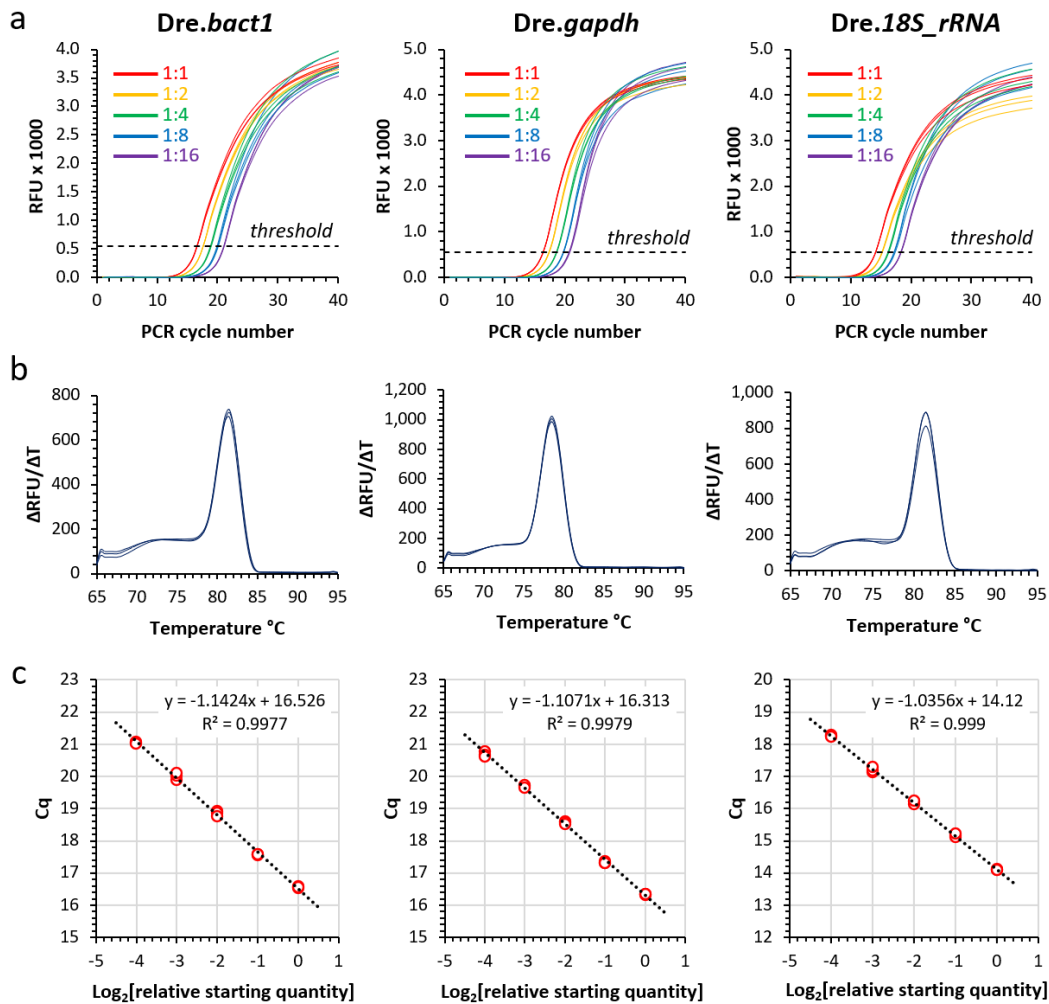
The table shows the primer sequences used for real-time quantitative PCR analysis of gene expression in Supplementary Figures S2 – S5 and S11. Primers were designed to (i) avoid alternatively spliced regions of transcripts; (ii) distinguish between closely related genes; (iii) yield amplicons of similar size; (iv) avoid duplex formation and self-annealing.

Supplementary Figure S2 – Verification of gene primers for reverse transcription PCR



Prior to validating primer pairs for quantitative real-time PCR analysis, we completed 35-cycle PCR amplification of first strand cDNA from 5dpf Tau zebrafish. PCR products were separated by electrophoresis on a 4% LMW agarose gel. The picture shows the ethidium-stained gel photographed under UV illumination. Each primer pair generated a product of the expected size. Amplification was specific to RNA samples that had undergone reverse transcription (RT+). These data validate use of each primer pair to detect the intended target transcript in first-strand cDNA from Tau zebrafish.

Supplementary Figure S3 – Verification of reference gene primers for real-time quantitative RT-PCR



First-strand cDNA from 5dpf Tau zebrafish was subjected to real-time qPCR analysis, using a BioRad CFX Maestro system and software to quantify SYBR-Green fluorescence during amplification with primers for the reference genes *Dre.bact1* (left), *Dre.gapdh* (center), and *Dre.18S_rRNA* (right).

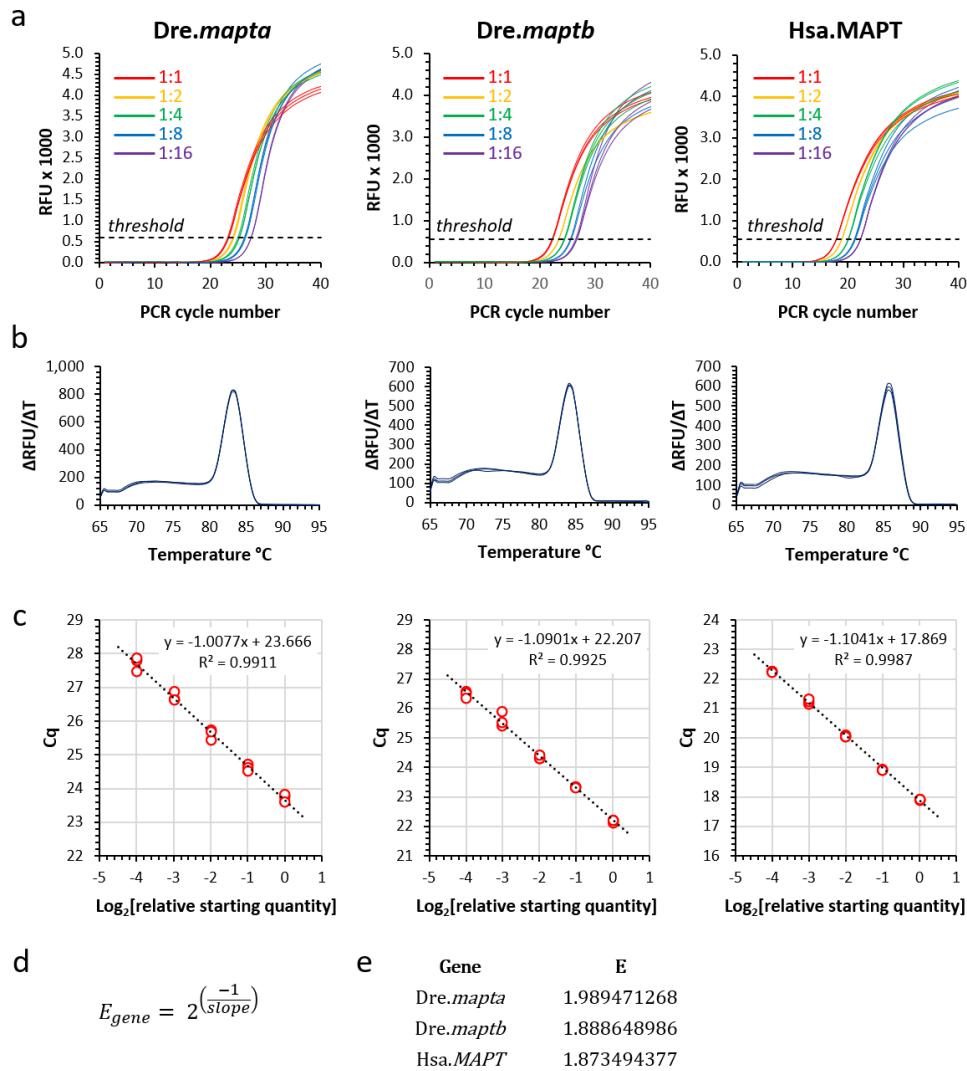
a: Amplification curves showing relative fluorescence units (proportional to product abundance; y-axis) as a function of PCR cycle (x-axis) for technical triplicates of each serial 2-fold dilution of the starting cDNA (color-coded according to the legend). Background subtraction and curve fitting were completed by the CFX-Maestro software. Threshold fluorescence for quantification was determined by the software algorithm to ensure each curve crossed the threshold during the exponential phase of amplification.

b: Melt curve analysis for each amplicon showing change in fluorescence signal with temperature (y-axis) as a function of temperature (x-axis). A single sharp peak, indicating a single amplification product, is seen for each primer pair. For clarity three technical replicates are shown of the amplicon from undiluted cDNA.

c: Graphs showing cycle of quantification (Cq; cycle at which amplification curve crosses threshold fluorescence in panel A) as a function of \log_2 [relative cDNA starting quantity ($\propto 1/\text{dilution factor}$)]. Three technical replicates are shown at each dilution. The linear regression line and equation are shown for each primer pair. R^2 values were > 0.99 in all cases.

These data validate use of these reference gene primer pairs for real-time qPCR analysis of Tau zebrafish.

Supplementary Figure S4 – Verification of human and zebrafish Tau primers for real-time quantitative RT-PCR



First-strand cDNA from 5dpf Tau zebrafish was subjected to real-time PCR analysis, similar to Supplementary Figure S3, but using primers for the dual zebrafish Tau paralogues, *Dre.mapta* (left) and *Dre.maptb* (center), and the human Tau transgene, *Hsa.MAPT* (right).

a: Amplification curves similar to Supplementary Figure S3a.

b: Melt curve analysis similar to Supplementary Figure S3b. A single sharp peak, indicating a single amplification product, is seen for each primer pair.

c: Graphs showing cycle of quantification as a function of \log_2 [relative cDNA starting quantity], similar to Supplementary Figure S3c. The linear regression line and equation are shown for each primer pair. R² values were > 0.99 in all cases.

These data validate the use of these primer pairs for real-time qPCR analysis of Tau zebrafish.

Supplementary Table 2 – Amplification efficiency of each primer pair

Gene	E
Dre. <i>mapta</i>	1.989471268
Dre. <i>maptb</i>	1.888648986
Hsa. <i>MAPT</i>	1.873494377

The amplification efficiency, E , for each Tau primer pair was calculated using the equation:

$$E_{gene} = 2^{\left(\frac{-1}{slope}\right)}$$

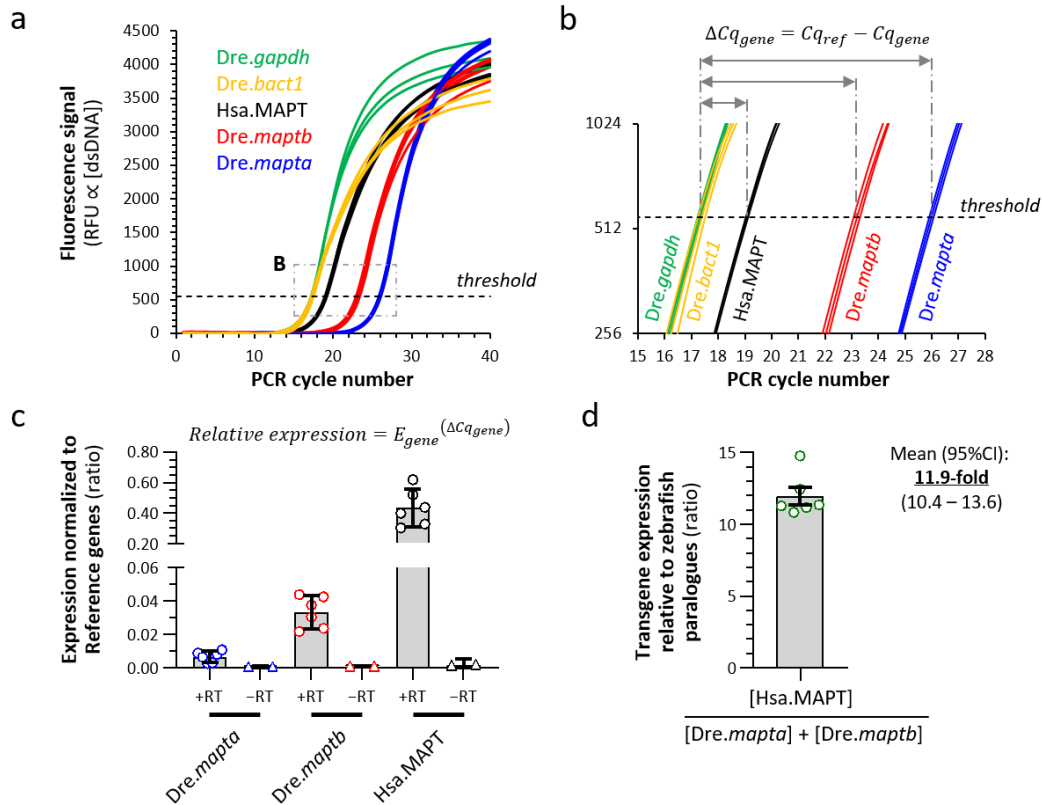
Where $slope$ = the gradient of the linear regression line for each gene in Supplementary Figure S4C.

The amplification efficiency relates the starting abundance, A , of the target cDNA in the sample to the abundance of the amplicon, P , after n cycles of PCR:

$$P = A \times E^n$$

Correction for the differing amplification efficiency of each primer pair is essential for meaningful comparison of the abundance of different target mRNA species using this method.

Supplementary Figure S5 – Expression of human Tau transgene relative to the endogenous zebrafish Tau paralogues *mapta* and *maptb*



First-strand cDNA from Tau zebrafish at 5dpf was amplified by real-time quantitative PCR using primers for two zebrafish reference genes (*Dre.bact1*, *Dre.gapdh*), the dual zebrafish Tau paralogues *Dre.mapta* and *Dre.maptb*, and the Human Tau transgene, Hsa.MAPT. Three technical replicates were completed for each of six biological replicates (i.e. six different first-strand cDNA libraries derived from different Tau zebrafish at 5dpf), run across two replicate experiments.

a: Amplification curves are shown for one biological replicate. The curves for all 3 technical replicates of all 5 primer pairs are superimposed (genes are color coded according to the legend). The boxed area is shown in panel (b). The quantification threshold was determined by the software algorithm to ensure amplification of each target transcript was in its exponential phase at threshold.

b: The boxed area from panel (a) is expanded to illustrate the linear relationship between \log_2 [fluorescence signal (\propto product abundance)] and PCR cycle around the quantification threshold. The difference between Cq for each gene of interest and mean Cq for the reference genes was calculated in each biological replicate, allowing comparison of the abundance of *mapta*, *maptb* and MAPT relative to the reference genes in each sample.

c: Normalized expression of each gene relative to the reference genes was calculated using the formula $E_{gene}^{(\Delta Cq_{gene})}$, as shown. Each point shows the mean value of three technical replicates for each different biological replicate, bars show group mean \pm SE. Note the discontinuous y-axis to accommodate widely differing relative expression levels. RNA samples that were not reverse transcribed were also amplified in each experimental replicate to reveal any contribution to the measured signal from genomic DNA carry over. Whole-larval human Tau transgene mRNA was expressed at approximately 40% abundance of the reference genes, whereas the endogenous zebrafish Tau paralogues were expressed at much lower levels.

d: For each biological replicate, the ratio of transgene Tau (in reference gene units) to the sum of the two endogenous paralogues (also in reference gene units) was calculated. Data points show each biological replicate, bars show mean \pm 95% CI. Overall, transgenic human MAPT mRNA was \approx 12-fold more abundant than the two endogenous paralogues, in whole zebrafish at 5dpf.

Panels c and d are identical to Figure 1c and 1c' of the manuscript and are reproduced here for clarity.

Supplementary Table 3 – Abbreviations and genotypes of zebrafish lines used in this study

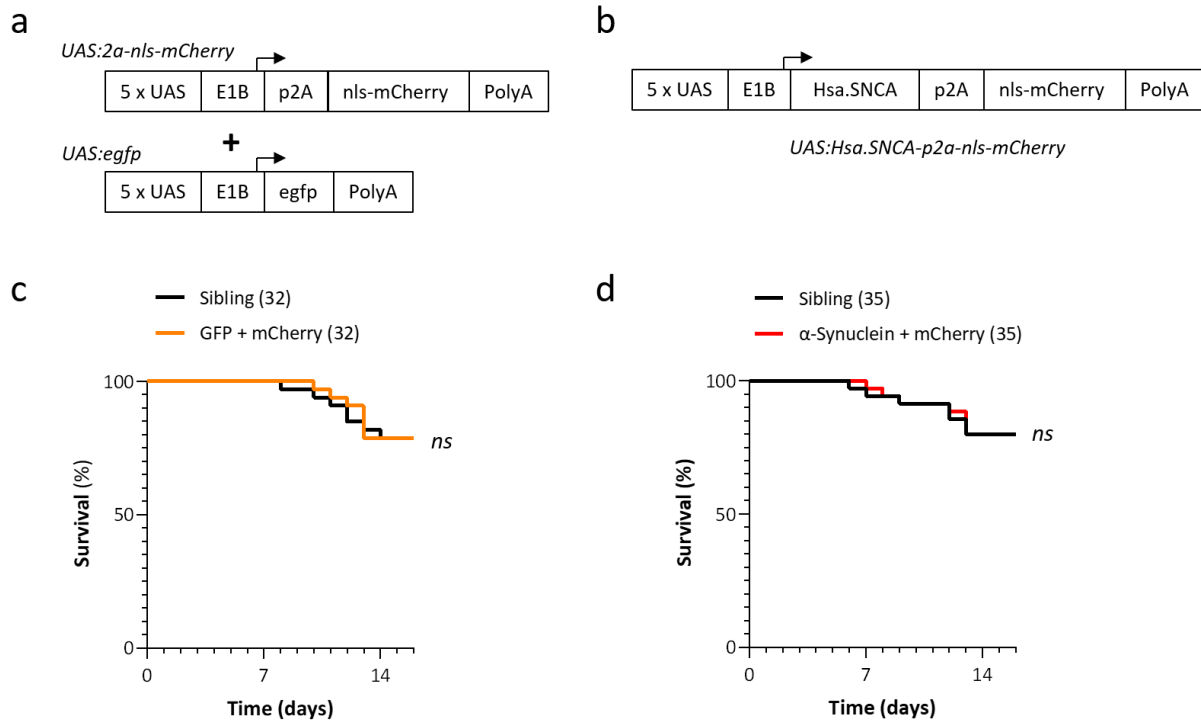
Abbreviation	Genotype
Tau	Tg(<i>elavl3:gal4-vp16</i>); Tg(<i>UAS:Hsa.MAPT-p2a-nls-mCherry</i>)
Ctrl	Tg(<i>elavl3:gal4-vp16</i>); Tg(<i>UAS:p2a-nls-mCherry</i>)
Sib	Siblings of Tau zebrafish without mCherry expression, includes a 1:1:1 ratio of: (i) WT (ii) Tg(<i>elavl3:gal4-vp16</i>) (iii) Tg(<i>UAS:Hsa.MAPT-p2a-nls-mCherry</i>)
GFP	Tg(<i>elavl3:gal4-vp16</i>); Tg(<i>UAS:egfp</i>)
mCherry + GFP	Tg(<i>elavl3:gal4-vp16</i>); Tg(<i>UAS:p2a-nls-mCherry</i>); Tg(<i>UAS:egfp</i>)
α -Syn	Tg(<i>elavl3:gal4-vp16</i>); Tg(<i>UAS:Hsa.SNCA-p2a-nls-mCherry</i>)

Supplementary Table 4 – Statistical analysis of survival in Tau zebrafish

Group	Parameter	Replicate #1	Replicate #2	Replicate #3
Ctrl vs. Tau	Mantel-Cox χ^2 (df)	50.44 (1)	40.15 (1)	77.02 (1)
	Mantel-Cox p	0.000000000001230	0.000000000234980	$< 10^{-15}$
	Mantel-Haenszel hazard ratio (95% CI)	13.51 (6.6 – 27.7)	11.61 (5.4 – 24.8)	31.00 (14.4 – 66.8)
Sib	Median survival	*undefined	*undefined	*undefined
Ctrl		*undefined	*undefined	*undefined
Tau		8 days	9 days	8 days

The table shows Mantel-Cox χ^2 and p , and Mantel-Haenszel hazard ratio \pm 95% confidence intervals for survival of Tau zebrafish in comparison with Ctrl zebrafish in each of the three replicate cohorts shown in Figure 1D. Similar results were found when comparing Tau and Sib zebrafish, and the statistical significance for both comparisons persisted after correction for multiple comparisons. In the lower part of the table, the calculated median survival for Tau zebrafish in each cohort is shown. The median survival for Ctrl and non-expressing sibling zebrafish in our zebrafish system is > 2 years and so was not reached (*undefined) in these experiments, which were deemed completed when no Tau zebrafish remained.

Supplementary Figure S6 - Survival of [GFP + mCherry] and [α -Synuclein + mCherry] zebrafish



To test whether the compromised viability of Tau zebrafish (Figure 1d, e) is a non-specific consequence of simultaneously over-expressing two heterologous proteins (human WT 4R/ON-Tau and mCherry), we analyzed survival in two additional models that each express two transgenes under the same Tg(*elavl3:gal4-vp16*) driver used in the Tau model:

a: Tg(*elavl3:gal4-vp16*); Tg(*UAS:p2a-nls-mCherry*); Tg(*UAS:egfp*) zebrafish express both GFP and mCherry

b: Tg(*elavl3:gal4-vp16*); Tg(*UAS:Hsa.SNCA-p2a-nls-mCherry*)^{pt423} zebrafish express both human α -Synuclein and mCherry. The UAS responder construct in this line is identical to Tau zebrafish, except that the human 4R/ON-Tau sequence is replaced by a cDNA encoding WT human α -Synuclein. We reported construction and validation of the pt423 transgenic line elsewhere¹.

c: Survival of Tg(*elavl3:gal4-vp16*); Tg(*UAS:p2a-nls-mCherry*); Tg(*UAS:egfp*) zebrafish (orange) compared with non-expressing siblings (black).

d: Survival of Tg(*elavl3:gal4-vp16*); Tg(*UAS:Hsa.SNCA-p2a-nls-mCherry*) zebrafish (red) compared with non-expressing siblings (black). This panel is identical to Figure 1f and is reproduced here for clarity and comparison.

For c and d, the starting numbers of zebrafish in each cohort are indicated in each graph legend.

Together with the statistical analysis shown in supplementary table 5, these data do not support the interpretation that the impaired survival of Tau zebrafish is a non-specific artifact of heterologous protein over-expression. Instead, this phenotype likely reflects a pathogenic property of human ON/4R-Tau in this model.

Supplementary Table 5 – Statistical analysis of survival in [GFP + mCherry] and [α -Synuclein + mCherry] zebrafish

Comparison	Parameter		
	Mantel-Cox χ^2 (df)	Mantel-Cox p	Mantel-Haenszel hazard ratio (95% CI)
Sib vs. mCherry + GFP	0.0052 (1)	0.94	0.96 (0.33 – 2.79)
Sib vs. Human α -Synuclein + mCherry	0.0012 (1)	0.97	0.98 (0.34 – 2.80)
<i>Sib vs. Human 4R/ON-Tau + mCherry*</i>	<i>71.68 (1)</i>	<i>0.000000000003842</i>	<i>24.71 (11.76 – 51.91)</i>
<i>* Replicate #3 from Figure 1D, reanalyzed to compare Sib and Tau, similar to the other comparisons in this table</i>			

The table shows Mantel-Cox χ^2 and p , and Mantel-Haenszel hazard ratio \pm 95% confidence intervals for survival of GFP/mCherry (Supplementary Figure S6C) or α -Synuclein/mCherry (Figure 1f, Supplementary Figure S6d) zebrafish in comparison with non-expressing Sibling zebrafish. The last row (in gray font) shows replicate #3 of Tau zebrafish (Figure 1d) reanalyzed to compare with non-expressing siblings, to provide a representative comparison with the additional controls.

Supplementary Table 6 – ANOVA summary for Figure 2d (Acridine Orange labeling)

2-way ANOVA (genotype, age) table:

Source of Variation	% of total variation	<i>p</i>
<i>Interaction</i>	10.76	0.000000000000239
<i>Age</i>	10.59	0.000000000000367
<i>Genotype (Ctrl versus Tau)</i>	48.13	<0.000000000000001

	SS (Type III)	DF	MS	F (DFn, DFd)	<i>p</i>
<i>Interaction</i>	24385.55	5	4877.11	F (5, 194) = 16.21	P=0.000000000000239
<i>Age</i>	24005.98	5	4801.20	F (5, 194) = 15.96	P=0.000000000000367
<i>Genotype</i>	109092.54	1	109092.54	F (1, 194) = 362.60	P<0.000000000000001
<i>Residual</i>	58366.43	194	300.86		

Šidák multiple comparisons test

Comparison group 1	Comparison group 2	Predicted (LS) mean diff.	95.00% CI of diff.	Adjusted <i>p</i> Value
Ctrl, 2 dpf	Tau, 2 dpf	-12.25	-29.09 to 4.59	0.285789213561081
Ctrl, 3 dpf	Tau, 3 dpf	-46.81	-62.72 to -30.90	0.000000000001960
Ctrl, 4 dpf	Tau, 4 dpf	-79.61	-95.25 to -63.96	<0.000000000000001
Ctrl, 5 dpf	Tau, 5 dpf	-65.07	-81.50 to -48.64	<0.000000000000001
Ctrl, 6 dpf	Tau, 6 dpf	-51.60	-66.04 to -37.16	<0.000000000000001
Ctrl, 7 dpf	Tau, 7 dpf	-25.91	-42.69 to -9.12	0.000359347541892

Supplementary Table 7 – ANOVA summary for Figure 2e (TUNEL labeling)

2-way ANOVA (genotype, age) table:

Source of Variation	% of total variation	<i>p</i>
<i>Interaction</i>	22.63	<0.0000000000000001
<i>Age</i>	39.03	<0.0000000000000001
<i>Genotype (Ctrl versus Tau)</i>	25.11	<0.0000000000000001

	SS (Type III)	DF	MS	F (DFn, DFd)	<i>p</i>
<i>Interaction</i>	211377.76	5	42275.55	F (5, 91) = 28.63	P<0.0000000000000001
<i>Age</i>	364563.85	5	72912.77	F (5, 91) = 49.37	P<0.0000000000000001
<i>Genotype</i>	234577.60	1	234577.60	F (1, 91) = 158.84	P<0.0000000000000001
<i>Residual</i>	134387.46	91	1476.79		

Šidák multiple comparisons test

Comparison group 1	Comparison group 2	Predicted (LS) mean diff.	95.00% CI of diff.	Adjusted <i>p</i> Value
Ctrl, 2 dpf	Tau, 2 dpf	-12.25	-29.09 to 4.59	0.001395687044297
Ctrl, 3 dpf	Tau, 3 dpf	-46.81	-62.72 to -30.90	<0.0000000000000001
Ctrl, 4 dpf	Tau, 4 dpf	-79.61	-95.25 to -63.96	0.0000000000000055
Ctrl, 5 dpf	Tau, 5 dpf	-65.07	-81.50 to -48.64	0.012198377958896
Ctrl, 6 dpf	Tau, 6 dpf	-51.60	-66.04 to -37.16	0.999939505322290
Ctrl, 7 dpf	Tau, 7 dpf	-25.91	-42.69 to -9.12	0.729813635807312

Supplementary Table 8 – ANOVA summary for Figure 2f (activated Caspase-3 labeling)

2-way ANOVA (genotype, age) table:

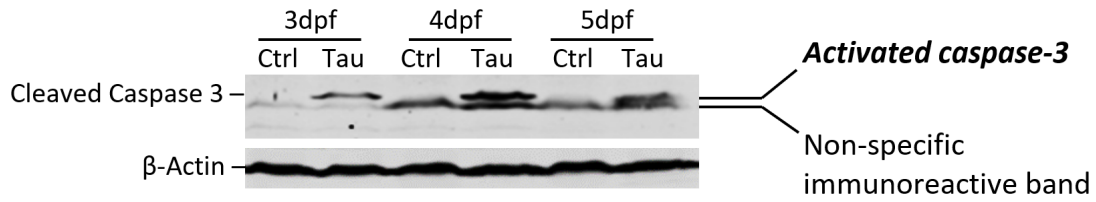
Source of Variation	% of total variation	<i>p</i>
<i>Interaction</i>	15.14	0.000000060713328
<i>Age</i>	25.04	0.000000000008366
<i>Genotype (Ctrl versus Tau)</i>	34.76	<0.000000000000001

	SS (Type III)	DF	MS	F (DFn, DFd)	<i>p</i>
<i>Interaction</i>	28418.35	5	5683.67	F (5, 78) = 10.85	P=0.000000060713328
<i>Age</i>	47000.02	5	9400.00	F (5, 78) = 17.94	P=0.000000000008366
<i>Genotype</i>	65239.59	1	65239.59	F (1, 78) = 124.54	P<0.000000000000001
<i>Residual</i>	40858.57	78	523.83		

Šidák multiple comparisons test

Comparison group 1	Comparison group 2	Predicted (LS) mean diff.	95.00% CI of diff.	Adjusted <i>p</i> Value
Ctrl, 2 dpf	Tau, 2 dpf	-12.25	-29.09 to 4.59	0.000146835705452
Ctrl, 3 dpf	Tau, 3 dpf	-46.81	-62.72 to -30.90	0.000000000000087
Ctrl, 4 dpf	Tau, 4 dpf	-79.61	-95.25 to -63.96	0.000000000459424
Ctrl, 5 dpf	Tau, 5 dpf	-65.07	-81.50 to -48.64	0.004836978515467
Ctrl, 6 dpf	Tau, 6 dpf	-51.60	-66.04 to -37.16	0.120399415095435
Ctrl, 7 dpf	Tau, 7 dpf	-25.91	-42.69 to -9.12	0.999742633267315

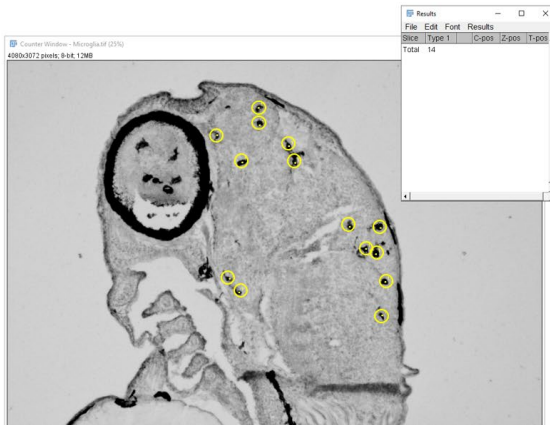
Supplementary Figure S7 – Caspase 3 cleavage by Western blot in Tau zebrafish at 3 – 5 dpf



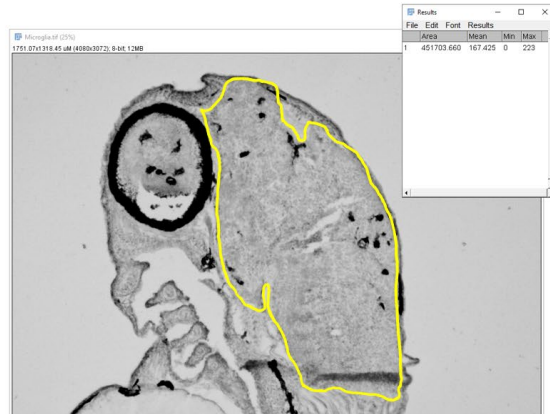
Western blots of larval zebrafish lysates at 3 – 5 dpf were probed with an antibody to cleaved (activated) Caspase-3 (upper panel) and the blot then re-probed with an antibody to β -Actin to confirm equal protein loading in all lanes (bottom panel). Lysates from Tau zebrafish at 3, 4 and 5 dpf, but not Ctrl zebrafish at the same ages, showed a prominent band at 26kDa representing activated Caspase-3. A non-specific band running immediately below activated Caspase-3 is present in every lane as indicated.

Supplementary Figure S8 – Quantification of labeled CNS cells in zebrafish larval sections

Since larval zebrafish brains are small, exhaustive counts of labeled cells are possible in each section. However, the brain area in each image varies according to the plane of the section, necessitating correction as follows:



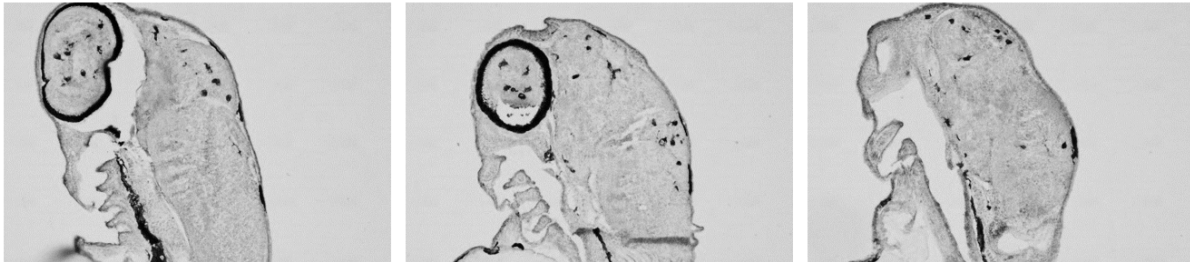
1. Count immunolabeled cells within region of interest (brain) on each section ($n=14$ in image shown)



2. Determine area of region of interest on each section ($= 451703.6 \mu\text{m}^2$
 $= 0.452\text{mm}^2$ in image shown)

3. Calculate 7.4.C4 immunolabeled cells (microglia) per unit area: $14 \times 10^6 / 451703.6 = \underline{\underline{30.99 \text{ microglia/mm}^2}}$ for the section shown above

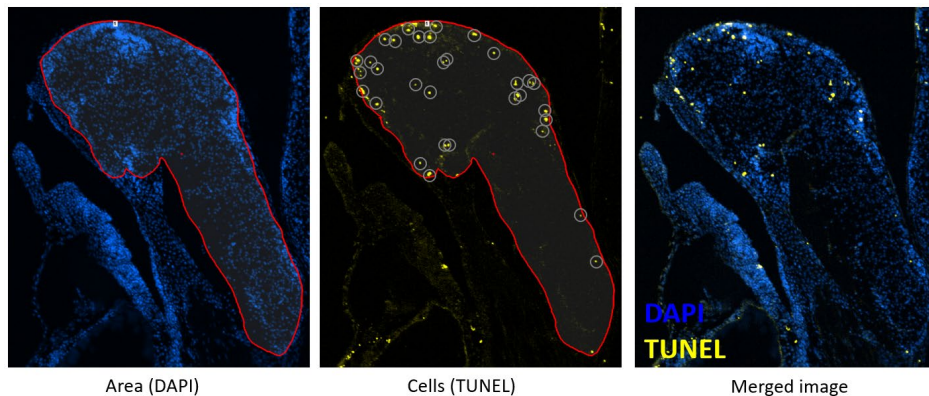
4. The same analysis is completed on 10 – 12 serial sections from each zebrafish:



5. Mean labeling density (cell/mm^2) is calculated for each zebrafish.

6. Analysis is completed for multiple zebrafish in each experimental group at each time point to arrive at data shown in Figure 2f and 2i.

7. Identical analysis is carried out in immunofluorescence sections such as TUNEL labeling in Figure 2b, 2e, except the area of interest is defined using anatomical landmarks in the DAPI labeled image, while blinded to the TUNEL image to increase rigor. The mask is then transferred to the TUNEL image for manual counting:



Supplementary Table 9 – Exact p -values for Figure 2g

Panel	Statistical test	Comparison group 1	Comparison group 2	p value
2g	One sample t-test comparing normalized Tau value to 1	Ctrl = 1	Tau TH	0.002601978242698
		Ctrl = 1	Tau GAD	0.006680996854756
		Ctrl = 1	Tau SYP	0.005405732187820
		Ctrl = 1	Tau PSD95	0.004708719289634

Supplementary Table 10 – ANOVA summary for Figure 2i (7.4.C4⁺ microglia)

2-way ANOVA (genotype, age) table:

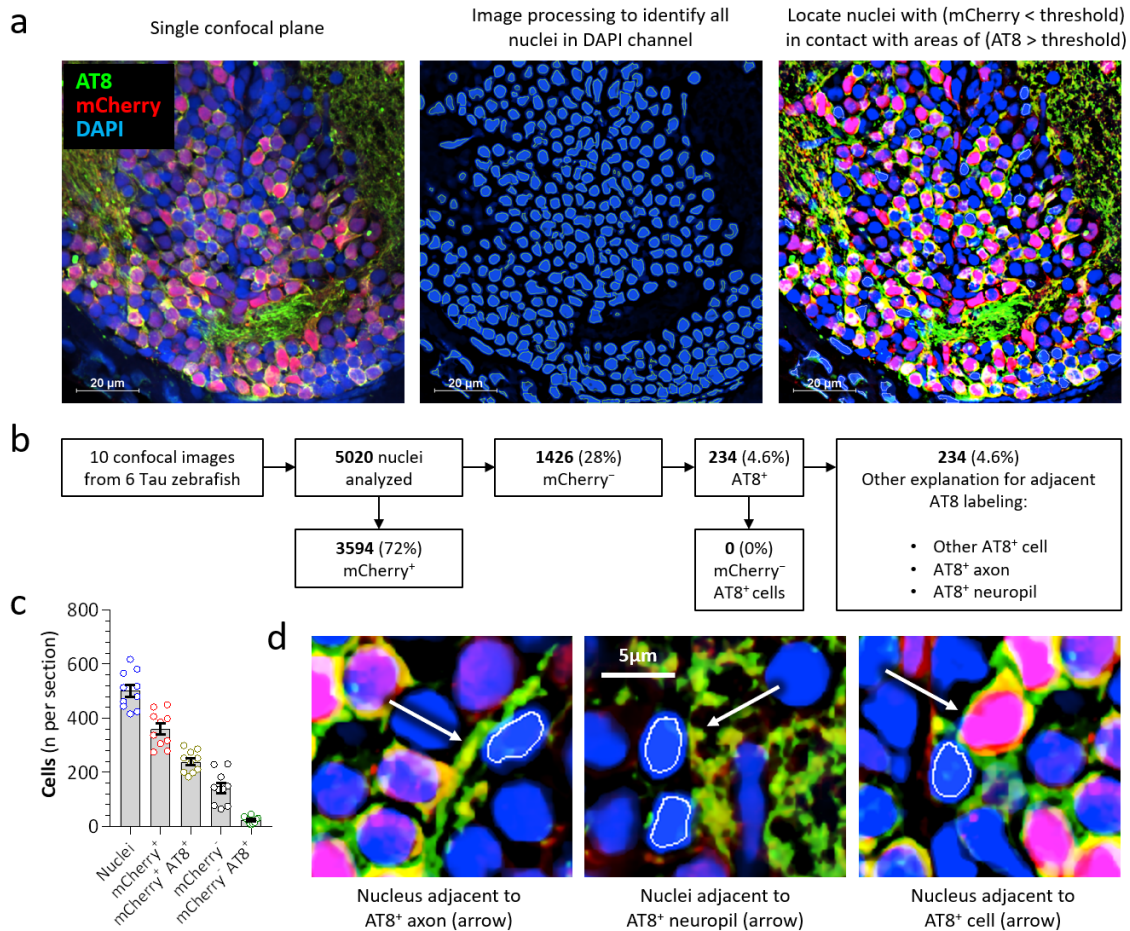
Source of Variation	% of total variation	<i>p</i>
<i>Interaction</i>	7.85	0.000000103003859
<i>Age</i>	41.53	<0.0000000000000001
<i>Genotype (Ctrl versus Tau)</i>	19.08	<0.0000000000000001

	SS (Type III)	DF	MS	F (DFn, DFd)	<i>p</i>
<i>Interaction</i>	1883.67	5	376.73	F (5, 114) = 9.66	P=0.000000103003859
<i>Age</i>	9959.19	5	1991.84	F (5, 114) = 51.10	P<0.0000000000000001
<i>Genotype</i>	4576.22	1	4576.22	F (1, 114) = 117.40	P<0.0000000000000001
<i>Residual</i>	4443.66	114	38.98		

Šidák multiple comparisons test

Comparison group 1	Comparison group 2	Predicted (LS) mean diff.	95.00% CI of diff.	Adjusted <i>p</i> Value
Ctrl, 2 dpf	Tau, 2 dpf	-1.05	-12.87 to 10.77	0.999956229578887
Ctrl, 3 dpf	Tau, 3 dpf	-8.02	-15.18 to -0.87	0.019633861731373
Ctrl, 4 dpf	Tau, 4 dpf	-24.34	-30.78 to -17.90	<0.0000000000000001
Ctrl, 5 dpf	Tau, 5 dpf	-23.29	-29.83 to -16.74	0.0000000000000002
Ctrl, 6 dpf	Tau, 6 dpf	-17.34	-23.55 to -11.13	0.000000000103689
Ctrl, 7 dpf	Tau, 7 dpf	-6.93	-16.23 to 2.37	0.257070044455303

Supplementary Figure S9 – No evidence that human Tau is transferred to cells not expressing the transgene



We examined Tau zebrafish brain sections for evidence that human Tau is taken up by cells adjacent to transgene-expressing neurons. An automated image analysis workflow identified candidate Tau-recipient cells (defined by AT8 immunoreactivity adjacent to nuclei lacking mCherry expression) for further manual analysis.

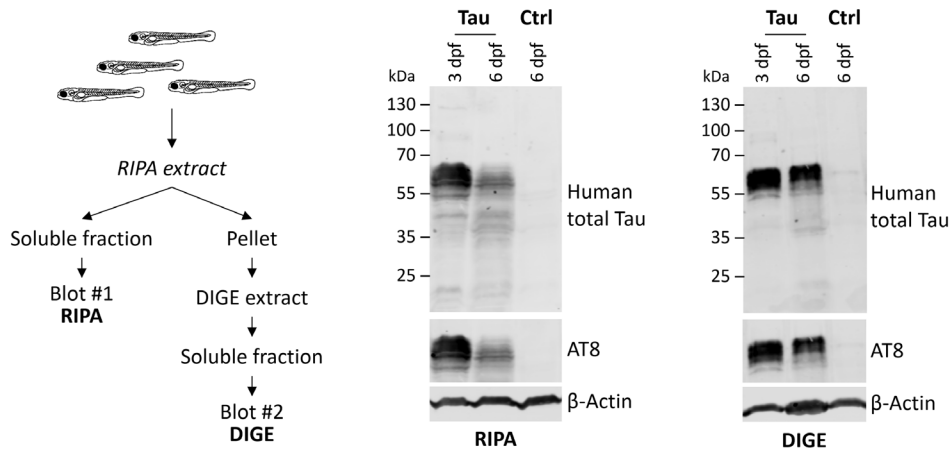
a: Image analysis workflow. The left panel shows a single confocal plane with three channels (DAPI, nuclei, blue; AT8, human [pS202, pT205]-Tau, green; mCherry, transgene expression, red) overlaid. The middle panel shows all nuclei identified in the DAPI channel after applying local contrast enhancement, thresholding, boundary smoothing and separation. The right image shows the processed channels overlaid; nuclei that did not express mCherry but were in contact with areas of AT8 immunoreactivity are outlined in white.

b, c: The algorithm identified 5020 nuclei in 10 confocal planes from 6 Tau zebrafish, of which 3594 (72%) were within neurons expressing the mCherry transgene. Of the remaining 1426 mCherry⁻ (non-expressing) nuclei, 234 were identified as being of potential interest by proximity to areas of AT8 labeling and were evaluated manually. All 234 mCherry⁻ nuclei were adjacent to AT8-immunoreactive structures in other cells, such as a neighboring cell body, axon, or neuropil. No definite AT8 immunoreactivity was found within mCherry⁻ cells. The graph in panel c shows these data by section (data points) with the group mean \pm SE.

d: Enlarged regions from panel (a) showing nuclei of cells identified as mCherry⁻/AT8⁺ by the algorithm (outlined in white) but found to show AT8 signal in an adjacent axon (left), neuropil (center), or cell body (right).

These data suggest that cell-to-cell transfer of human Tau in this model occurs rarely, or at quantities below threshold levels for detection, or does not occur. These experiments do not exclude human Tau seeds templating the misfolding of zebrafish Tau in adjacent cells, detection of which would require antibodies to misfolded zebrafish Tau paralogues.

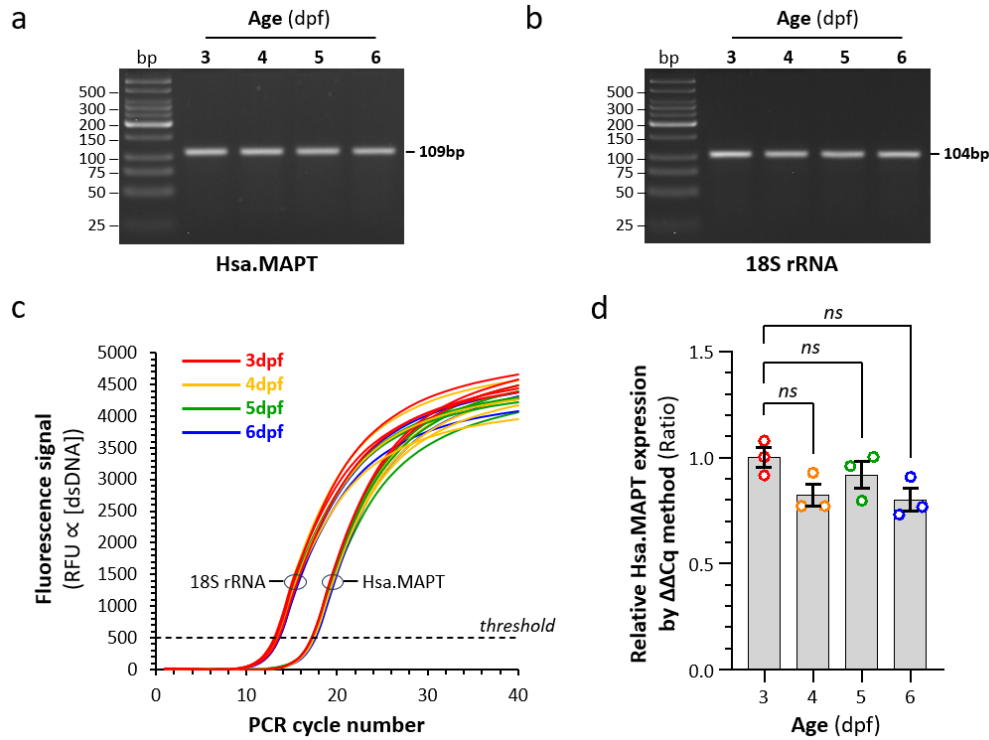
Supplementary Figure S10 – Serial extraction of Tau zebrafish in RIPA then DIGE



The blots in Figure 4b show separate zebrafish samples extracted using either RIPA or DIGE buffers in parallel. In this figure, the same zebrafish samples were extracted serially using RIPA first, and then the RIPA-insoluble pellet was re-extracted with DIGE, as summarized in the schematic to the left. The two western blots show the RIPA- (left) and DIGE- (right) extracted samples for 3dpf and 6dpf Tau zebrafish and 6dpf Ctrl zebrafish, probed with antibodies to human total Tau (top), human Phospho[S202, T205]-Tau (AT8; middle) and β -Actin (bottom).

This procedure is technically challenging in zebrafish as the starting material is small. However, the large reduction in Tau immunoreactivity in the RIPA-extracted samples between 3 dpf and 6 dpf is much less prominent in the DIGE-extracted samples. Together with the blots shown in Figure 4a – 4b, these data support the interpretation that human ON/4R-Tau becomes less soluble in Tau zebrafish between 3dpf and 6dpf.

Supplementary Figure S11 – Relative expression of human MAPT mRNA during development in transgenic Tau zebrafish



We employed real-time qRT-PCR to determine whether expression of the Tau transgene changes during development. Since expression of the common reference genes *bact1* (decrease) and *gapdh* (increase) change significantly during zebrafish development (not shown) we instead used a primer pair for 18S ribosomal RNA as a reference gene, providing an internal control for total RNA (see Supplementary Figure S3 and Supplementary table 1 for validation of the 18S-rRNA primer pair in this assay).

a, b: 25-cycle PCR amplification of first-strand cDNA from Tau zebrafish at 3-, 4-, 5- and 6-days post-fertilization (dpf) using primers to (a) Hsa.MAPT or (b) 18S rRNA. The PCR products were separated in a 4% LMP agarose gel. The images show the ethidium-stained gel photographed under UV illumination. A single product of expected size was generated by each primer pair at every developmental point. These data validate using these primers for detecting transgene expression and rRNA in Tau zebrafish and show that Hsa.MAPT transgene mRNA is expressed at all time points 3 – 6 dpf.

c: Real-time quantitative PCR amplification of first-strand cDNA from Tau zebrafish at 3 – 6 dpf using primers for 18S rRNA and the human Tau transgene. Three technical replicates were completed for each of three biological replicates (i.e. three different first-strand cDNA libraries derived from different zebrafish at each time point 3 – 6 dpf). The figure shows superimposed amplification curves for all 3 technical replicates at all four time points for one biological replicate (time points are color coded according to the legend). The curves within each set cross the quantification threshold at near-identical x-coordinates, suggesting abundance of RNA for both genes is similar in each of the samples.

d: Expression of the MAPT transgene relative to expression at 3dpf using the $\Delta\Delta Cq$ method. Each data point shows the mean value of three technical replicates for each biological replicate. Bars show group mean \pm SE. Data were analyzed using 1-way ANOVA with Dunnett’s multiple comparisons to test to compare Hsa.MAPT cDNA abundance at each time point to 3dpf. Although a small ($\approx 15\%$) decrease was seen in Hsa.MAPT between 3 and 6dpf, this was not statistically significant and may be accounted for by assay variability. This panel is identical to Figure 4c and is reproduced here for clarity.

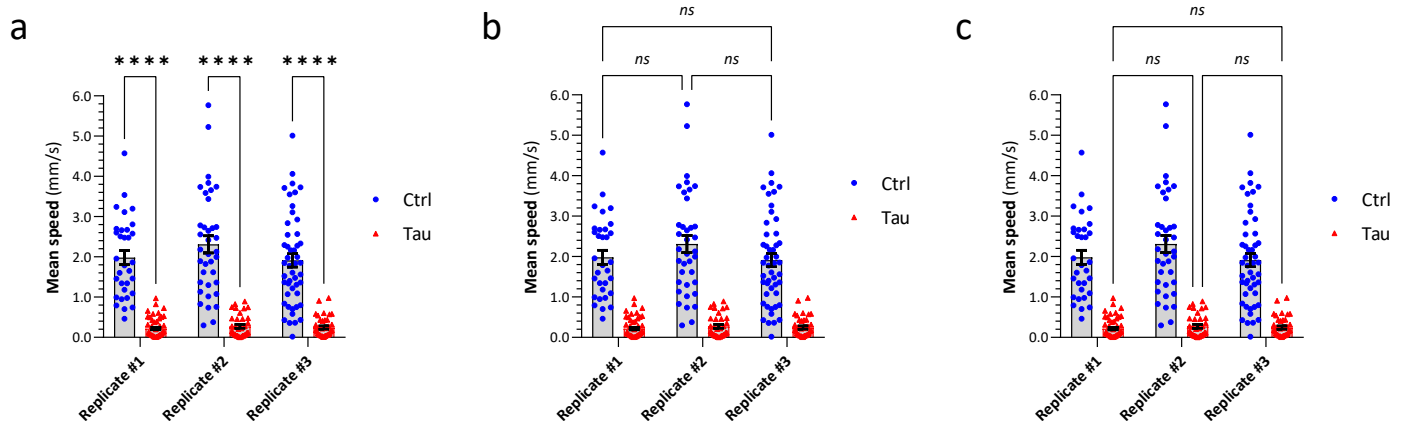
Supplementary Table 11 – Šidák multiple comparisons test for Figure 5b

N1 = 48 N2 = 48 Df = 2,820

Time bin	Mean difference	95.00% CI of difference	Adjusted <i>p</i> value	<i>t</i>
1 ($0 \leq t \leq 2$)	1.20706	0.427597 to 1.98652	0.000036738918828	4.86218
3	1.47632	0.696864 to 2.25579	0.000000092117170	5.94682
5	1.44248	0.663022 to 2.22194	0.000000207777493	5.81050
7	1.59446	0.815003 to 2.37392	0.000000004697050	6.42270
9	1.57605	0.796585 to 2.35551	0.000000007575102	6.34851
11	1.45742	0.677960 to 2.23688	0.000000145412921	5.87068
13	1.50133	0.721869 to 2.28079	0.000000049941436	6.04755
15	1.65403	0.874565 to 2.43349	0.000000000966657	6.66263
17	1.70375	0.924286 to 2.48321	0.000000000247904	6.86291
19	1.69835	0.918890 to 2.47781	0.000000000287872	6.84117
21	1.68007	0.900612 to 2.45953	0.000000000476104	6.76755
23	1.67524	0.895778 to 2.45470	0.000000000543400	6.74808
25	1.51013	0.730665 to 2.28959	0.000000040174474	6.08298
27	1.48953	0.710073 to 2.26899	0.000000066742357	6.00003
29	1.33722	0.557759 to 2.11668	0.000002332954064	5.38649
31	1.34872	0.569259 to 2.12818	0.000001806082129	5.43281
33	1.58773	0.808270 to 2.36719	0.000000005597149	6.39558
35	1.52918	0.749715 to 2.30864	0.000000024975194	6.15972
37	1.42203	0.642567 to 2.20149	0.000000336853786	5.72811
39	1.29875	0.519292 to 2.07821	0.000005412699527	5.23154
41	1.11090	0.331437 to 1.89036	0.000238467585333	4.47484
43	1.26937	0.489913 to 2.04883	0.000010138302967	5.11320
45	1.33415	0.554692 to 2.11361	0.000002496948210	5.37414
47	1.29290	0.513441 to 2.07236	0.000006139794112	5.20797
49	1.28724	0.507778 to 2.06670	0.000006932828705	5.18516
51	1.38607	0.606610 to 2.16553	0.000000775541793	5.58327
53	1.38548	0.606024 to 2.16495	0.000000786022282	5.58091
55	1.66705	0.887586 to 2.44651	0.000000000679326	6.71508
57	1.73399	0.954530 to 2.51345	0.000000000106378	6.98474
59	1.70589	0.926433 to 2.48535	0.000000000233561	6.87156

The movement traces in Figure 5b were analyzed by calculating the mean swimming speed for each of the 48 zebrafish in each group, within contiguous 2-minute time bins spanning the 60 minutes of recording. For each time bin, Tau and Ctrl group means were compared using 2-way repeated-measures ANOVA (experimental group, time point) with Šidák multiple comparisons test. The adjusted *p* value is shown for each time bin.

Supplementary Figure S12 – Biological replicate motor activity assays comparing Tau and Ctrl zebrafish



3 biological replicate experiments (same transgenic allele, different parents, crossed different days) comparing the mean speed of Tau and Ctrl zebrafish over 60 minutes of spontaneous swimming in bright white ambient illumination at 5 dpf. Data points show individual zebrafish, bars show group mean \pm SE. Experimental groups and replicates were compared using 2-way ANOVA (genotype, replicate) with a single Tukey multiple comparisons test (see Supplementary Table S12). The same data are shown three times for clarity.

- a: There was a robust difference between Tau and Ctrl in each assay
- b: There was no difference between assays for Ctrl
- c: There was no difference between assays for Tau

Given the absence of significant differences between the assays, it was admissible to combine these data to generate Figures 5c – 5g.

Supplementary Table 12 – ANOVA summary for Supplementary Figure S12

Details of the 2-way ANOVA (genotype, replicate) used in Supplemental Figure S12 to compare Ctrl and Tau zebrafish in 3 biological replicate assays.

Source of Variation	% of total variation	P
<i>Interaction</i>	0.3809	0.350146138610801
<i>Experimental replicate</i>	0.5807	0.202605208323934
<i>Ctrl versus Tau</i>	54.44	<0.0000000000000001

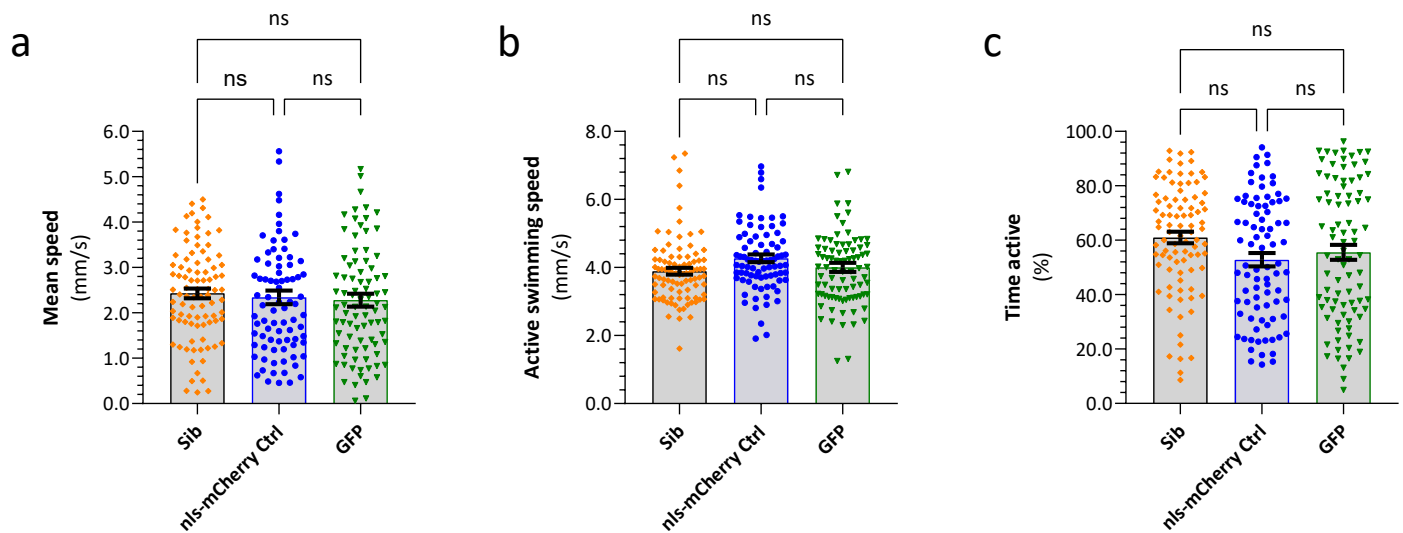
	SS (Type III)	DF	MS	F (DFn, DFd)	P
<i>Interaction</i>	1.395	2	0.6976	F (2, 241) = 1.054	P=0.350146138610801
<i>Experimental replicate</i>	2.127	2	1.064	F (2, 241) = 1.607	P=0.202605208323934
<i>Ctrl vs Tau</i>	199.4	1	199.4	F (1, 241) = 301.3	P<0.0000000000000001
<i>Residual</i>	159.5	241	0.6619		

Tukey multiple comparisons test

	Comparison	Predicted (LS) mean diff.	95.00% CI of diff.	Adjusted P Value
a: Ctrl vs. Tau each replicate	Replicate #1:Ctrl vs. Replicate #1:Tau	1.765	1.406 to 2.124	<0.0000000000000001
	Replicate #2:Ctrl vs. Replicate #2:Tau	2.036	1.661 to 2.411	<0.0000000000000001
	Replicate #3:Ctrl vs. Replicate #3:Tau	1.671	1.331 to 2.012	<0.0000000000000001
b: Compare Ctrl between replicates	Replicate #1:Ctrl vs. Replicate #2:Ctrl	-0.3263	-0.7895 to 0.1368	0.222191178051007
	Replicate #1:Ctrl vs. Replicate #3:Ctrl	0.07036	-0.3675 to 0.5082	0.923925766974799
	Replicate #2:Ctrl vs. Replicate #3:Ctrl	0.3967	-0.02304 to 0.8164	0.068410230248918
c: Compare Tau between replicates	Replicate #1:Tau vs. Replicate #2:Tau	-0.05549	-0.4699 to 0.3589	0.946530094330830
	Replicate #2:Tau vs. Replicate #3:Tau	-0.02320	-0.4222 to 0.3758	0.989693422254547
	Replicate #1:Tau vs. Replicate #3:Tau	0.03229	-0.4059 to 0.4705	0.983492703865083

A single Tukey test was completed to encompass all 9 comparisons, but data are shown in three groups of 3 for clarity.

Supplementary Figure S13 – Three different control groups behave similarly in motor activity assays



In Figure 5, we show data comparing Tau and Ctrl zebrafish, which contain exactly the same complement of transgenes, with the exception that human Tau is not expressed in Ctrl zebrafish. However, since there is substantial genetic heterogeneity in WT zebrafish that can influence outcomes in neurological assays, the possibility that some of the phenotypes are caused by genetic variation unrelated to the transgene should be considered.

To address this question, we tested two additional controls in this assay: (i) Siblings of Tau zebrafish that do not show mCherry fluorescence and therefore do not express human Tau (Sib; orange). These are a mixture of WT, driver and responder zebrafish that share background genetics with their Tau siblings. (ii) *Tg(elavl3:gal4-*vp16*); Tg(UAS:egfp)* zebrafish (GFP; green) that express a second responder allele unrelated to the *Tg(UAS:2a-nls-mCherry)* allele present in Ctrl zebrafish.

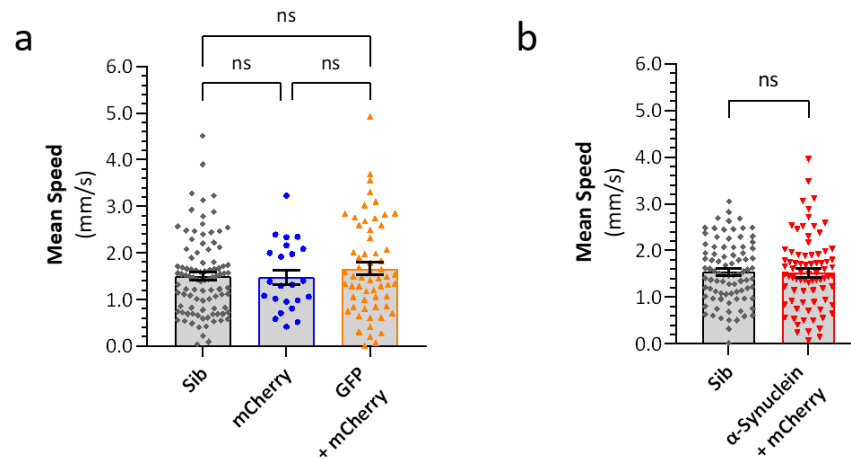
Motor activity assays were run and analyzed identically to those shown in Figure 5^{2,3}. The graphs show:

- a: Mean speed
- b: Active swimming speed
- c: % time active

In each graph, data points show individual zebrafish, bars show mean \pm SE. Comparison between groups was carried out using 1-way ANOVA with Tukey multiple comparison test.

There were no statistically significant differences between the groups. Together with direct comparisons between Tau zebrafish and each of these controls, and replicate phenotypes in multiple transgenic Tau lines, these data strongly support our interpretation that the observed phenotypes in Figure 5 are attributable to expression of human ON/4R-Tau. These data also support the use of these controls interchangeably in subsequent experiments.

Supplementary Figure S14 – Heterologous protein over-expression does not alone cause motor phenotypes



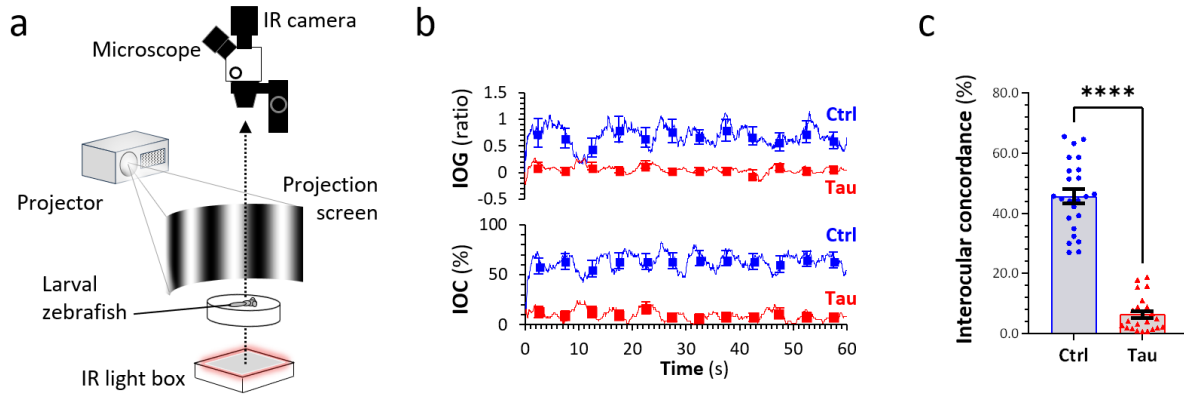
In Figure 5, we show data comparing Tau and Ctrl zebrafish, which contain exactly the same complement of transgenes, with the exception that human Tau is not expressed in Ctrl zebrafish. However, this means that Ctrl zebrafish express one less transgene than Tau zebrafish, and so these experiments do not fully exclude the possibility that phenotypes in Tau zebrafish are non-specific and arise from over-expression of multiple heterologous transgenes. To address this question, we analyzed two additional models that express the same number of transgenes as Tau zebrafish, using the same 96-well plate motor function assay. In each graph, data points show individual zebrafish, bars show mean \pm SE (data in each panel are combined from biological replicates that did not differ significantly from each other, exactly as analyzed in Supplementary Figure 12).

a. *Tg(elavl3:gal4-vp16); Tg(UAS:egfp); Tg(UAS:p2a-nls-mCherry)* zebrafish (orange) express both GFP and mCherry simultaneously, replicating the same number of heterologous genes expressed under the same driver as Tau zebrafish. Control groups were siblings with mCherry fluorescence only (blue), and siblings lacking both mCherry and GFP fluorescence (grey). Comparison between groups was carried out using 1-way ANOVA with Tukey's multiple comparison test.

b. *Tg(elavl3:gal4-vp16); Tg(UAS:Hsa.SNCA-p2a-nls-mCherry)^{pt423}* zebrafish express the same bicistronic responder cassette under the same driver as Tau zebrafish, but with human WT α -Synuclein cDNA replacing the human ON/4R-Tau coding sequence. This replicates the expression system of the Tau model exactly, and also expresses an independent heterologous human protein. Controls were siblings lacking mCherry expression. Comparison between groups was carried out using a 2-tailed *t*-test with Welch's correction for unequal variance.

There were no statistically significant differences between the groups in either set of assays, showing that expressing mCherry with a second transgene (either GFP or human α -Synuclein) under the same pan-neuronal driver does not result in a motor phenotype. These data do not support the interpretation that the hypokinetic motor phenotype of Tau zebrafish is a non-specific artifact of heterologous protein over-expression. Instead, this phenotype likely reflects a pathogenic property of human ON/4R-Tau in this model.

Supplementary Figure S15 – Methodology and abnormalities of ocular movement in Tau zebrafish

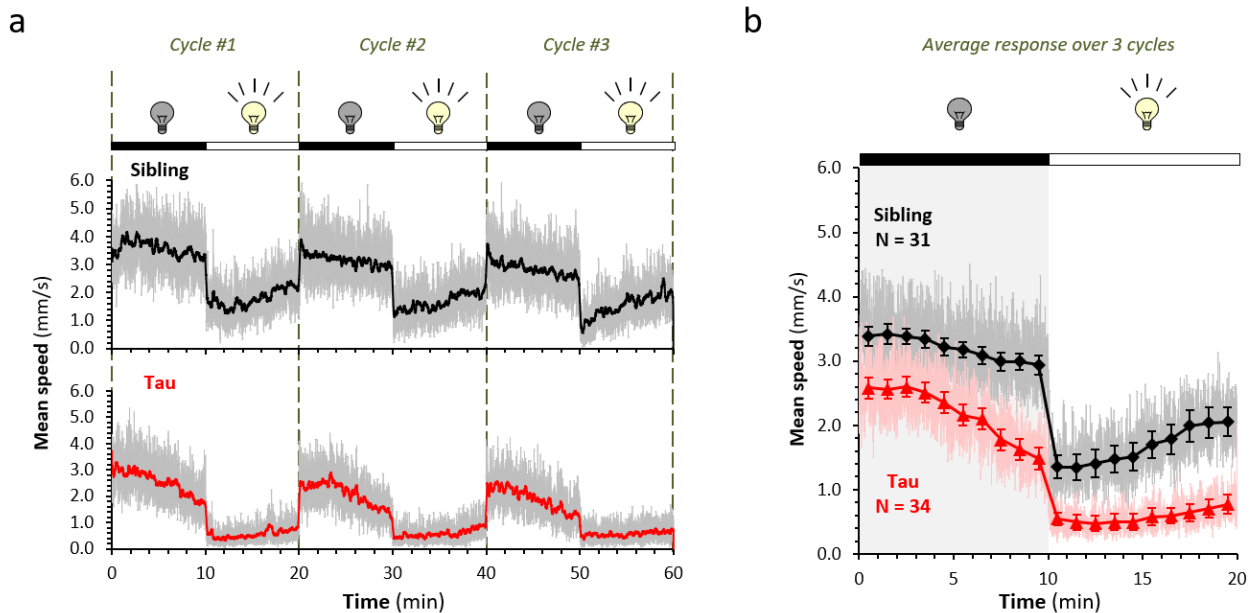


a: Illustration of the experimental configuration⁴ used to elicit optokinetic reflexes in Figure 6. Note that the visual stimulus is presented to the left (stimulated) eye only.

b: Unilateral stimulus presentation in this assay allows analysis of the coordination between L and R eyes during the response. These graphs show how interocular gain (IOG; the ratio of change in angle of stimulated eye to change in angle of contralateral eye at each frame transition; see also Figure 6h) and interocular concordance (IOC; the proportion of frame transitions at which there was movement of both eyes in the same direction) vary in Ctrl (blue) and Tau (red) zebrafish during the same example segment of recording shown in Figure 6b.

c: Quantitative analysis of mean IOC for Ctrl (blue) and Tau (red) zebrafish. Data points show individual zebrafish, bars show mean \pm SE. **** $p < 0.0001$, Ctrl vs. Tau, 2-tailed unpaired t -test with Welch's correction for unequal variance.

Supplementary Figure S16 – Abnormalities of the visual motor response in Tau zebrafish



In order to optimize an assay of motor activity for high-throughput screening, it was necessary to reduce variability as far as possible. This was achieved by using the zebrafish responses to alternating periods of bright ambient light and darkness, as evoked responses tend to be less variable than spontaneous behavior, and responses to multiple stimuli can be averaged. In addition, to simplify the breeding scheme for executing a screen, and further reduce variability by ensuring the controls shared similar genetic background and were at exactly the same developmental age as Tau zebrafish, the assay was optimized using non-expressing siblings as controls. This is valid because siblings showed identical responses to other controls in all assays tested (Supplementary Figure S13).

a: Motor responses for 31 Sib and 34 Tau zebrafish over three consecutive stimulus cycles of [10 minutes darkness + 10 minutes light] as shown above the graph. The gray traces show mean group centroid displacement at each video frame transition scaled to show mean speed (y-axis); the colored lines (Sib, black; Tau, red) show the same data averaged over a 50-frame moving window.

b: The three stimulus cycles were averaged to provide mean activity waveforms for each individual zebrafish over a single cycle; the averaged traces for each experimental group are shown (gray). The mean speed for each zebrafish was calculated in contiguous 1-minute time bins over the 20-minute averaged stimulus cycle. This allowed calculation of group mean speed (solid markers) and SE (error bars) in each time bin across the averaged response cycle.

These analyses reduced response variability and increased statistical power to detect differences between smaller samples of zebrafish in each group, providing an essential basis for the screening assays shown in Figure 7. Since the difference between Ctrl and Tau was proportionately greater in the light phase of the response, and this was more quantitatively reproducible between biological replicates than the dark phase abnormalities, we used VMR light phase swimming speed as the readout for the screen.

Supplementary Table 13 – Šidák multiple comparisons table for Supplementary Figure S16b

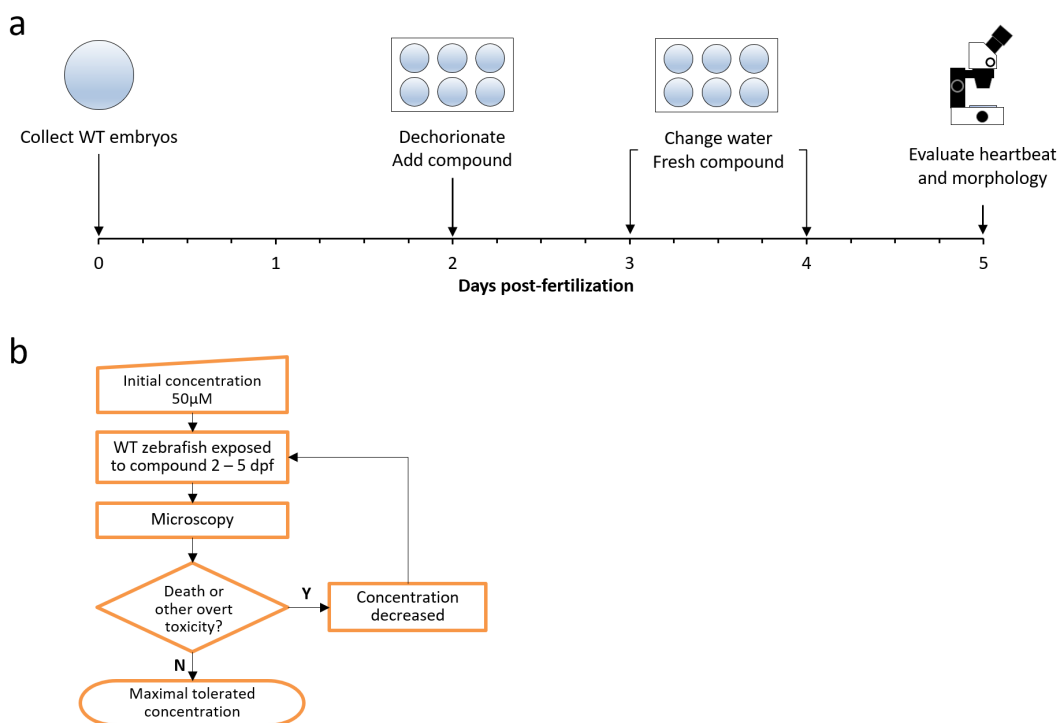
Time (Min)	Predicted (LS) mean diff.	95.00% CI of diff.	Adjusted P Value
0.5 (0 ≤ t <1)	0.806912641366225	0.110909956833643 to 1.50291532589881	0.009458477660351
1.5	0.856180163187854	0.160177478655273 to 1.55218284772044	0.004191672094418
2.5	0.783846788425048	0.0878441038924668 to 1.47984947295763	0.013636095234470
3.5	0.832441664136623	0.136438979604041 to 1.52844434866920	0.006238104819818
4.5	0.868476591081594	0.172473906549012 to 1.56447927561418	0.003398073653293
5.5	1.01484090891840	0.318838224385823 to 1.71084359345099	0.000227994715967
6.5	0.988876888994308	0.292874204461726 to 1.68487957352689	0.000378316585406
7.5	1.21731838519924	0.521315700666660 to 1.91332106973182	0.000002950694177
8.5	1.36357402371917	0.667571339186584 to 2.05957670825175	0.000000082594425
9.5	1.45304057115750	0.757037886624914 to 2.14904325569008	0.000000007755137
10.5	0.810600031309298	0.114597346776716 to 1.50660271584188	0.008913110573539
11.5	0.853784509487666	0.157781824955085 to 1.54978719402025	0.004365266187774
12.5	0.928790748576850	0.232788064044268 to 1.62479343310943	0.001167796835428
13.5	0.977701580645162	0.281698896112580 to 1.67370426517774	0.000468767742351
14.5	1.01941306736243	0.323410382829847 to 1.71541575189501	0.000208291705206
15.5	1.12485552277040	0.428852838237817 to 1.82085820730298	0.000023443366506
16.5	1.18968867267552	0.493685988142940 to 1.88569135720810	0.000005566046220
17.5	1.35094928842505	0.654946603892466 to 2.04695197295763	0.000000114080609
18.5	1.33412558728653	0.638122902753946 to 2.03012827181911	0.000000174705283
19.5	1.28679395825427	0.590791273721686 to 1.98279664278685	0.000000564786257

The data shown in Supplementary Figure S16b were analyzed by 2-way repeated measures ANOVA (group, time) with Šidák multiple comparisons test to evaluate the difference between Ctrl and Tau at each time point during the response. The table shows the predicted least squares difference between experimental groups in each time bin, 95% CI of the difference and adjusted *p*.

Supplementary Table 14 – Small molecule screening data

Category	Parameter	Description
Assay	Type of assay	Machine vision analysis of zebrafish motility
	Target	Agnostic/phenotypic screen
	Primary measurement	Rescue of Tau zebrafish hypokinesia
	Key reagents	Tau and Sib zebrafish
	Assay protocol	Measurement of light phase swimming speed during the visual motor response. See <i>Methods</i> .
Library	Library size	147 small molecules
	Library composition	Inhibitors of epigenetic reader, writers and erasers
	Source	Cayman Chemical, Ann Arbor, MI
Screen	Format	96 well plate
	Concentration(s) tested	Maximum tolerated concentration in WT zebrafish (0.5 – 50 μ M)
	Plate controls	Untreated Tau and Sibling zebrafish
	Reagent/ compound dispensing system	Manual
	Detection instrument and software	IR video from FL3-U3-13Y3M-C camera, Point Gray Research; video analyzed by MATLAB running <i>LSRtrack</i>
	Assay validation/QC	See Figure 7 and S19. QC based on untreated Tau and Sib controls in each assay.
	Correction factors	None
	Normalization	Assay output normalized to controls in each assay as shown in Figure 7d'
Post-HTS analysis	Hit criteria	Library mean + 3*SD
	Hit rate	3/147
	Additional assay(s)	Survival analysis, cell death, transgene expression, microgliosis, synapse abundance, microglial phagocytosis of synaptic material, see Figures 8 – 9
	Confirmation of hit purity and structure	Results replicated with repurchased compound

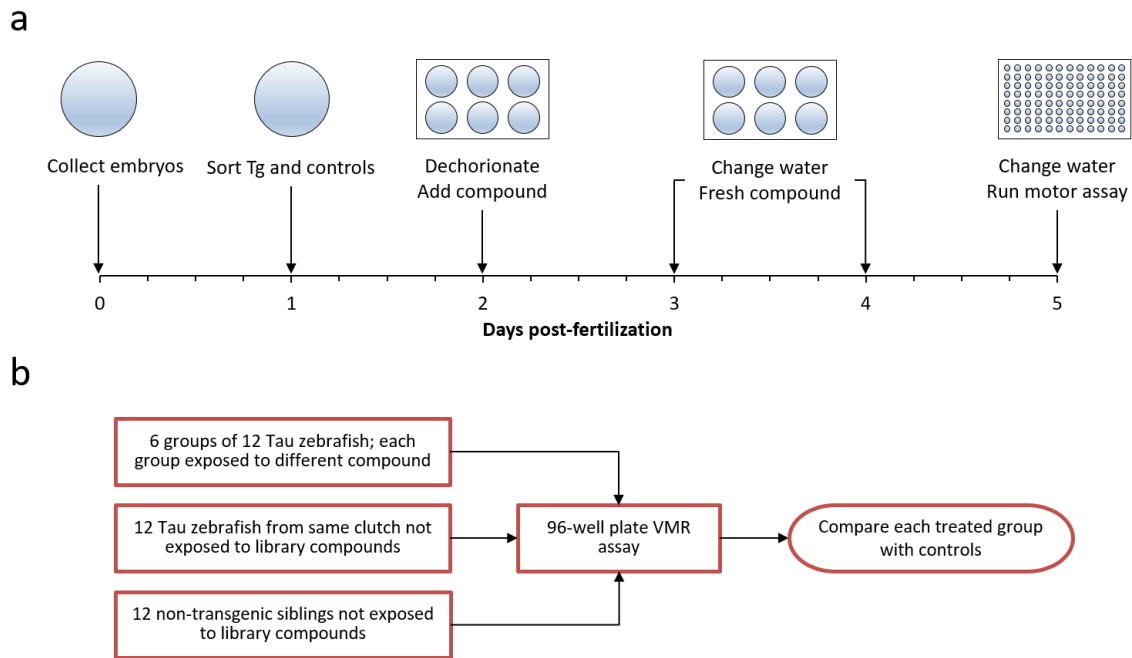
Supplementary Figure S17 – Small molecule screen part 1: Determination of maximum tolerated concentration



a: WT zebrafish embryos were collected after fertilization and housed in 6-well plates with daily changes of E3 buffer. The larvae were dechorionated at 2dpf and buffer replaced with fresh E3 containing library compound. The buffer was replaced with fresh E3 containing the compound at 3dpf and 4dpf, then microscopy carried out at 5dpf to evaluate for viability (heartbeat) and morphology.

b: Each compound was evaluated initially at 50µM final concentration in the buffer. If toxicity was found after exposure, the concentration was reduced. Iterative testing eventually provided the maximum tolerated concentration (MTC) for each small molecule in the library.

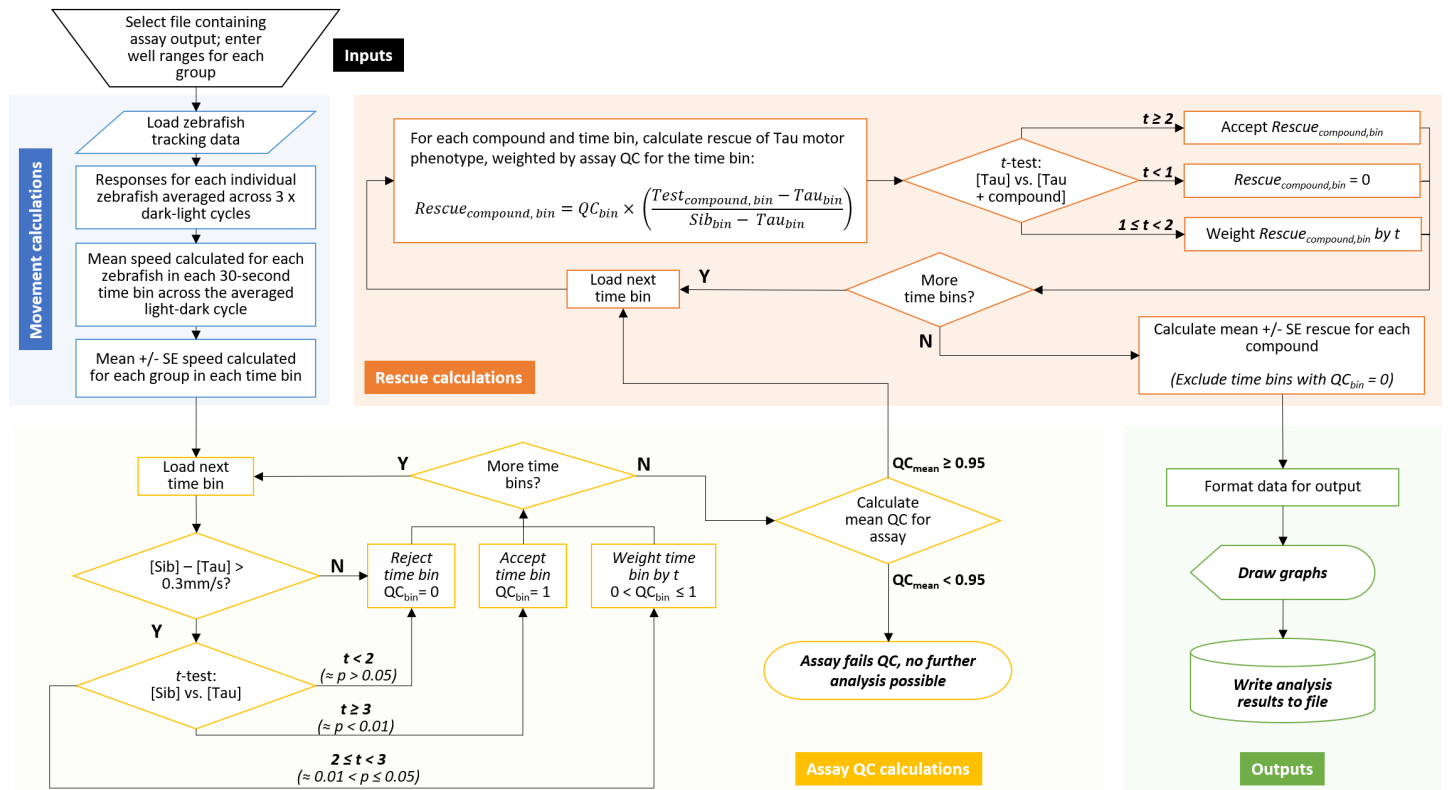
Supplementary Figure S18 – Small molecule screen part 2: Rescue of motor phenotype in Tau zebrafish



A: Zebrafish embryos from a $Tg(elavl3:gal4-vp16) \times Tg(UAS:Hsa.MAPT-p2a-nls-mCherry)$ cross were collected and housed in in 6-well plates with daily changes of E3 buffer. Embryos were genotyped by mCherry fluorescence at 1dpf and sorted into Tau and Sib groups. Larvae were then dechorionated at 2dpf, genotypes verified, and buffer replaced with fresh E3 containing library compound. There were 7 groups of Tau zebrafish: 6 of the groups received E3 containing a different small molecule at its MTC (as defined in part 1 of the screen), the 7th group received E3 only. A single group of 12 Sib zebrafish also received E3 only. Buffer was replaced with fresh E3 \pm compound at 3dpf and 4dpf.

B: At 5dpf, compounds were washed off and replaced with fresh E3 and the VMR elicited as shown in Supplementary Figure S16 for quantitative analysis as shown in Supplementary Figure S19. The entire library was tested, 6 compounds at a time, in this way.

Supplementary Figure S19 – Algorithm logic for analysis of video tracking data from rescue screening assays



The flowchart depicts the algorithm used to calculate rescue of the abnormal VMR phenotype in Tau zebrafish by small molecule exposure. Calculations are split into 4 consecutive processes:

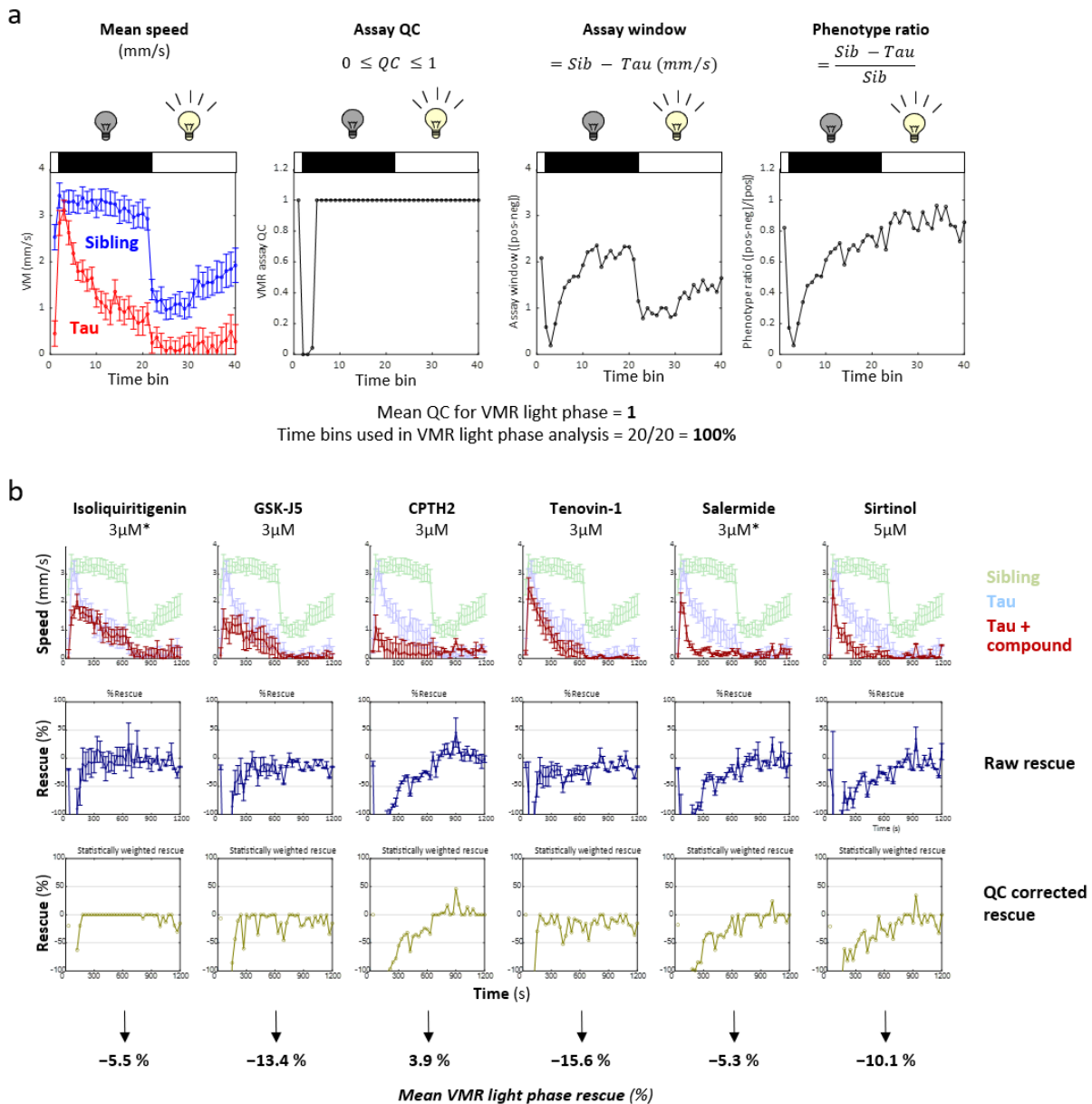
1. Movement calculations (blue) – individual zebrafish responses are averaged over 3 cycles of dark-light stimuli as shown in Supplementary Figure S16, then mean speed for each zebrafish calculated in contiguous 30-second time bins across the averaged stimulus cycle. Mean and SE speed are then calculated for each experimental group in each time bin across the stimulus cycle.

2. Assay quality control (QC) calculations (yellow) – the responses of untreated Tau and Sib zebrafish are compared to ensure that the phenotype in Tau zebrafish was sufficiently robust to make rescue calculations meaningful. Individual time bins where $Speed_{Sib} - Speed_{Tau} < 0.3$ mm/s are assigned $QC=0$ and rejected. Each accepted time bin is then analyzed to ensure that $Speed_{Sib}$ and $Speed_{Tau}$ are statistically significantly different at $p < 0.01$ by t -test; if so, the time bin is assigned a QC score of 1 and accepted. If $p > 0.05$, the bin is assigned $QC=0$ and rejected. For $0.01 < p < 0.05$, QC is weighted linearly between 1 and 0. Mean QC is then calculated for the assay. If $QC < 0.95$ the assay has failed quality control, and no further analysis is possible. This stringent QC process overall rejected $< 5\%$ of assays and ensured that data relating to phenotypic rescue were only accepted as part of the screen if the model behaved exactly as expected.

3. Rescue calculations (orange) – this calculates % rescue for each small molecule in each time bin according to the formula shown in Figure 7d' multiplied by the QC value for the bin. For each compound and each time bin, if $Speed_{Tau}$ and $Speed_{Tau+Chemical}$ are significantly different at $p < 0.05$ by t -test, the value for % rescue in that time bin is accepted. If $p > 0.1$, rescue is set to 0 for that time bin. For $0.1 < p < 0.05$, rescue is weighted by $(t - 1)^3$. These stringent criteria for accepting data points minimized any contribution to overall rescue score from time bins in which effects were marginal. Mean rescue for each chemical is then calculated for the light and dark phases of the VMR, omitting any time bins that were rejected at stage 2 (QC).

4. Outputs (green) – QC metrics and binned rescue data are output graphically (see Supplementary Figure S20) and numerical data are written into a spreadsheet for downstream analysis.

Supplementary Figure S20 – Example outputs from screening assay



a: Mean \pm SE speed of 12 Tau (red) and 12 Sib (blue) zebrafish in 30-second time bins, averaged across 3 x 20-minute dark-light stimulus cycles (first graph). There is a robust phenotype but overlap between Tau and Sib at the start of the dark phase would make rescue calculations impossible in these time bins. This is reflected in the QC score (second graph), which rejects bins 2 – 4 of the dark phase responses. The assay window (difference between Sib and Tau; third graph) and phenotype ratio (assay window as a fraction of Sib response) show the effect size attributable to Tau across the stimulus cycle. Overall, the VMR light phase in this experiment performed well as an assay to detect rescue of neurological function.

b: Automated outputs showing the effect of each of 6 compounds tested in the assay shown in panel A. In the top row, the responses of Tau zebrafish exposed to small molecules (red) are superimposed on the Tau (blue) and Sib (green) controls. None of the compounds improved the motor function of Tau zebrafish. The second and third rows show calculations for phenotypic rescue, either without (middle row) or with (bottom row) removal of points failing QC and correction for whether the effect was significant in each time bin. Compounds marked * were subsequently retested at lower concentrations.

Supplementary Table 15 – Summary of data from the small molecule screen in Figure 7d

Summary table of data from the epigenetic library screen. Rows show each compound, ranked by % rescue of the light phase of the VMR; hits shown in red, other compounds of potential interest shown in green. Columns (from left to right): rank; maximum tolerated concentration (i.e. concentration tested in this assay; μM); mean % rescue of the light phase of the VMR (negative values indicate that the compound worsened the motor phenotype of Tau zebrafish); SE of rescue; compound identity; molecular target.

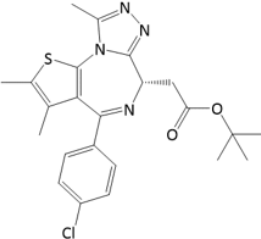
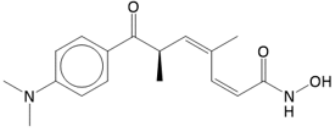
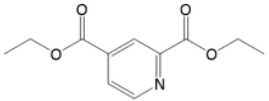
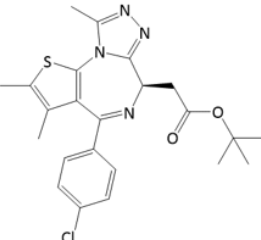
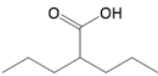
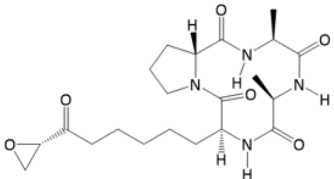
Rank	MTC (μM)	% Rescue	SE	Chemical	Target
1	2	74.89	7.88	(+)-JQ1	BET protein bromodomains
2	0.3	66.92	5.11	Trichostatin A	class I, II, and IV histone deacetylases (HDACs)
3	6	55.17	3.92	2,4-DPD	HIF- α prolyl hydroxylase
4	5	46.32	6.53	Valproic Acid (sodium salt)	class I histone deacetylases (HDACs)
5	25	40.51	3.61	HC Toxin	histone deacetylases (HDACs)
6	50	30.75	4.17	5-Methyl-2'-deoxycytidine	DNA methylation
7	50	30.7	4.16	PFI-3	SMARCA4 bromodomain and PB1(bromodomain 5)
8	10	29.55	9.6	Oxamflatin	histone deacetylases (HDACs)
9	50	28.29	6.96	Chidamide	histone deacetylases (HDACs)
10	37.5	26.39	6.14	SAHA-BPyrne	class I and class II histone deacetylases (HDACs)
11	50	25.92	4.55	N-Oxalylglycine	JMJD2A, JMJD2C, and JMJD2E histone demethylases
12	25	25.03	5.93	4-pentynoyl-Coenzyme A (trifluoroacetate salt)	lysine acetyltransferases
13	50	24.16	4.86	2',3',5'-triacetyl-5-Azacytidine	DNA methyltransferase
14	20	23.8	3.9	S-(5'-Adenosyl)-L-methionine (tosylate)	Methyl donor
15	0.75	23.59	4.19	Lestaurtinib	JAK2, FLT3, TrkA
16	30	22.39	4.07	S-(5'-Adenosyl)-L-methionine chloride (hydrochloride)	Methyl donor
17	50	20.67	5.09	BML-210	histone deacetylases (HDACs)
18	50	20.29	4.2	Tenovin-6	p53 activator
19	50	20.2	3.03	Butyrolactone 3	histone acetyltransferase Gcn5
20	50	19.96	10.06	BIX01294 (hydrochloride hydrate)	G9a histone methyltransferase
21	40	19.78	4.42	CAY10398	histone deacetylase (HDAC1)
22	40	19.11	4.24	trans-Resveratrol	SIRT1 activator, multiple actions
23	20	19.1	3.43	Bromosporine	Bromodomain proteins
24	1.5	17.81	1.64	Isoliquiritigenin	Guanyl cyclase activator
25	40	17.39	5.69	Ellagic Acid	coactivator-associated arginine methyltransferase 1
26	20	17.31	3.7	OTX015	BRD2, 3 and 4
27	50	16.95	7.67	EPZ5676	DOT1L histone methyltransferase
28	1	16.62	5.1	3,3'-Diindolylmethane	histone deacetylases (HDACs) and DNA MTs
29	50	15.46	2.85	Sodium Butyrate	histone deacetylases (HDACs)
30	12.5	13.96	4.96	Chaetocin	HMTs
31	50	13.5	7.93	I-BET151	BRD2, 3, 4
32	20	12.58	5.2	MC 1568	Class Iia HDACs

33	1.5	12.51	7.63	SGL-1027	DNA MTs
34	50	12.27	2.89	UNC0224	G9a histone methyltransferase
35	50	11.22	3	GSK-J1 (sodium salt)	H3K27 histone demethylase JMJD3
36	50	11.11	4.45	RG-108	DNA MTs
37	50	10.7	4.44	Tubastatin A	HDAC6
38	50	9.6	2.21	Suramin (sodium salt)	Topoisomerase II
39	50	9.33	4.54	2,4-Pyridinedicarboxylic Acid	Jumonji HDMs
40	30	8.99	6.25	Zebularine	DNA MTs
41	50	8.78	4.12	Etoposide	Topoisomerase II
42	50	8.4	2.21	I-BET762	BET proteins
43	20	8.08	6.79	Anacardic Acid	HAT activity P300 and PCAF
44	50	8.05	7.04	Rucaparib (phosphate)	PARP1
45	50	7.83	2.5	(+)-Abscisic Acid	Chromatin structure gene expression
46	12.5	7.63	7.12	AK-7	SIRT2
47	50	7.51	2.43	AGK2	SIRT2
48	50	6.7	1.76	Daminozide	HDMs KDM2A, PHF8, KDM7A
49	50	6.34	1.73	(R)-PFI-2 (hydrochloride)	SET7/9 HMT
50	6	6.26	5.42	(-)-JQ1	Negative control for (+)-JQ1
51	0.7	6.12	5.07	CAY10669	HAT PCAF
52	50	5.9	5.14	CPI-203	BRD4
53	1.5	4.93	2.37	IOX1	JMJ2DA HDM
54	50	4.37	2.28	Decitabine	DNA MTs
55	50	4.19	1.68	LAQ824	HDACs
56	50	3.9	1.58	AMI-1 (sodium salt)	Arginine methyltransferases
57	3	3.89	3.19	CPTH2 (hydrochloride)	histone acetyltransferase Gcn5
58	50	3.43	1.63	I-CBP112 (hydrochloride)	CBP EP300
59	50	3.34	4	UNC0642	G9a and GLP HMTs
60	6	3.3	2.87	PCI 34051	HDAC8
61	0.75	3.12	1.86	CAY10591	SIRT1 class III HDACs
62	50	3.11	2.39	Tubacin	HDAC6
63	12.5	2.92	3.46	BSI-201	PARP1
64	1	2.89	1.54	Splitomicin	Sir2p HDAC activity
65	50	2.85	3.44	RVX-208	BET bromodomains BD2
66	1.5	2.81	4.23	Apicidin	HDACs
67	17.5	2.75	2.05	SIRT1/2 Inhibitor IV	SIRT 1 and SIRT2
68	50	2.72	1.58	UNC0646	G9a and GLP HMTs
69	50	2.6	1.79	RSC-133	HDAC and DNA MTs
70	50	2.57	1.46	B32B3	H2A T120 phosphorylation
71	50	2.14	0.96	5-Methylcytidine	DNA methylation
72	50	1.93	0.88	3-Deazaneplanocin A (hydrochloride)	H3 K27 methyltransferase EZH2
73	50	1.26	0.58	WDR5-0103	Histone MTs
74	1.5	1.1	0.3	C646	p300 HAT
75	50	0.92	0.9	UNC1215	L3MBTL3 methyl lysine reader
76	50	0.86	0.55	GSK126	H3 K27 methyltransferase EZH2
77	50	0.82	0.71	BRD73954	HDAC6, 8

78	50	0.77	0.47	Nicotinamide	HDAC
79	1.5	0.61	0.64	Garcinol	p300 PCAF HATs
80	50	0.53	4.34	MI-2 (hydrochloride)	HMTs
81	4	0.53	0.64	Scriptaid	HDACs
82	50	0.45	0.62	Nullscript	Negative control for Scriptaid
83	1.5	0.43	0.34	GSK4112	HDAC3 activator
84	50	0.35	0.34	UNC0631	G9a and GLP HMTs
85	50	0.27	0.11	6-Thioguanine	DNA methylation inhibitor
86	50	0.24	0.09	CBHA	HDACs
87	1.5	0.15	0.81	CCG-100602	Rho/MKL1/SRF transcription
88	50	0.04	0.28	Gemcitabine	DNA methylation
89	50	-0.02	0.97	Piceatannol	Resveratrol analog, multiple actions
90	50	-0.2	0.11	S-Adenosylhomocysteine	DNA MTs
91	50	-0.26	0.21	ITF 2357	Class I and II HDACs
92	6	-0.32	0.46	Lomeguatrib	O ⁶ -Methylguanine-DNA methyltransferase (MGMT) inhibitor
93	50	-0.33	0.93	SGC0946	DOT1 H3K79 methylation
94	50	-0.39	0.3	Octyl- α -ketoglutarate	Promotes demethylase function
95	50	-0.52	0.6	GSK-J2 (sodium salt)	Negative control for GSK-J1
96	50	-0.61	0.31	coumarin-SAHA	Class I and II HDACs
97	50	-0.69	0.62	SB939	HDACs
98	50	-1.06	1.79	PFI-1	BRD2 and 4 bromodomains
99	5	-1.11	0.42	Salermide	SIRT1 and SIRT2 HDAC
100	25	-1.12	0.85	Sodium 4-Phenylbutyrate	HDACs
101	50	-1.13	1.16	CUDC-101	Class I and II HDACs, HER1 and 2
102	0.5	-1.22	0.54	2-hexyl-4-Pentynoic Acid	HDACs (derivative of VPA)
103	50	-1.23	0.41	Cl-Amidine (trifluoroacetate salt)	Protein arginine deaminases
104	50	-1.23	1.86	HPOB	HDAC6
105	50	-1.67	1.15	GSK-LSD1 (hydrochloride)	Lysine demethylase 1
106	50	-1.78	2.27	MS-436	BRD4 bromodomain 1
107	50	-1.79	1.82	EPZ005687	EZH2 blocks trimethylation H3K27
108	50	-2.16	1.78	CI-994	Class I HDAC
109	50	-2.26	1.59	AZ 505	SMYD2 lysine N-methyltransferase
110	50	-2.4	1.85	α -Hydroxyglutaric Acid (sodium salt)	HDMs and DNA hydroxylases
111	50	-2.72	1.76	AGK7	Negative control for AGK2
112	50	-2.79	0.84	5-Azacytidine	DNA MTs
113	10	-2.84	2.3	UNC0638	G9a and GLP HMTs
114	50	-3.14	5.05	CAY10683	HDAC2 and 6
115	50	-3.62	1.92	UNC1999	EZH2 blocks trimethylation H3K27
116	3	-3.64	1.95	HNHA	HDACs
117	50	-3.65	1.9	3-Deazanepanocin A	EZH2 blocks trimethylation H3K27
118	50	-4	3.07	CAY10603	HDAC6
119	50	-4.15	2.24	F-Amidine (trifluoroacetate salt)	Protein arginine deaminases PAD1 and 4
120	0.5	-4.17	2.19	JIB-04	Jumonji HDMs

121	50	-4.73	2.8	Tubastatin A (trifluoroacetate salt)	HDAC6
122	50	-4.97	1.88	GSK343	EZH2 blocks trimethylation H3K27
123	3	-5.46	2.03	Phthalazinone pyrazole	Aurora kinases
124	50	-6.74	3.09	Suberohydroxamic Acid	HDAC1 and 3
125	50	-6.82	1.89	Mirin	Mre11-Rad50-Nbs1 phosphorylation of H2AX
126	50	-7.7	3.92	Delphinidin (chloride)	p300/CBP HATs
127	25	-7.79	2.82	Panobinostat	class I, II, and IV histone deacetylases (HDACs)
128	50	-7.96	2.84	Sinefungin	methyltransferases
129	50	-8.24	3.95	(-)-Neplanocin A	methyltransferases
130	12.5	-8.44	2.77	GSK-J4 (hydrochloride)	H3K27 histone demethylase JMJD3
131	50	-8.85	2.45	Pimelic Diphenylamide 106	Class I HDACs
132	50	-9.42	5.18	RGFP966	HDAC3
133	50	-9.82	2.25	M 344	HDAC1, 6
134	5	-10.12	3.75	Sirtinol	SIRT1, 2
135	50	-10.19	4.06	UNC0321 (trifluoroacetate salt)	G9a HMT
136	50	-10.63	4.03	JGB1741	SIRT1
137	20	-11.38	4.51	DMOG	HIF- α prolyl hydroxylase
138	50	-11.51	4.35	MS-275	HDAC1
139	50	-12.81	2.67	Pyroxamide	HDAC1
140	3	-13.41	2.9	GSK-J5 (hydrochloride)	Negative control for GSK-J4
141	50	-14.16	4.38	4-iodo-SAHA	Class I and II HDACs
142	40	-14.98	5.08	2-PCPA (hydrochloride)	Lysine-specific demethylase 1 (LSD1)
143	3	-15.56	2.69	Tenovin-1	SIRT1 and 2
144	40	-17.76	4.4	SAHA	Class I, II and IV HDACs
145	3	-20.87	4.95	SGC-CBP30	CBP EP300
146	50	-22.51	5.09	3-amino Benzamide	PARPs
147	12.5	-35.23	7.43	EX-527	SIRT1

Supplementary Figure S21 – Hits recovered from epigenetic library screen

a		Hit #1	Hit #2	Hit #3	
					
		(+)-JQ1	Trichostatin-A	2,4-Diethylpyridine dicarboxylate	
Concentration:	2 μ M	Concentration:	0.3 μ M	Concentration:	6 μ M
VMR light rescue (QC 1.0):	75 \pm 7.9 %	VMR light rescue (QC 1.0):	67 \pm 5.1 %	VMR light rescue (QC 1.0):	55 \pm 4.0 %
VMR dark rescue (QC 0.96):	14 \pm 2.5 %	VMR dark rescue (QC 0.95):	-6.2 \pm 6.2 %	VMR dark rescue (QC 0.95):	9.3 \pm 4.4 %
Spontaneous activity in light rescue (QC 0.28):	91 \pm 15.7 %	Spontaneous activity in light rescue (QC 0.48):	61 \pm 13.2 %	Spontaneous activity in light rescue (QC 0.81):	18 \pm 8.1 %
Target:	BET bromodomain inhibitor	Target:	Reversible HDAC I, II, IV inhibitor	Target:	Reversible HIF-PH inhibitor
b		c			
Negative control		Other compound of potential interest #1		Other compound of potential interest #2	
					
(-)-JQ1		Valproic acid		HC Toxin	
Concentration:	5 μ M	Concentration:	5 μ M	Concentration:	20 μ M
VMR light rescue (QC 1.0):	6.3 \pm 5.4 %	VMR light rescue (QC 1.0):	46 \pm 6.5 %	VMR light rescue (QC 1.0):	41 \pm 3.6 %
VMR dark rescue (QC 0.96):	-8.1 \pm 4.4 %	VMR dark rescue (QC 1.0):	-0.6 \pm 0.5 %	VMR dark rescue (QC 0.96):	-7.8 \pm 7.6 %
Spontaneous activity in light rescue (QC 0.28):	-3.7 \pm 2.5 %	Spontaneous activity in light rescue (QC 0.24):	68 \pm 19.1 %	Spontaneous activity in light rescue (QC 0.99):	88 \pm 5.9 %
Target:	Inactive stereoisomer of (+)-JQ1	Target:	Reversible multi-HDAC inhibitor	Target:	Reversible multi-HDAC inhibitor

The chemical structures, maximum tolerated concentrations, phenotypic rescue, and molecular targets are summarized for compounds identified as active in this screen.

a: The three compounds that satisfied *a priori* criteria for a 'hit'

b: (-)JQ1 is a negative control stereoisomer of (+)JQ1; its lack of activity in this assay is strongly suggestive that (+)JQ1 exerts its effect through a specific receptor-ligand interaction

c: Other compounds that did not satisfy *a priori* criteria as 'hits', but appeared to show some activity in this assay and may therefore be of interest.

Supplementary Table 16 – Data summary by target

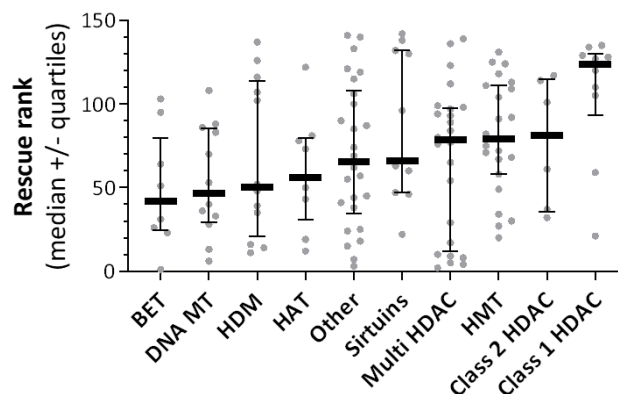
	BET BDs	Multi HDAC	DNA MT	HAT	Other	HMT	Class 2 HDAC	HDM	Class 1 HDAC	Sirtuins
Number of values	10	24	12	9	25	23	6	12	10	11
Minimum	-1.778	-17.76	-2.792	-7.701	-22.51	-10.19	-4.726	-14.98	-12.81	-35.23
25% Percentile	1.873	-1.127	0.0989	0.518	-3.208	-3.618	-4.181	-3.73	-10.24	-10.63
Median	10.95	0.6497	6.683	3.893	2.566	0.5313	0.9371	5.814	-7.798	2.755
75% Percentile	22	24.96	15.59	14.14	9.195	3.339	11.17	19.6	-0.7922	7.506
Maximum	74.89	66.92	30.75	25.03	55.17	19.96	12.58	25.92	19.78	19.11
Mean	16.98	9.796	8.997	6.417	4.295	1.699	2.739	6.052	-4.137	-2.695
Std. Deviation	22.68	20.45	10.56	10.26	15.38	7.789	7.448	13.16	9.726	14.58
Std. Error of Mean	7.174	4.175	3.048	3.422	3.077	1.624	3.041	3.798	3.076	4.395
Lower 95% CI of mean	0.7528	1.16	2.289	-1.473	-2.056	-1.669	-5.077	-2.307	-11.09	-12.49
Upper 95% CI of mean	33.21	18.43	15.71	14.31	10.65	5.067	10.56	14.41	2.821	7.099
<i>One sample t test</i>										
Theoretical mean	0	0	0	0	0	0	0	0	0	0
Actual mean	16.98	9.796	8.997	6.417	4.295	1.699	2.739	6.052	-4.137	-2.695
Discrepancy	16.98	9.796	8.997	6.417	4.295	1.699	2.739	6.052	-4.137	-2.695
95% CI of discrepancy	0.7528 to 33.21	1.160 to 18.43	2.289 to 15.71	-1.473 to 14.31	-2.056 to 10.65	-1.669 to 5.067	-5.077 to 10.56	-2.307 to 14.41	-11.09 to 2.821	-12.49 to 7.099
t, df	t=2.367, df=9	t=2.346, df=23	t=2.952, df=11	t=1.875, df=8	t=1.396, df=24	t=1.046, df=22	t=0.9008, df=5	t=1.593, df=11	t=1.345, df=9	t=0.6131, df=10
P value (two tailed)	0.0421	0.0279	0.0132	0.0976	0.1755	0.3069	0.409	0.1394	0.2115	0.5535
Significant?	Yes	Yes	Yes	No	No	No	No	No	No	No

Supplementary Figure S22 – Ranked phenotypic rescue activity by target

a

Target class	Number of compounds	Mean % rescue	Median rank
BET	10	16.98	42
Multi HDAC	24	9.796	78.5
DNA MT	12	8.997	46.5
HAT	9	6.417	56
HDM	12	6.052	50
Other	25	4.295	65.5
Class 2 HDAC	6	2.739	81
HMT	23	1.699	79
Sirtuins	11	-2.695	66
Class 1 HDAC	10	-4.137	123.5

b



Rescue data grouped by pharmacological target, similar to Figure 7e and Supplementary Table 16, but analyzed by rank rather than % rescue.

a: Table showing mean % rescue and median rank by pharmacological target

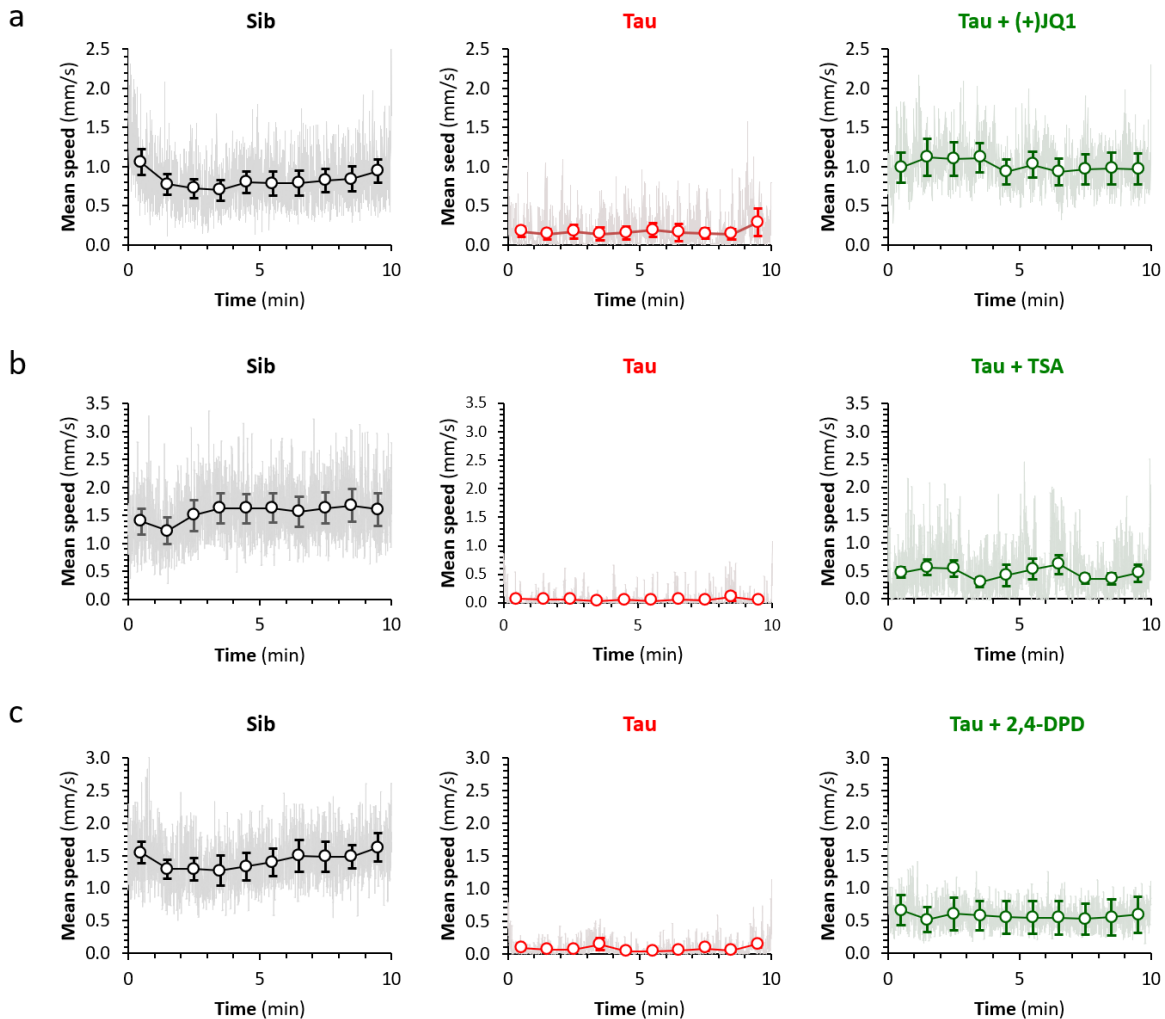
b: Graph showing rescue rank by target. Data points show individual chemicals, bars show median and quartiles.

The data show similar trends to Figure 7e, with BET bromodomain inhibitors showing the lowest median rescue rank.

Supplementary Table 17 – Properties of compounds categorized as ‘other’ in Figure 7e

Rank	Mean % rescue	Compound	Target
3	55.16842	2,4-DPD	HIF- α prolyl hydroxylase
15	23.59271	Lestaurtinib	JAK2, FLT3, TrkA
18	20.29308	Tenovin-6	p53 activator
24	17.80692	Isoliquiritigenin	Guanyl cyclase activator
25	17.38939	Ellagic Acid	coactivator-associated arginine methyltransferase 1
38	9.604486	Suramin (sodium salt)	Topoisomerase II
41	8.784877	Etoposide	Topoisomerase II
44	8.049176	Rucaparib (phosphate)	PARP1
45	7.831244	(+)-Abscisic Acid	Chromatin structure gene expression
55	3.898963	AMI-1 (sodium salt)	Arginine methyltransferases
57	3.425327	I-CBP112 (hydrochloride)	CBP EP300
62	2.921351	BSI-201	PARP1
69	2.565975	B32B3	H2A T120 phosphorylation
74	0.915359	UNC1215	L3MBTL3 methyl lysine reader
85	0.148336	CCG-100602	Rho/MKL1/SRF transcription
87	-0.02275	Piceatannol	Resveratrol analog, multiple actions
90	-0.31731	Lomeguatrib	O ⁶ -Methylguanine-DNA methyltransferase (MGMT)
100	-1.22962	Cl-Amidine (trifluoroacetate salt)	Protein arginine deaminases
106	-2.26145	AZ 505	SMYD2 lysine N-methyltransferase
115	-4.15488	F-Amidine (trifluoroacetate salt)	Protein arginine deaminases PAD1 and 4
119	-5.46097	Phthalazinone pyrazole	Aurora kinases
121	-6.81759	Mirin	Mre11-Rad50-Nbs1 phosphorylation of H2AX
133	-11.3792	DMOG	HIF- α prolyl hydroxylase
140	-20.8708	SGC-CBP30	CBP EP300
141	-22.5056	3-amino Benzamide	PARPs

Supplementary Figure S23 – Verification of hits by analysis of repurchased compound



Library molecules that rescued motor phenotypes in the primary screen were repurchased and tested at the same purported concentrations in motor rescue assays to verify the molecular identities of the hits. Sibling controls (left column; black) and untreated Tau zebrafish (center column; red), were compared with Tau zebrafish exposed to compound following dechoriation at 2dpf until 5dpf (right column, green). 96-well plate motor assays were run at 5dpf as shown in Figures 5 and 8. The graphs show mean speed during the light phase of the VMR. The light traces show mean frame-to-frame displacement scaled to speed; colored markers and bars show 1-minute binned group mean \pm SE, similar to Figure 8a.

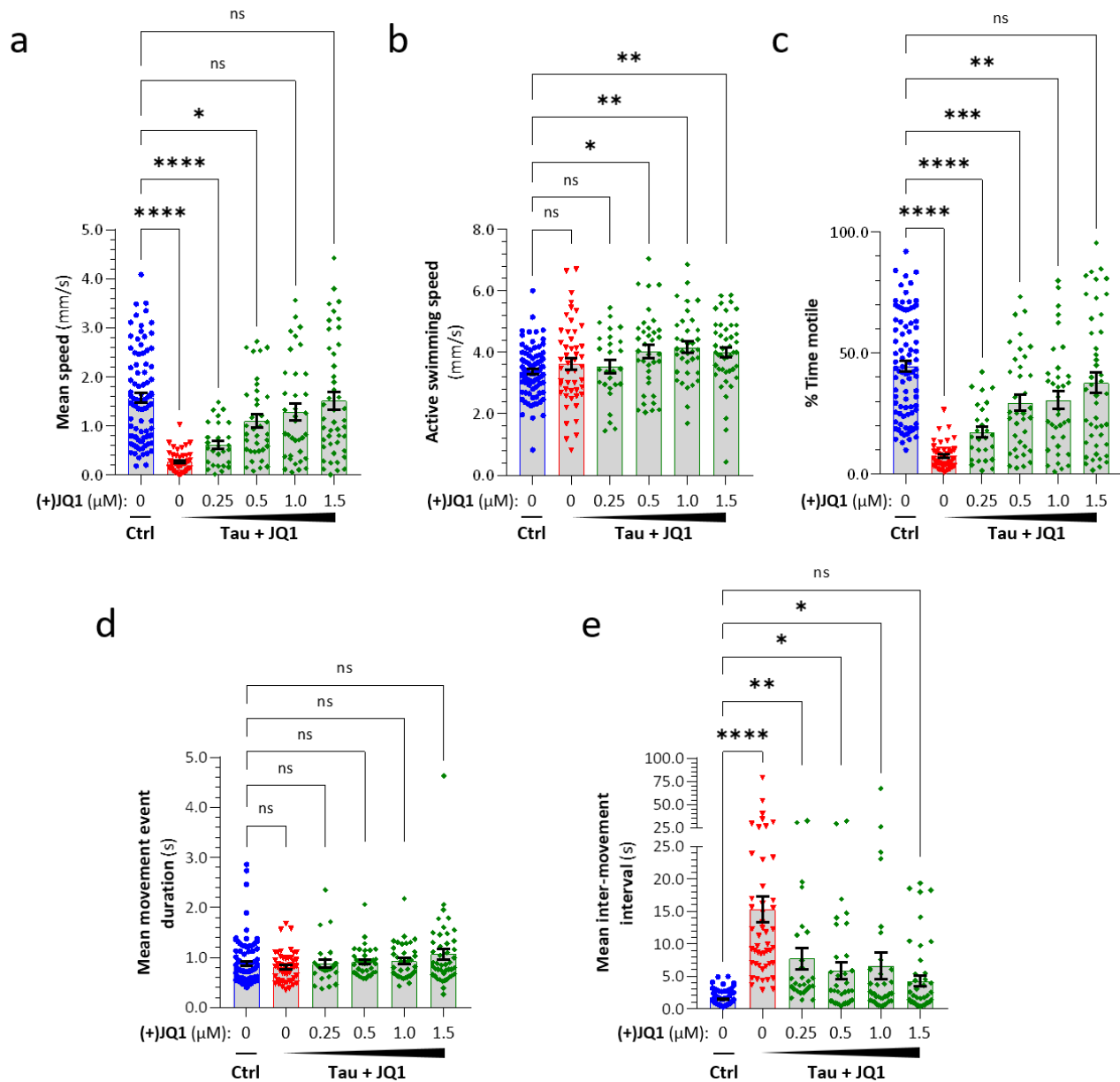
a: (+)JQ1 (1.5 μ M) repurchased from Sigma (batch # 0000083981; these are the same data as Figure 8a reproduced here for clarity)

b: Trichostatin-A (0.2 μ M) repurchased from Cayman Chemical (batch # 0437853431)

c: 2,4-Diethylpyridine dicarboxylate (6 μ M) repurchased from Cayman Chemical (batch # 181397-27)

All three compounds partially rescued VMR light phase hypokinesia in Tau zebrafish, verifying the identities of the hits found in the primary screen using the same assay.

Supplementary Figure S24 – Concentration-dependent rescue of motor function in Tau zebrafish by (+)JQ1



Similar analyses to Figure 5c – 5g, showing how abnormalities of motor activity in Tau zebrafish at 5dpf were altered by exposure to (+)JQ1 between 2 – 5 dpf, at incremental concentrations from 0.25 to 1.5 μM. In each graph, data points show individual zebrafish, bars show mean ± SE. **** $p < 0.0001$, *** $p < 0.001$, ** $p < 0.01$, * $p < 0.05$, Ctrl vs. experimental group, 1-way ANOVA with Dunnett’s multiple comparison test.

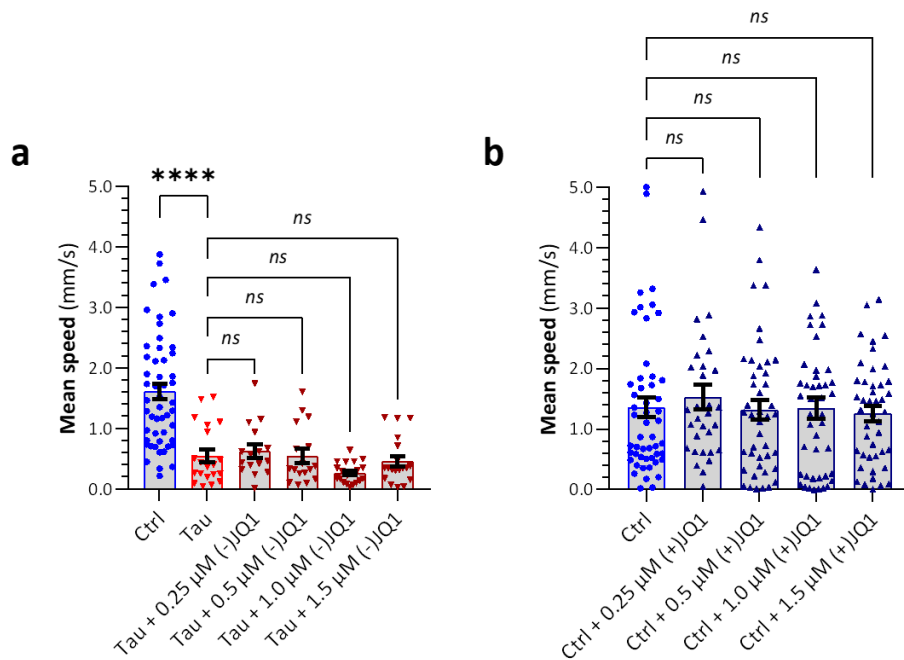
- a: Mean speed (scalar distance traveled by zebrafish centroid/time of assay)
- b: Active swimming speed (mean scalar speed of zebrafish centroid during movement events)
- c: Time active % (proportion of video frame transitions at which displacement occurred)
- d: Mean movement event duration (mean duration of movement episodes)
- e: Mean inter-movement interval (mean duration of stationary periods between movements)

Motor abnormalities in Tau zebrafish improved with increasing concentrations of (+)JQ1.

Supplementary Table 18 - Exact *p*-values for Figure 8b, 8d – 8i

Panel	Statistical test	Comparison group 1	Comparison group 2	Adjusted <i>p</i> value
8b	One-way ANOVA with Dunnett multiple comparisons test	Ctrl	Tau	0.000000000000083
			Tau + 0.25µM (+)JQ1	0.000003472349992
			Tau + 0.5µM (+)JQ1	0.029010139082927
			Tau + 1.0 µM (+)JQ1	0.359887638918267
			Tau + 1.5 µM (+)JQ1	0.997796583767877
8d	One-way ANOVA with Šidák multiple comparisons test	Ctrl	Ctrl + (+)JQ1	0.999942977282417
		Ctrl	Tau	0.000000006937303
		Tau	Tau + (+)JQ1	0.000489002947961
8e	2-tailed t-test with Welch correction	Tau	Tau + (+)JQ1	0.008717663859809
8f	One-way ANOVA with Dunnett multiple comparisons test	Ctrl	Tau	0.000000000005670
		Tau	Tau + (+)JQ1	0.992031122504968
8g	One-way ANOVA with Šidák multiple comparisons test	Ctrl	Ctrl + (+)JQ1	0.998757810893752
		Ctrl	Ctrl + (-)JQ1	0.999993794290067
		Ctrl	Tau	<0.000000000000001
		Tau	Tau + (+)JQ1	0.000000013851543
		Tau	Tau + (-)JQ1	0.483623885971886
8h	One-way ANOVA with Šidák multiple comparisons test	Ctrl	Ctrl + (+)JQ1	0.010057465092475
		Ctrl	Ctrl + (-)JQ1	0.987460255302511
		Ctrl	Tau	0.000000000000095
		Tau	Tau + (+)JQ1	<0.000000000000001
		Tau	Tau + (-)JQ1	0.999907116208083
8i	One-way ANOVA with Tukey multiple comparisons test	Ctrl	Tau	0.000018040608642
		Tau	Tau + (+)JQ1	0.419406610554096
		Ctrl	Tau + (+)JQ1	0.000352844802280

Supplementary Figure S25 – Specificity controls for (+)JQ1 rescue of motor function in Tau zebrafish



Mean swimming speed of Ctrl and Tau zebrafish during the light phase of the VMR is shown at 5 dpf following exposure to small molecules as indicated from 2 – 5 dpf.

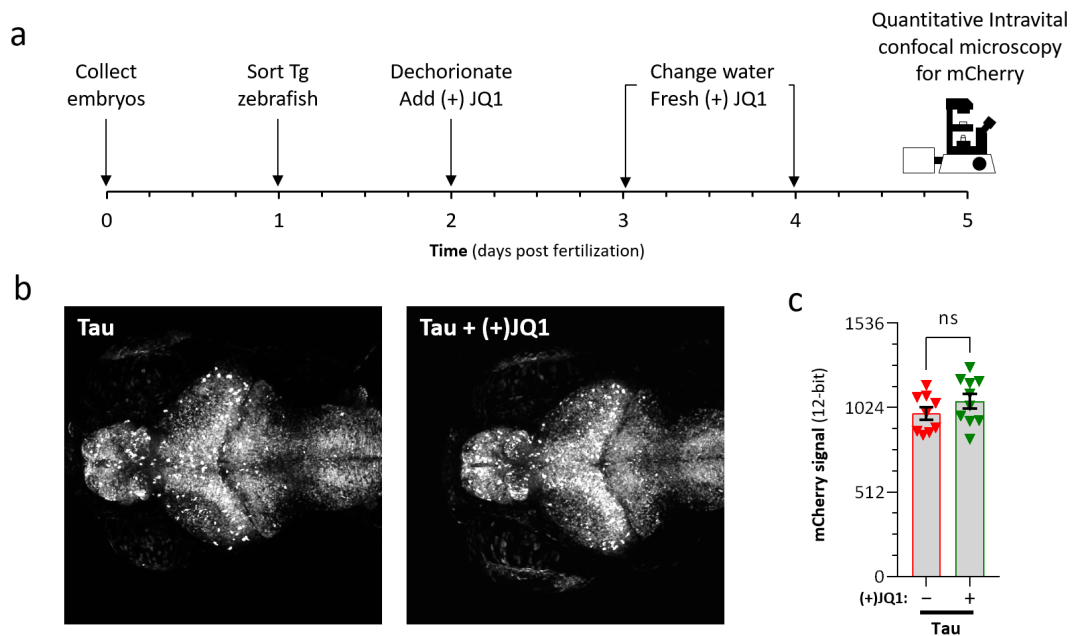
a: Tau zebrafish exposed to incremental concentrations of the negative control stereoisomer (-)JQ1 that does not bind to protein bromodomains. Untreated Tau and Ctrl zebrafish are shown for comparison.

b: Ctrl zebrafish exposed to incremental concentrations of (+)JQ1. Untreated Ctrl zebrafish are shown for comparison.

In each graph, data points show individual zebrafish, bars show mean \pm SE. **** $p < 0.0001$, 1-way ANOVA with Dunnett's multiple comparisons test to compare each group to untreated (a) Tau or (b) Ctrl zebrafish.

In contrast to the robust (+)JQ1 dose-dependent rescue of VMR light phase hypokinesia in Tau zebrafish (Figures 8a – 8b, Supplementary Figure S24), the stereoisomer (-)JQ1 is inactive in this assay, strongly suggesting that the activity of (+)JQ1 is dependent on a specific interaction with a protein bromodomain. The lack of increased motor activity in Ctrl zebrafish exposed to (+)JQ1 further indicates that this compound does not influence zebrafish motility non-specifically, but instead acts by rescuing the phenotype caused by ON/4R-Tau over-expression.

Supplementary Figure S26 – (+)JQ1 does not silence transgene expression in Tau zebrafish



A critical validation for the screen shown in Figure 7 is to ensure that small molecules identified as rescuing phenotypes did not do so by silencing transgene expression, as compounds with this activity would likely be uninformative about the biology of tauopathy, instead reflecting properties of the transgene expression system. Co-expression of nls-mCherry with Tau in the model provides a marker of transgene expression and a rapid way to evaluate screen ‘hits’ for activity in interfering with transgene expression.

a: Schematic showing the design of the validation assay. Zebrafish were exposed to (+)JQ1 in an identical way to the screen, but instead of a movement assay, the endpoint was intravital confocal imaging.

b: Representative confocal Z-plane maximum intensity projections showing dorsal views of mCherry expression in live Tau zebrafish exposed to (+)JQ1 or no inhibitor as indicated.

c: Quantification of fluorescence signal in 9 zebrafish per group using NIS-Elements. Data points show individual zebrafish, bars show mean \pm SE. Data analyzed by 2-way unpaired *t*-test.

There was no evidence of transgene expression being lost after exposure to (+)JQ1. Note that the steady-state level of 0N/4R-Tau could be influenced by other factors separate from transgene expression (such as Tau degradation, clearance, etc.). This is dealt with in Figure 8f.

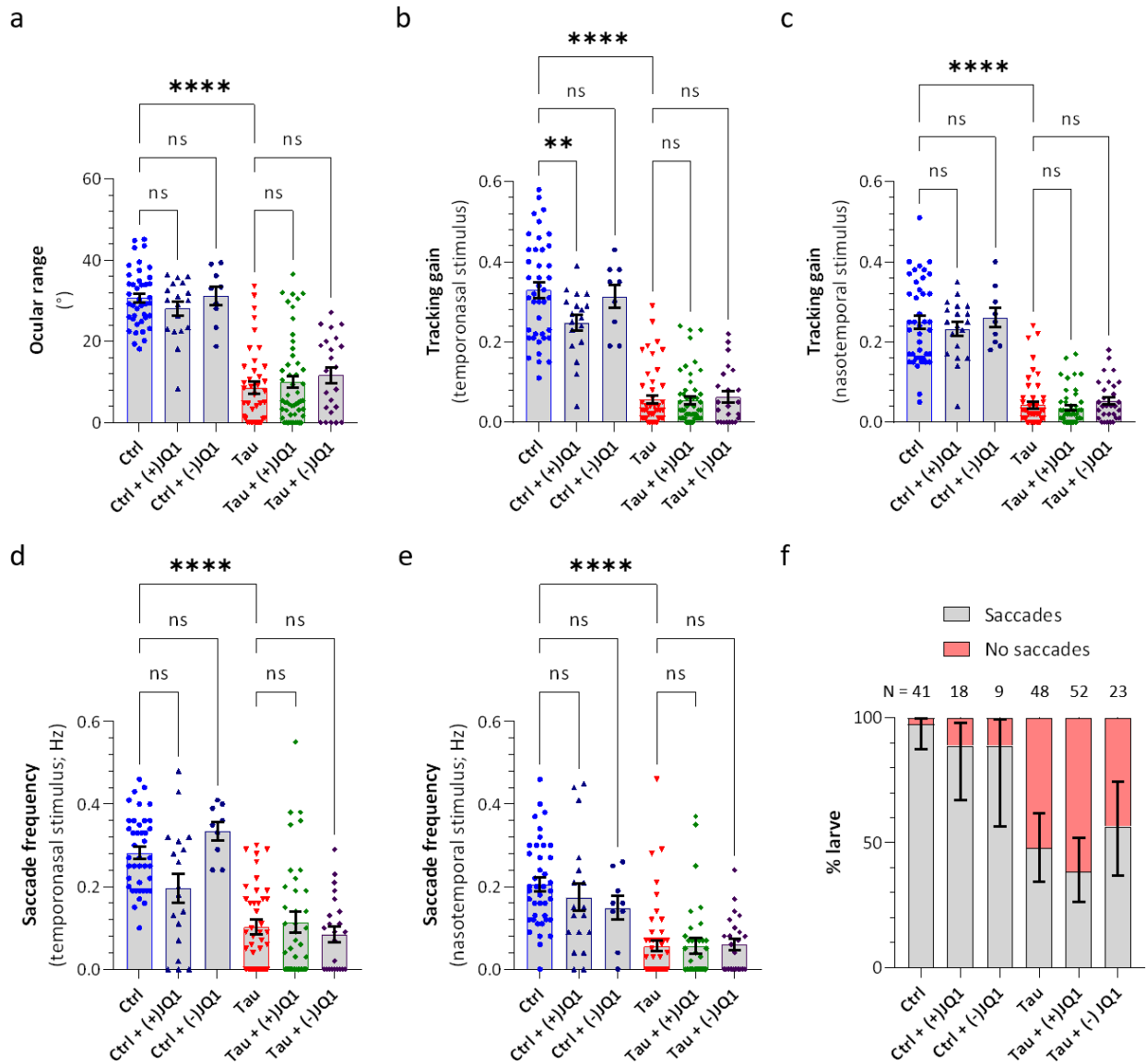
Supplementary Table 19 – Statistical analysis of Tau zebrafish survival in presence or absence of (+)JQ1

Group	Parameter	Replicate #1	Replicate #2	Replicate #3
Tau vs. Tau + JQ1	Mantel-Cox χ^2 (df)	16.4063968503581 (1)	19.2694441904945 (1)	20.1818785115746 (1)
	Mantel-Cox p	0.000051112445882	0.000011350844466	0.000034474380916
	Mantel-Haenszel hazard ratio (95% CI)	6.44997684996026 (3.85 – 28.37)	9.53997776573499 (3.60 – 27.00)	3.82608678934647 (2.13 – 6.87)
Tau	Median survival	11	11.5	11.5
Tau + JQ1		14	14	13

Supplementary Table 20 – Statistical analysis of Ctrl zebrafish survival in presence or absence of (+)JQ1

Group	Parameter	Replicate #1	Replicate #2	Replicate #3
Ctrl vs. Ctrl + JQ1	Mantel-Cox χ^2 (df)	0.226102965462962 (1)	0.0362666071172773 (1)	0.0882470940061729 (1)
	Mantel-Cox p	0.634428598517294	0.848965973660078	0.766417553251096
	Mantel-Haenszel hazard ratio (95% CI)	1.41471464022798 (0.34 – 6.0)	0.883623837091171 (0.26 – 3.08)	0.869975645802120 (0.35 – 2.18)

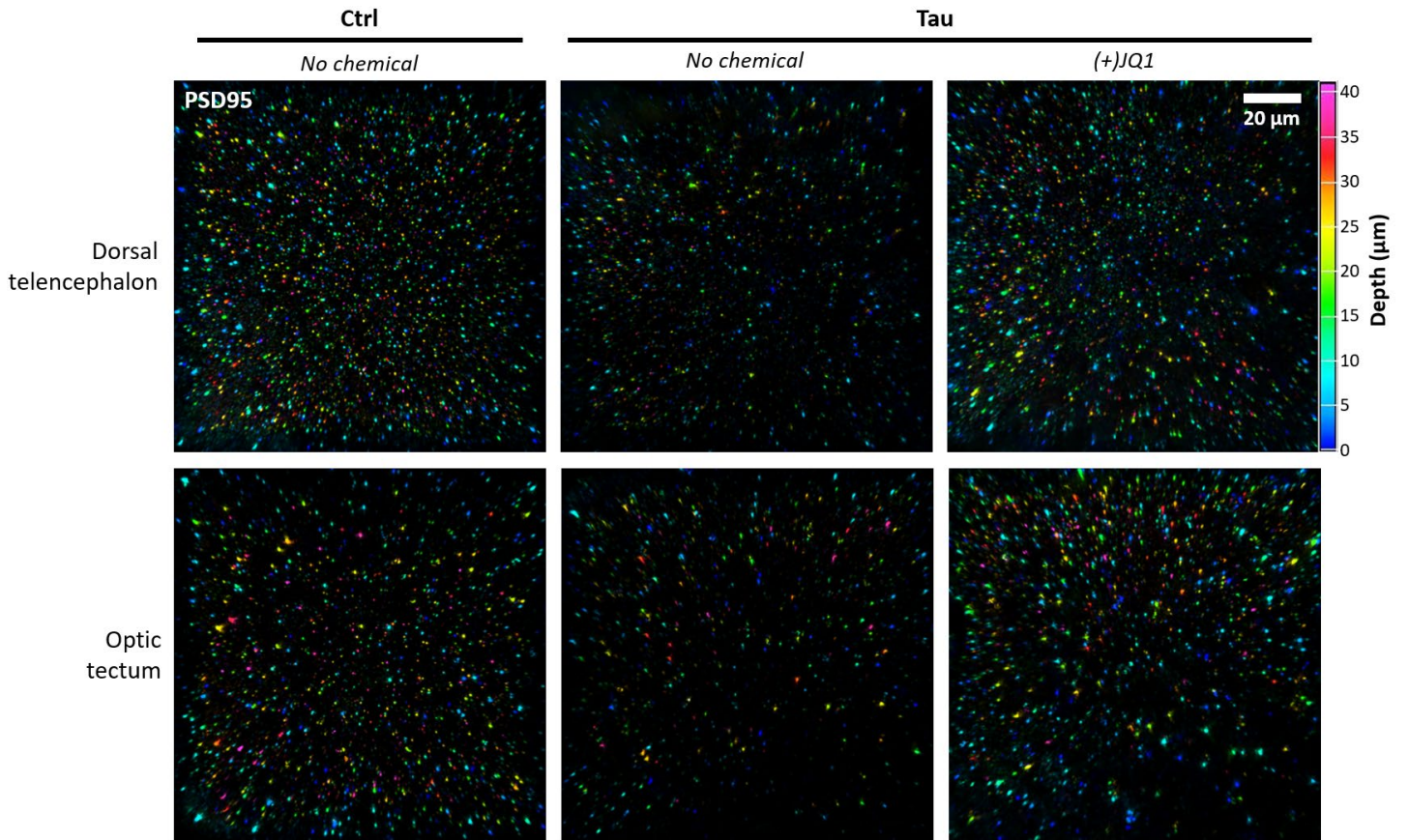
Supplementary Figure S27 – (+)JQ1 does not rescue OKR deficits in Tau zebrafish



Similar analyses to Figure 6 and Supplementary Figure S15, showing quantification of optokinetic reflexes in Ctrl and Tau zebrafish at 5dpf after no treatment, exposure to (+)JQ1, or exposure to (-)JQ1 from 2 – 5 dpf. In graphs a – e, data points show individual zebrafish, bars show mean \pm SE. **** p <0.0001, ** p <0.01, 1-way ANOVA with Šidák multiple comparison test. In panel (f), bars show proportion \pm 95% CI of zebrafish with and without saccadic movements during exposure to OKR stimuli.

In contrast to motor function and survival, there was no evidence that (+)JQ1 rescued OKR deficits in the Tau model after treatment at these time points.

Supplementary Figure S28 – Volumetric imaging of synapse abundance in zebrafish larval brain

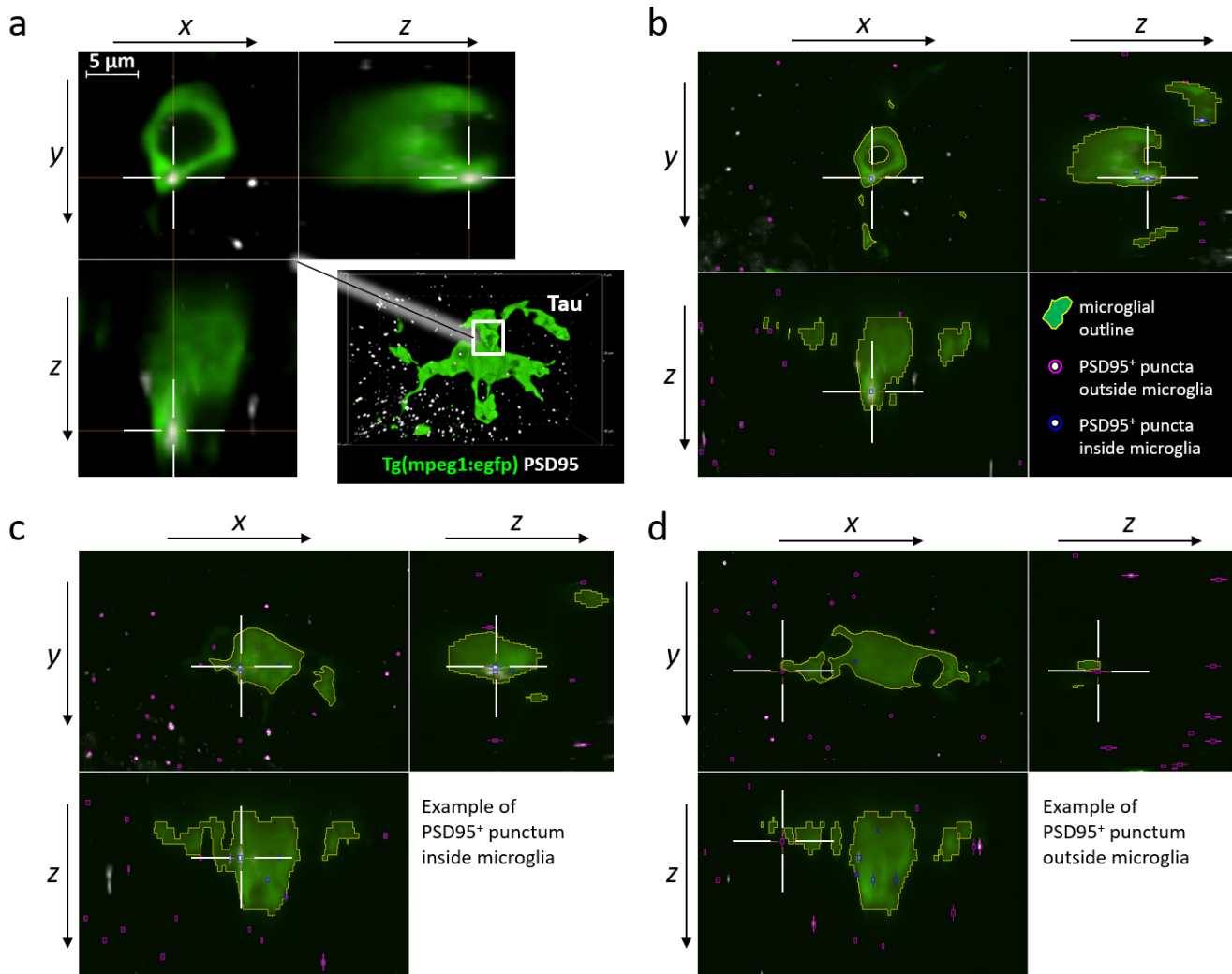


PSD95 whole mount immunolabeling and volumetric image acquisition in the telencephalon (upper row) and optic tectum (lower row) were carried out in Ctrl (left), Tau (center) and [Tau + (+)JQ1] (right) zebrafish. The figure shows the same samples as Figure 9a, but the images here are alpha-blended and pseudocolored to show depth within the image stack, illustrating the large volume of PSD95 expression data that was captured by this method.

Supplementary Table 21 – Exact *p*-values for Figure 9b, 9c, 9e, 9g

Panel	Statistical test	Comparison group 1	Comparison group 2	Adjusted <i>p</i> value
9b	One-way ANOVA with Šidák multiple comparisons test	Ctrl	Ctrl + (+)JQ1	0.919409980094170
		Ctrl	Tau	0.000003356940192
		Tau	Tau + (+)JQ1	0.000993889661747
		Ctrl	Tau + (+)JQ1	0.166096447592438
9c	One-way ANOVA with Šidák multiple comparisons test	Ctrl	Ctrl + (+)JQ1	0.893099808802923
		Ctrl	Tau	0.000000000173235
		Tau	Tau + (+)JQ1	0.025239927938240
		Ctrl	Tau + (+)JQ1	0.000024080791842
9e	One-way ANOVA with Tukey multiple comparisons test	Ctrl	Tau	0.000000000007919
		Tau	Tau + (+)JQ1	0.000000002081638
		Ctrl	Tau + (+)JQ1	0.966489749127617
9g	One-way ANOVA with Šidák multiple comparisons test	GFP	GFP + (+)JQ1	0.998900495477148
		GFP	Tau	0.000000022461457
		Tau	Tau + (+)JQ1	0.000000161286393
		GFP	Tau + (+)JQ1	0.974162547746396

Supplementary Figure S29 – Quantification of PSD95-immunoreactive synaptic material inside zebrafish microglia



Confocal image stacks were acquired through whole mount zebrafish brains after immunolabeling for GFP, expressed from the *Tg(mpeg1:egfp)* transgene (labels the cytoplasm of microglia; green), and PSD95 (localized to post-synaptic densities; white).

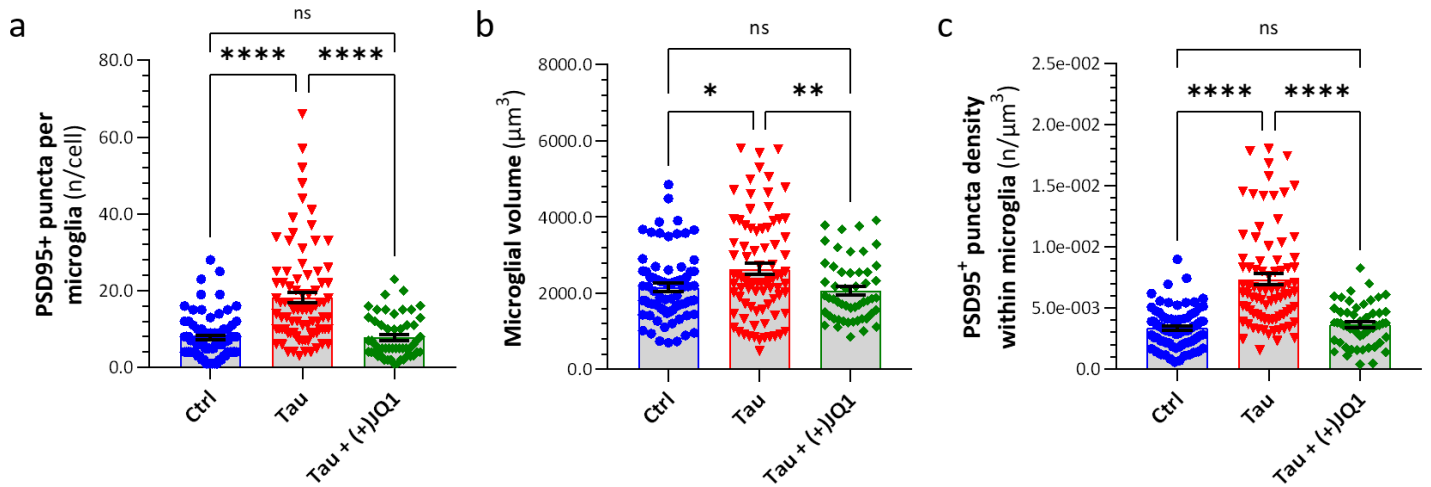
a: The inset shows an alpha-blended 3D representation of a microglia from a Tau zebrafish brain. The three images show a single confocal plane through part of the microglial cell (x-y, top left). A PSD95 punctum that appears to be inside the microglial cytoplasm is indicated by cross hairs. The other two images show x-z and y-z reconstructions through the planes of the cross hairs, indicating that the punctum is unequivocally localized within the microglial cytoplasm in all three views.

b: A custom algorithm (written using NIS-Elements GA3) was used to identify, in 3 dimensions, the boundaries of each microglia (yellow) and the locations of all PSD95⁺ puncta, then to assign each punctum to a position within (blue) or outside (magenta) microglia. The image shows the same confocal plane from panel (a), with multiple PSD95⁺ puncta correctly assigned to locations within or outside microglia.

c, d: Further examples are shown of different confocal planes, in which PSD95⁺ puncta are correctly assigned to positions (c) within the microglia, or (d) adjacent to but outside the microglia.

Using this algorithm, we were able to analyze the locations of a large number of PSD95 puncta with respect to a statistically robust sample of microglia (Figure 9d – 9e; Supplementary Figure S30).

Supplementary Figure S30 – (+)JQ1 mitigates microglial accumulation of PSD95-immunoreactive synaptic material in Tau zebrafish



The method shown in Supplementary Figure S29 was used to quantify PSD95-immunoreactive puncta inside microglia of whole mount brain samples from 4dpf Ctrl (blue), Tau (red) or JQ1-treated Tau (green) zebrafish. Each line was first crossed with *Tg(mpeg1:egfp)* zebrafish to label microglial cytoplasm, and then fixed brains were immunolabeled for GFP and PSD95. In all three graphs, data points show individual microglia, bars show mean \pm SE for the group. Multiple images were analyzed from 6 – 10 brains per group.

a: Number of PSD95⁺ puncta per microglial cell

b: Volume of each microglial cell

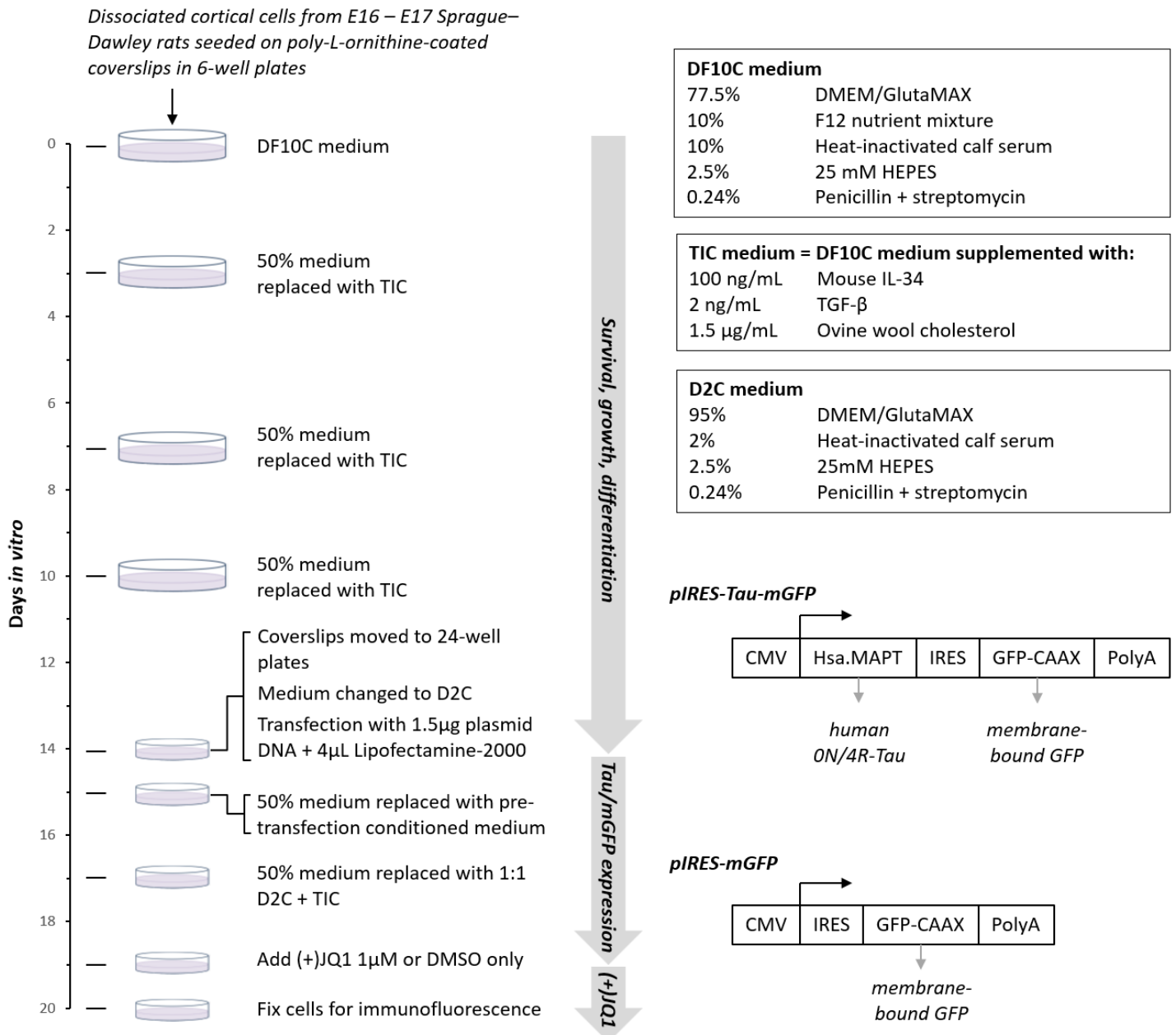
c: Number of PSD95⁺ puncta per cell normalized to the volume of the same cell to show density rather than abundance

In each graph **** $p < 0.0001$, ** $p < 0.01$, * $p < 0.05$, 1-way ANOVA with Tukey's multiple comparisons test.

Individual microglia in Tau zebrafish contained > 2-fold more PSD95-immunoreactive puncta than microglia from Ctrl zebrafish. Microglia from Tau zebrafish also showed slightly larger volume than Ctrl. The increase in microglial size in Tau zebrafish did not account for the increased abundance of PSD95⁺ puncta, as the density of PSD95⁺ puncta was also substantially increased in Tau zebrafish microglia compared with controls. These changes in PSD95⁺ puncta/microglia, PSD95⁺ puncta/volume, and microglial volume in Tau zebrafish were not seen after exposure to (+)JQ1.

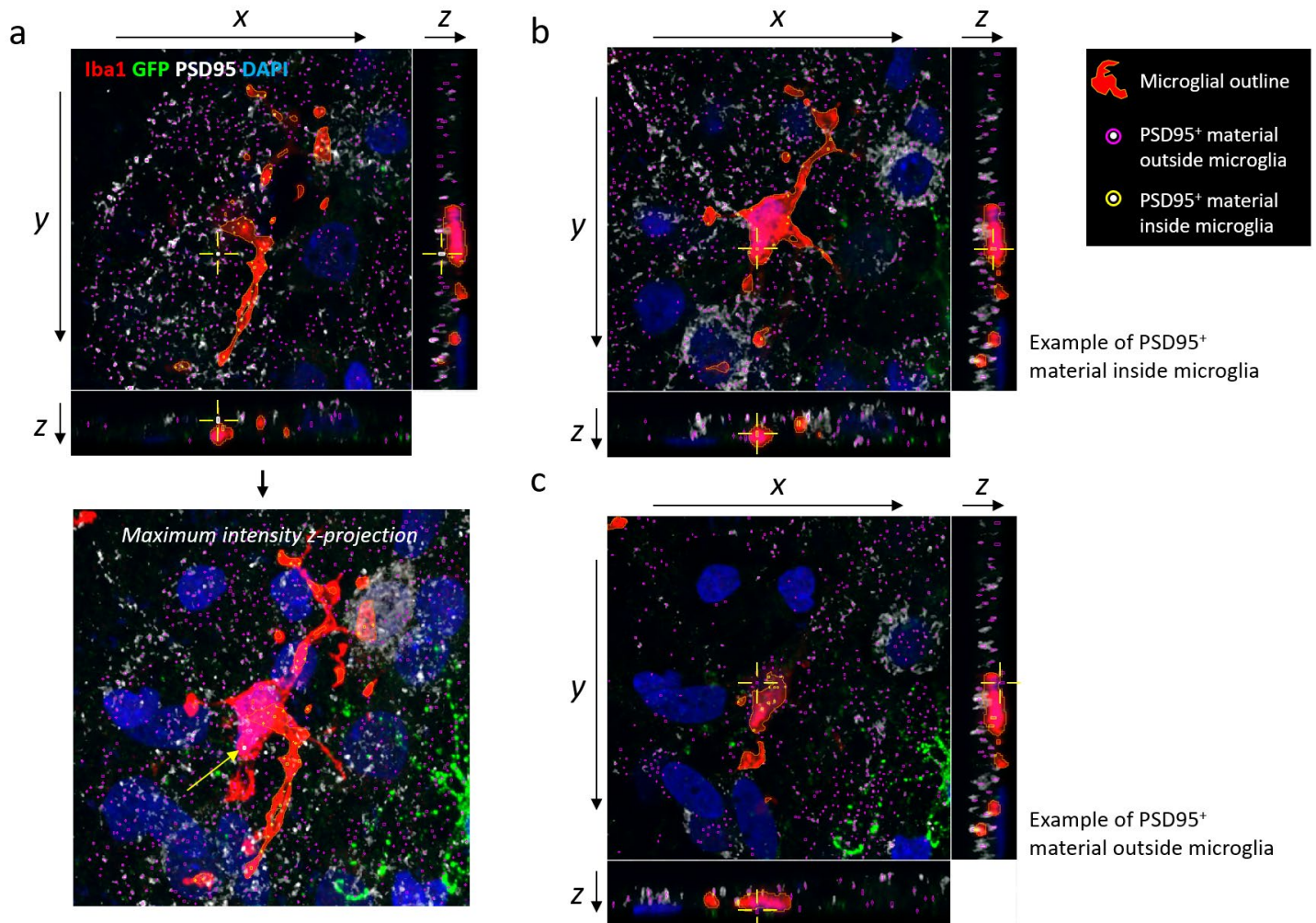
Together these data support a model in which: (i) microglial phagocytosis of synaptic material contributes to the reduced density of PSD95⁺ synaptic puncta seen in brains from Tau zebrafish; and (ii) (+)JQ1 decreases microglial phagocytosis of synaptic material.

Supplementary Figure S31 – Rat primary co-culture system to test the activity of (+)JQ1 in mammalian microglia



The left side of the schematic shows the procedure and time course for generating rat cortex primary cultures that contain neurons, astrocytes, and abundant microglia (this is modified from previous work⁵ to enhance the survival and proliferation of microglia⁶). The key reagents used in this experiment are shown on the right side of the schematic. At 14 DIV, the established co-cultures were transfected so that some neurons expressed either: (i) human 4R/ON-Tau and membrane bound GFP (mGFP) as separate proteins, or (ii) mGFP alone, using the plasmid constructs shown lower right. The neurons expressed the transgene for 5 days, and then (+)JQ1, or DMSO alone at the same final concentration, was added to the culture medium. 24 hours later, the cells were fixed for immunofluorescence and microscopic analysis of synaptic material within microglia.

Supplementary Figure S32 – Quantification of PSD95-immunoreactive puncta inside rat microglia



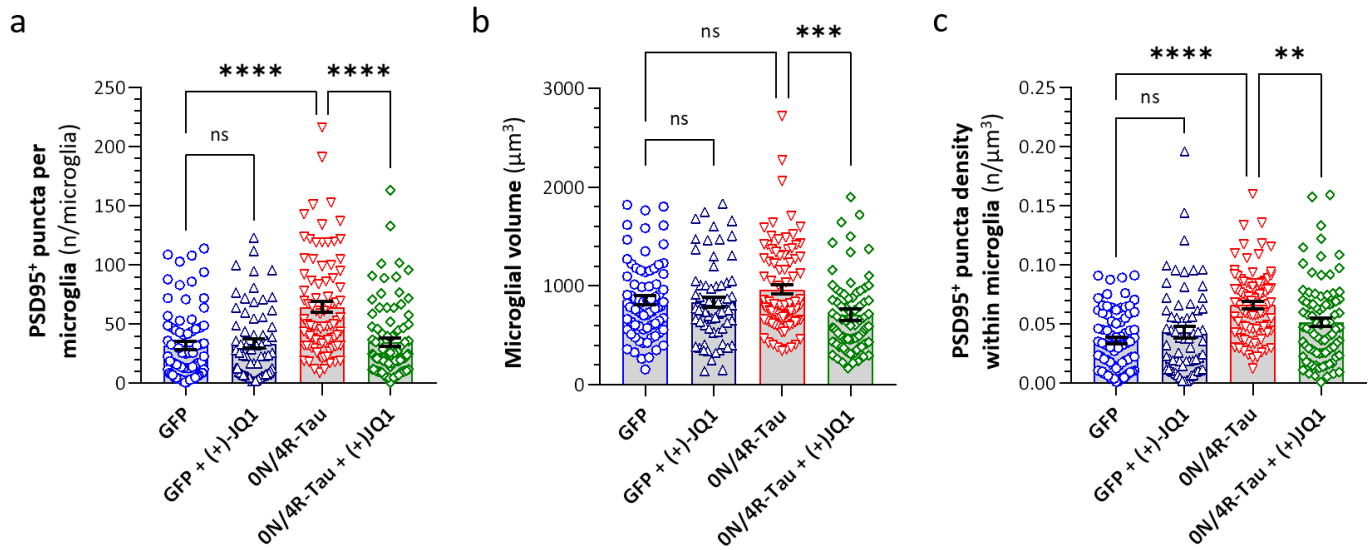
Confocal image stacks were acquired from rat primary cultures after immunolabeling for Iba1 (microglia; red), GFP (labels the plasma membrane of transfected neurons; green), PSD95 (post-synaptic densities; white) and DAPI (nuclei; blue). Similar to Supplementary Figure S29, a custom algorithm (written using NIS-Elements GA3) was used to identify, in 3 dimensions, the boundaries of each microglia (orange) and the locations of all PSD95⁺ puncta, then to assign each PSD95⁺ punctum to a position within (yellow) or outside (magenta) microglia.

a: Although contact cultures are flat compared with whole mount brain samples, the 3D analysis approach remains critical. The upper panel shows a single confocal plane through a microglial cell (x-y, top left), with x-z and y-z reconstructions through the planes of the cross hairs. A PSD95⁺ punctum is unequivocally localized outside the microglial cytoplasm in the x-y plane, and it is seen lying above the microglia in the z-reconstructions. As a result, analysis of a z-plane maximum intensity projection image (lower panel) would incorrectly assign the punctum as inside the microglia (yellow arrow). Using stringent analysis parameters to maximize specificity in all three image planes, the algorithm performed well in correctly identifying PSD95⁺ puncta inside microglia in this model.

b, c: Further examples are shown of different confocal planes, in which PSD95⁺ puncta are correctly assigned to positions (b) within the microglia, or (c) closely adjacent to, but outside, the microglia.

Using this algorithm, we were able to analyze the locations of a large number of PSD95 puncta with respect to a statistically robust sample of microglia (Figures 9f – 9g; Supplementary Figure S33).

Supplementary Figure S33 – (+)JQ1 mitigates accumulation of PSD95-immunoreactive puncta within rat microglia co-cultured with neurons transfected to express human ON/4R-Tau



The methods shown in Supplementary Figures S38 and S39 were employed to quantify PSD95-immunoreactive puncta within microglia of primary rat cortex cultures, in which neurons were transfected to express GFP and ON/4R-Tau, or GFP only, then exposed to D2C + TIC medium containing 1μM (+)JQ1, or medium containing the equivalent amount of DMSO only. Fixed cultures were immunolabeled for GFP (transfected neurons), Iba1 (microglia), and PSD95 (excitatory post-synaptic densities) and counter-labeled with DAPI (nuclei). In all three graphs, data points show individual microglia, bars show group mean ± SE.

a: Number of PSD95⁺ puncta per microglial cell

b: Volume of each microglial cell

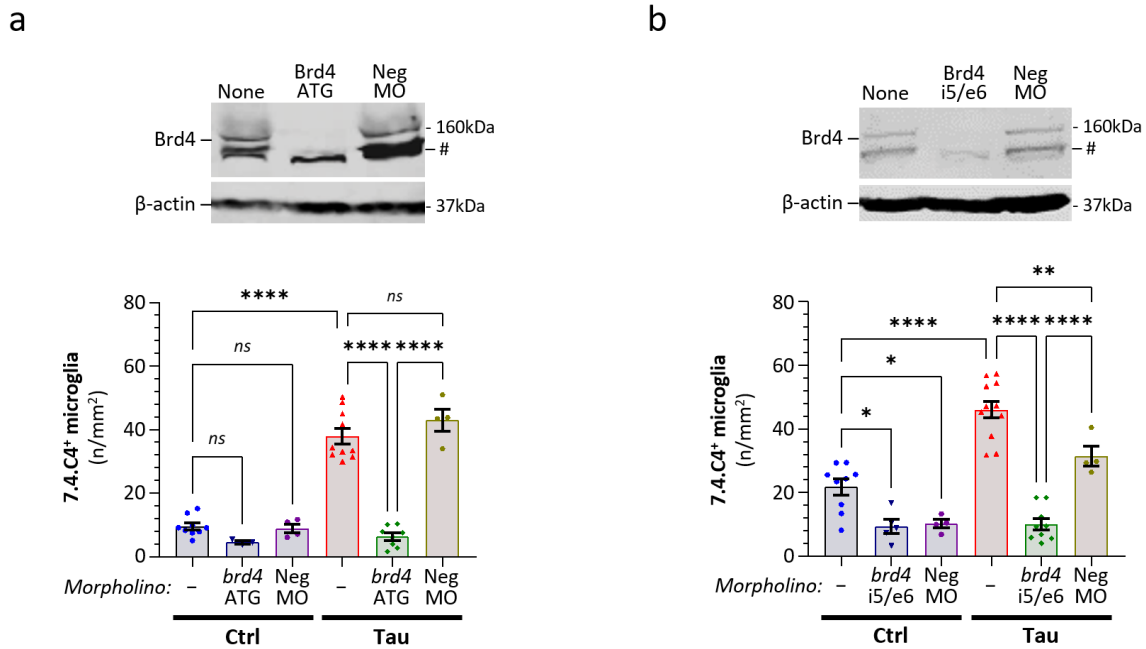
c: Number of PSD95⁺ puncta per cell divided by the volume of the same cell to show density rather than abundance

In each graph **** $p < 0.0001$, *** $p < 0.001$, ** $p < 0.01$, 1-way ANOVA with Šidák multiple comparisons test.

Individual microglia from cultures in which neurons expressed human ON/4R-Tau and GFP contained ≈ 2-fold more PSD95-immunoreactive puncta compared with microglia from control cultures, in which neurons were transfected to express GFP only. This increase was not present after treatment with (+)JQ1. Microglia from Tau-transfected cultures showed similar volumes to GFP-transfected cultures. A modest decrease in microglial volume in Tau-transfected cultures treated with (+)JQ1 did not account for the decreased abundance of microglial PSD95⁺ puncta, as the density of PSD95⁺ puncta was also substantially reduced after (+)JQ1 treatment.

Together these data provide an important validation that microglial phagocytosis of synaptic material in the presence of Tau over-expression, and its prevention by (+)JQ1, is phylogenetically conserved in a rat model. This suggests that the observations made in the zebrafish model may be translationally informative.

Supplementary Figure S34 – Transient knockdown of Brd4 in Tau zebrafish mitigates microgliosis at 4dpf



Morpholino oligonucleotides (MO) targeting *brd4* expression were used to evaluate the role of Brd4 in microgliosis in Tau zebrafish. Two different MO were used to increase confidence that any observed effects were attributable to loss of Brd4 expression:

a: MO targeting the translational start site and adjacent 5'UTR of the zebrafish *brd4* mRNA. This is predicted to decrease translation of Brd4.

b: MO targeting the splice acceptor sequence at the boundary between intron 5 and exon 6 of the primary *brd4* transcript. This is predicted to skip exon 6 during splicing and introduce a frame shift mutation and premature stop codon into the mRNA, as the splice boundary phases of i5/e6 and i6/e7 differ with respect to the ORF.

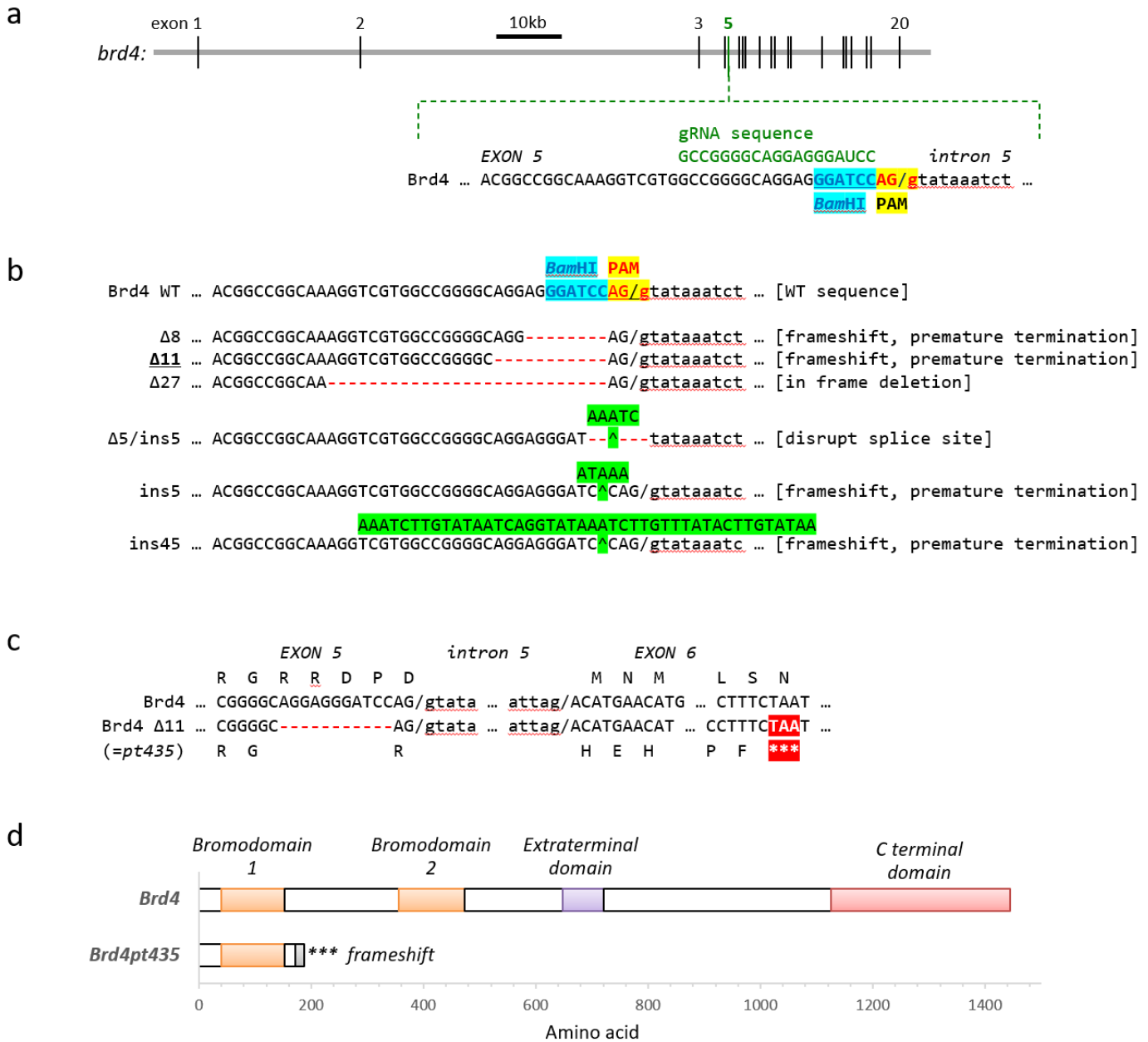
MO were microinjected at the single-cell stage and both MO were compared with a non-targeting negative control MO (neg MO) to exclude effects caused by microinjection, injection buffer, or nonspecific effects attributable to MO exposure.

In the upper panels, western blots were made from lysates of 2 dpf control, *brd4* MO-microinjected and neg MO-microinjected zebrafish, and then probed with an antibody to zebrafish Brd4 (a generous gift from Dr. Igor Dawid, NIH). At this early developmental point, the antibody recognizes a protein of 160kDa corresponding to the expected size of Brd4, in addition to other smaller proteins whose identity is unclear (#). In each case, the 160kDa band disappeared after *brd4* MO microinjection but not neg MO injection, confirming that Brd4 was targeted by both MO.

In the lower panels, 7.4.C4-immunoreactive microglia were quantified in sections by immunohistochemistry at 4dpf, identically to Figure 2H – J, in Ctrl or Tau zebrafish that were untreated, or microinjected with either Brd4 or non-targeting MO. In each graph, data points show individual zebrafish, bars show mean \pm SE. **** p <0.0001, ** p <0.01, * p <0.05, 1-way ANOVA with Šidák multiple comparison test.

The large increase in microglial abundance in Tau zebrafish was prevented by Brd4 knockdown, suggesting Brd4 is the target through which (+)JQ1 prevents microgliosis in this model.

Supplementary Figure S35 – Generation of a stable *brd4* null allele using Cas9/CRISPR



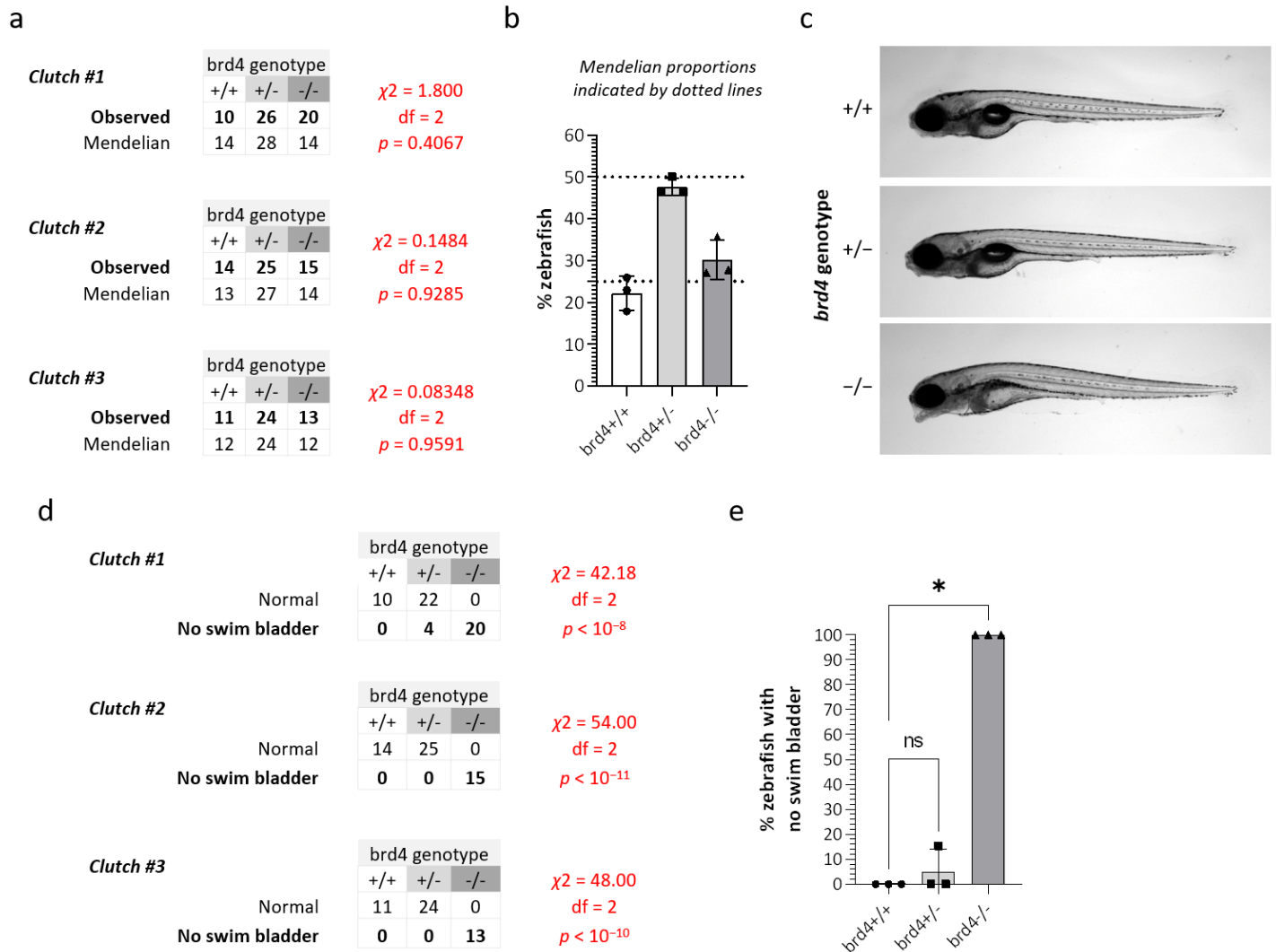
a: The *brd4*^{Pt435} allele described in the paper was made using CRISPR/Cas9 genome editing. A gRNA sequence was identified to target a PAM site overlapping a *Bam*HI restriction enzyme site in exon 6 of the *brd4* gene. This was chosen to allow easy genotyping by showing loss of the *Bam*HI site in a PCR amplicon spanning the mutation, without necessitating DNA sequencing.

b: Multiple mutant alleles were recovered at the F1 stage, including small deletions and insertions as shown. The 11bp deletion was chosen for further studies, as it abolished Brd4 expression (Figure 10b).

c: The Pt435 11bp deletion allele causes a frameshift mutation leading to a premature stop codon within exon 6.

d: The predicted translation of the Pt435 allele leads to a severely truncated protein that ends after the first bromodomain of Brd4. Genetic studies suggest this is a null allele (see below) and not a dominant negative, as there is no phenotype in heterozygotes. The protein fragment may be unstable.

Supplementary Figure S36 – Developmental phenotypes in *brd4*^{-/-} zebrafish



a: Genotypes from three independent clutches (same allele, different parents) of *brd4*^{-/-} zebrafish at 5dpf. There was no significant difference between the observed genotypes and the expected Mendelian ratios.

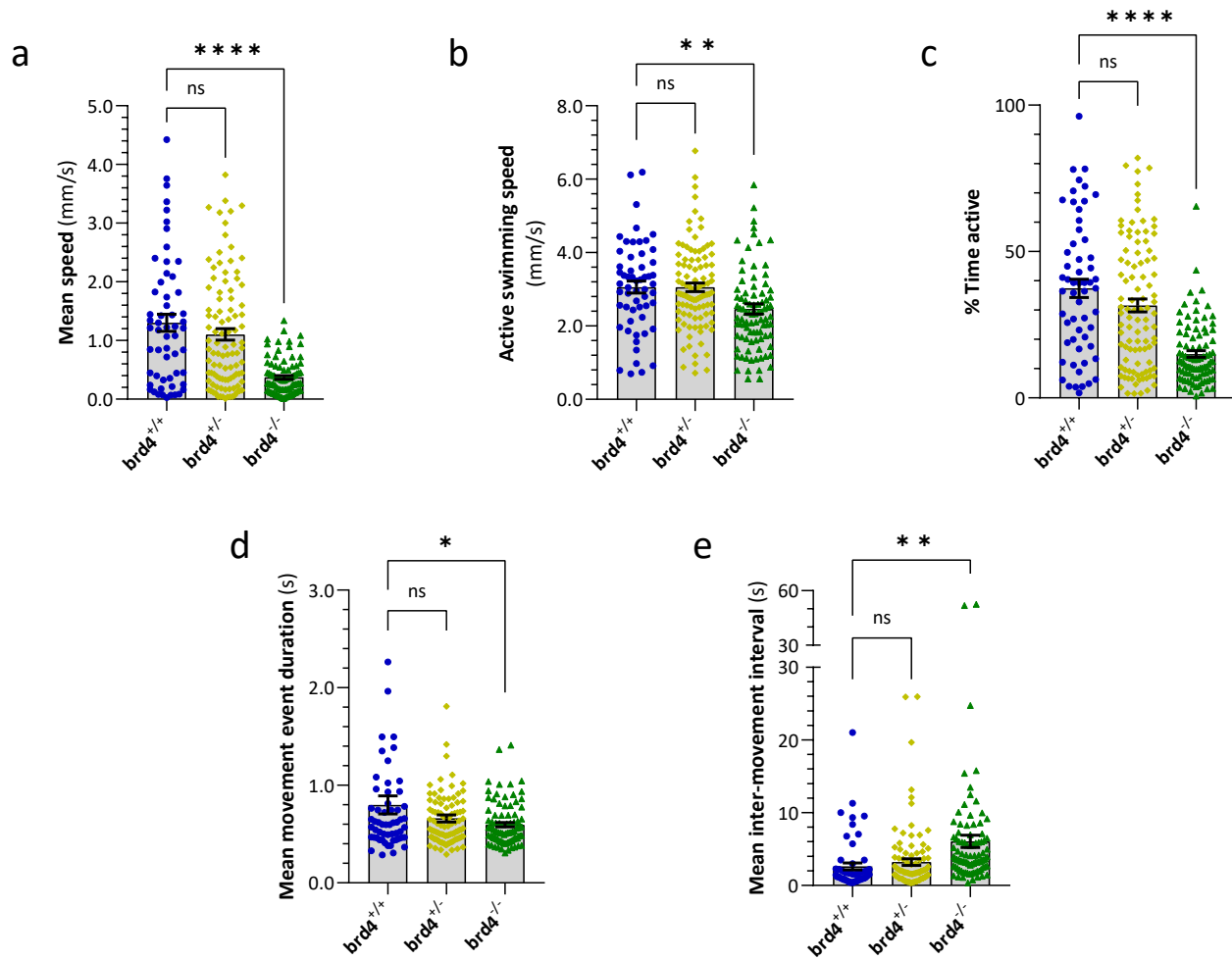
b: Genotype proportions for the three clutches overall did not differ from the expected Mendelian ratios at 5dpf. However, no homozygous *brd4*^{-/-} zebrafish adults were identified from >100 offspring of *brd4*^{+/-} in-crosses that were genotyped, strongly suggesting that *brd4*^{-/-} zebrafish are not viable to adulthood.

c: Morphological changes in *brd4*^{-/-} zebrafish, including jaw region dysgenesis, pericardial edema, failure of swim bladder insufflation, and kyphotic spinal curvature.

d: Relationship between genotype and presence of a swim bladder. There was a strong statistically-significant association between *brd4*^{-/-} genotype and failure of swim bladder insufflation in each of the three clutches analyzed in panel (a).

e: Genotype proportions for zebrafish from each of the three clutches without an observable swim bladder at 5dpf. The *brd4*^{-/-} genotype was strongly associated with absent swim bladder. * $p < 0.05$, 1-way ANOVA with Dunnett multiple comparisons test.

Supplementary Figure S37 – Motor activity abnormalities in *brd4*^{-/-} zebrafish

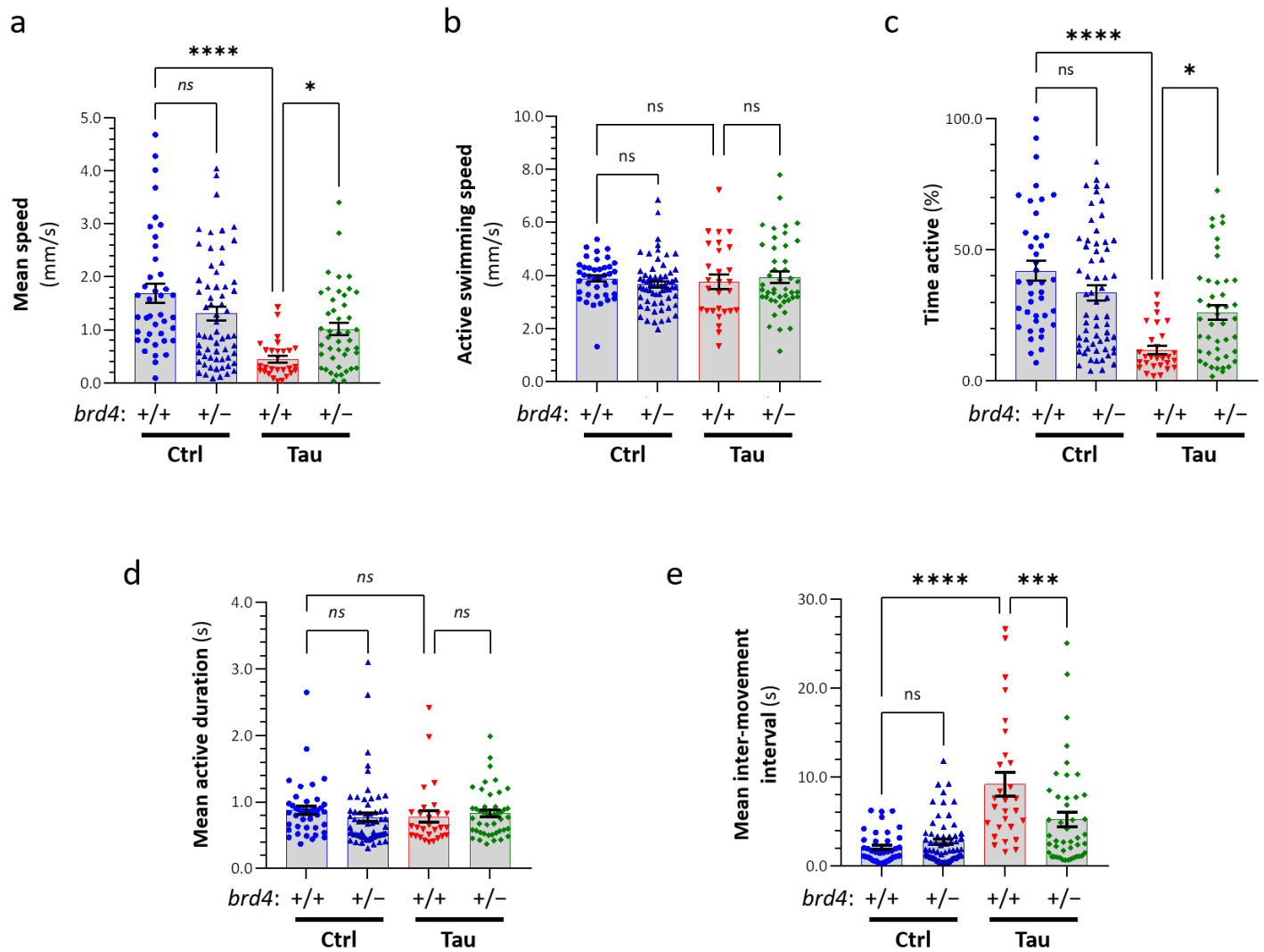


5dpf larvae resulting from *brd4*^{+/-} in-crosses were analyzed in a 96-well plate motor activity assay similar to Figure 5a – 5h, and then each larva was genotyped by PCR amplification and *Bam*HI restriction digest for the *brd4*^{Pt435} allele. In each graph, data points show individual zebrafish, bars show mean ± SE. *****p*<0.0001, ***p*<0.01, **p*<0.05, 1-way ANOVA with Dunnett multiple comparison test.

- a: Mean speed (scalar distance traveled by zebrafish centroid/time of assay)
- b: Active swimming speed (mean scalar speed of zebrafish centroid during movement events)
- c: Time active % (proportion of video frame transitions at which centroid displacement occurred)
- d: Mean movement event duration (mean duration of movement episodes)
- e: Mean inter-movement interval (mean duration of stationary periods between movements)

Together with Supplementary Figure S36, these data suggest that analysis of *brd4* as a genetic modifier of the Tau phenotype would be difficult to interpret using homozygous *brd4*^{-/-} mutants that have morphological and motor phenotypes of their own. However, heterozygous *brd4*^{+/-} mutants that have no detectable abnormalities should provide a valid means to determine if decreased Brd4 expression modulates the phenotype in Tau zebrafish.

Supplementary Figure S38 – Heterozygous *brd4*^{+/-} mutations partially rescue motor phenotypes in Tau zebrafish



5dpf Tau and Ctrl larvae were analyzed in a 96-well plate motor activity assay similar to Figure 5a – 5h, and then each larva was genotyped by PCR amplification and *Bam*HI restriction digest of genomic DNA to detect the *brd4* deletion allele. In each graph, data points show individual zebrafish, bars show mean \pm SE. **** p <0.0001, *** p <0.001, * p <0.05, 1-way ANOVA with Šidák multiple comparison test.

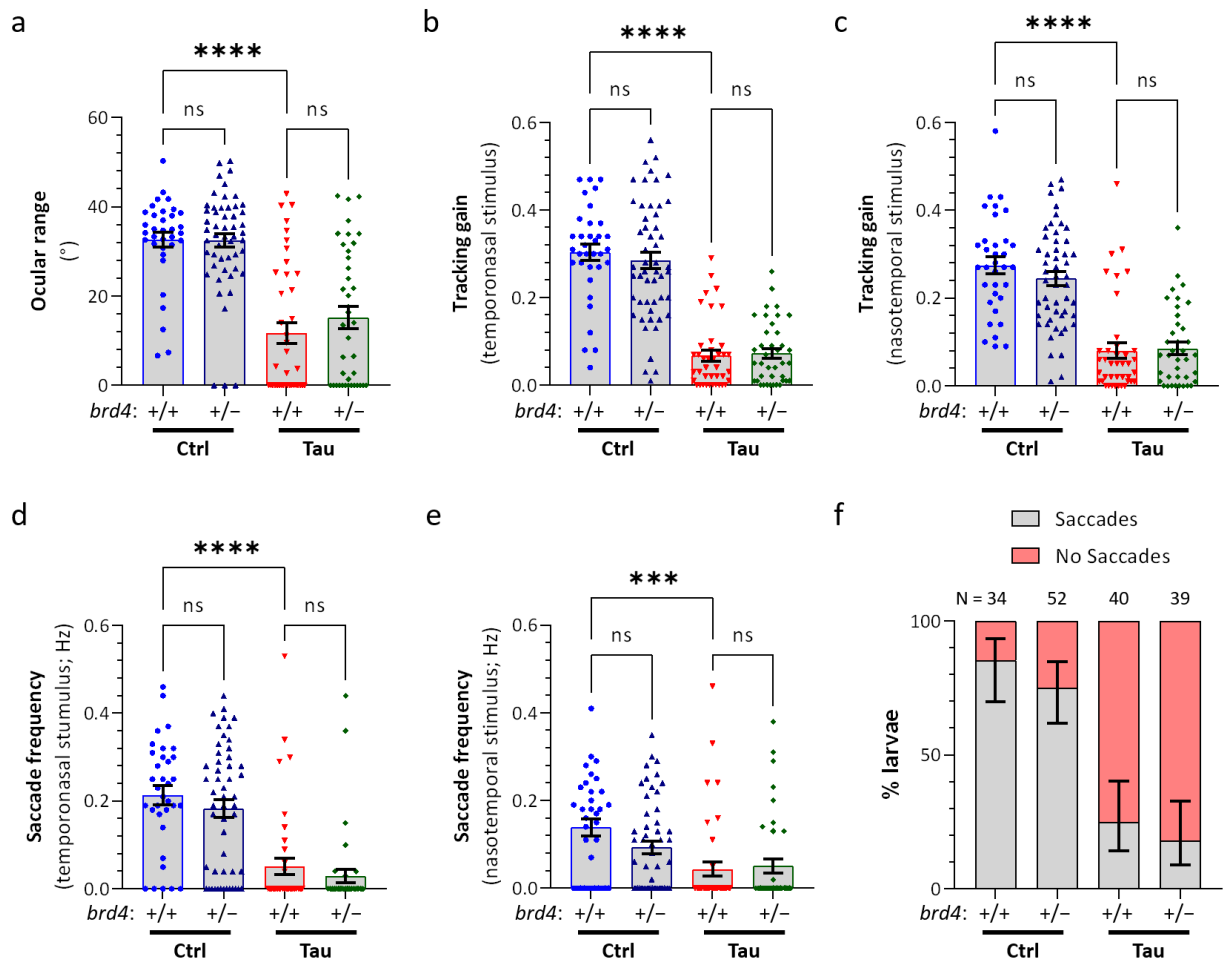
- a: Mean speed (scalar distance traveled by zebrafish centroid/time of assay)
- b: Active swimming speed (mean scalar speed of zebrafish centroid during movement events)
- c: Time active % (proportion of video frame transitions at which centroid displacement occurred)
- d: Mean movement event duration (mean duration of movement episodes)
- e: Mean inter-movement interval (mean duration of stationary periods between movements)

These data show that heterozygous *brd4*^{+/-} mutations partially rescue mean speed, % time active and inter-movement interval in Tau zebrafish. The modest abnormalities in active swimming speed and mean movement duration found in Tau zebrafish in Figure 5 were not detected in these larval clutches, which seemed to have a slightly weaker phenotype.

Supplementary Table 22 – Exact *p*-values for Figure 10d – 10i

Panel	Statistical test	Comparison group 1	Comparison group 2	Adjusted <i>p</i> value
10d	One-way ANOVA with Šidák multiple comparisons test	Ctrl; <i>brd4</i> ^{+/+}	Ctrl; <i>brd4</i> ^{+/-}	0.113707882660896
		Ctrl; <i>brd4</i> ^{+/+}	Tau; <i>brd4</i> ^{+/+}	0.000000292123687
		Tau; <i>brd4</i> ^{+/+}	Tau; <i>brd4</i> ^{+/-}	0.029082887963640
10e	One-way ANOVA with Šidák multiple comparisons test	Ctrl; <i>brd4</i> ^{+/+}	Ctrl; <i>brd4</i> ^{+/-}	0.999802006238610
		Ctrl; <i>brd4</i> ^{+/+}	Tau; <i>brd4</i> ^{+/+}	0.000000000031921
		Tau; <i>brd4</i> ^{+/+}	Tau; <i>brd4</i> ^{+/-}	0.362341368466568
10f	One-way ANOVA with Šidák multiple comparisons test	Ctrl; <i>brd4</i> ^{+/+}	Ctrl; <i>brd4</i> ^{+/-}	0.118543083544085
		Ctrl; <i>brd4</i> ^{+/-}	Ctrl; <i>brd4</i> ^{-/-}	0.969533891959084
		Ctrl; <i>brd4</i> ^{+/+}	Ctrl; <i>brd4</i> ^{-/-}	0.000009306670211
		Ctrl; <i>brd4</i> ^{+/+}	Tau; <i>brd4</i> ^{+/+}	0.000000000102355
		Tau; <i>brd4</i> ^{+/+}	Tau; <i>brd4</i> ^{+/-}	0.000000000019628
		Tau; <i>brd4</i> ^{+/-}	Tau; <i>brd4</i> ^{-/-}	0.006322344844991
		Tau; <i>brd4</i> ^{+/+}	Tau; <i>brd4</i> ^{-/-}	<0.000000000000001
10g	One-way ANOVA with Tukey multiple comparisons test	Ctrl; <i>brd4</i> ^{+/+}	Tau; <i>brd4</i> ^{+/+}	0.000000000101563
		Ctrl; <i>brd4</i> ^{+/+}	Tau; <i>brd4</i> ^{+/-}	0.000058615382397
		Tau; <i>brd4</i> ^{+/+}	Tau; <i>brd4</i> ^{+/-}	0.002120097691076
10h	One-way ANOVA with Tukey multiple comparisons test	Ctrl; <i>brd4</i> ^{+/+}	Tau; <i>brd4</i> ^{+/+}	0.000000000019925
		Ctrl; <i>brd4</i> ^{+/+}	Tau; <i>brd4</i> ^{+/-}	0.000005329924599
		Tau; <i>brd4</i> ^{+/+}	Tau; <i>brd4</i> ^{+/-}	0.000009862682856
10i	Two-way ANOVA with Šidák multiple comparisons test	Globus Pallidus Control	Globus Pallidus PSP	0.317711657542679
		Substantia nigra control	Substantia nigra PSP	0.998941139892130

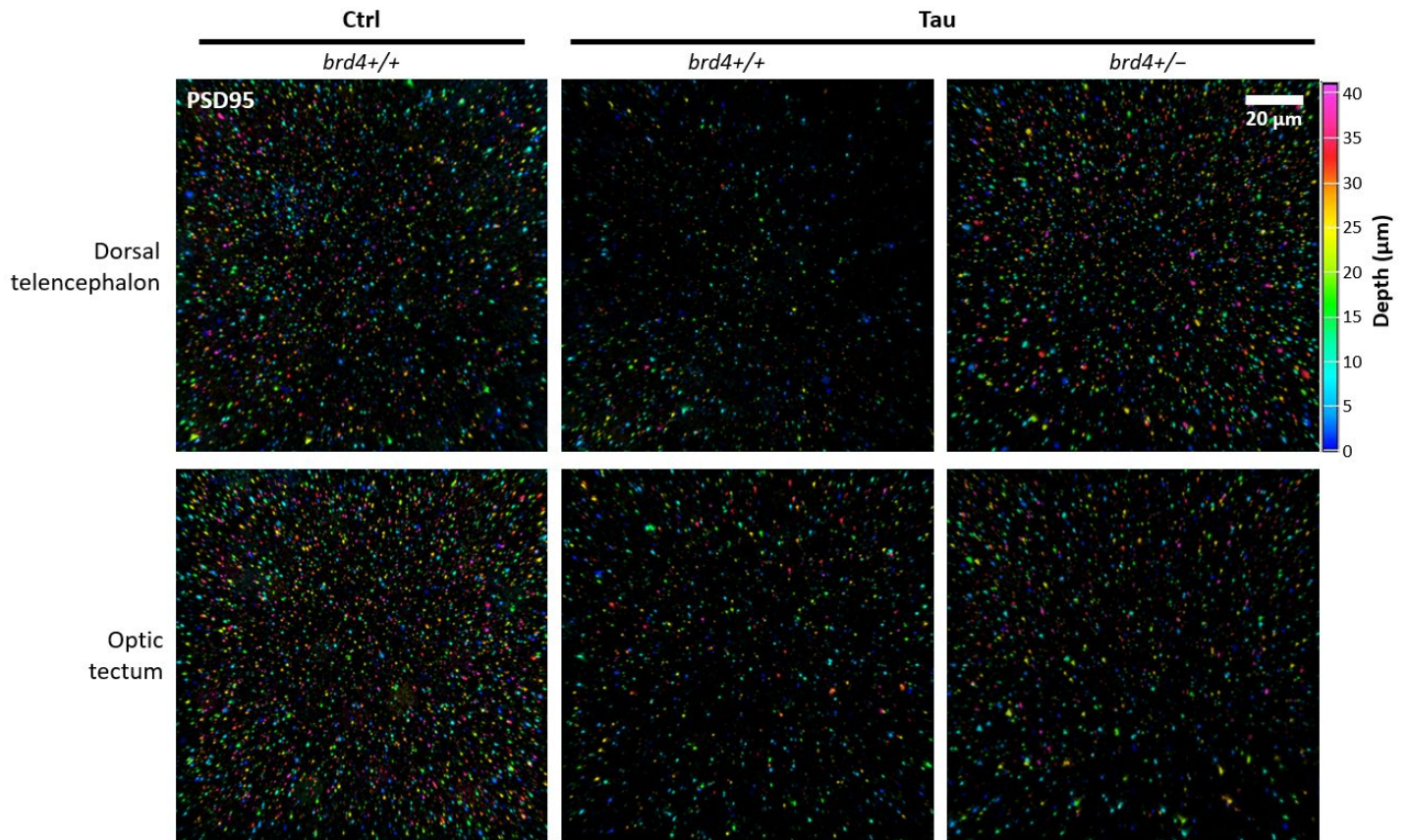
Supplementary Figure S39 – Heterozygous *brd4*^{+/-} mutation does not rescue OKR deficits in Tau zebrafish



5dpf Tau and Ctrl larvae resulting from [Tg(*elavl3:gal4-vp16*); *brd4*^{+/^{Pt435}}] x [Tg(*UAS:hsa.MAPT-p2a-nls-mCherry*) or Tg(*UAS:p2a-nls-mCherry*)] crosses were analyzed in OKR assays similar to Figure 6 and Supplementary Figures S15 and S27, and then each larva was genotyped by PCR amplification and *Bam*HI restriction digest for the *brd4*^{Pt435} allele. In panels (a) – (e), data points show individual zebrafish, bars show mean ± SE. *****p*<0.0001, ****p*<0.001, 1-way ANOVA with Šidák multiple comparison test. In panel (f), bars show proportion ± 95% CI of zebrafish with and without saccadic movements during exposure to OKR stimuli.

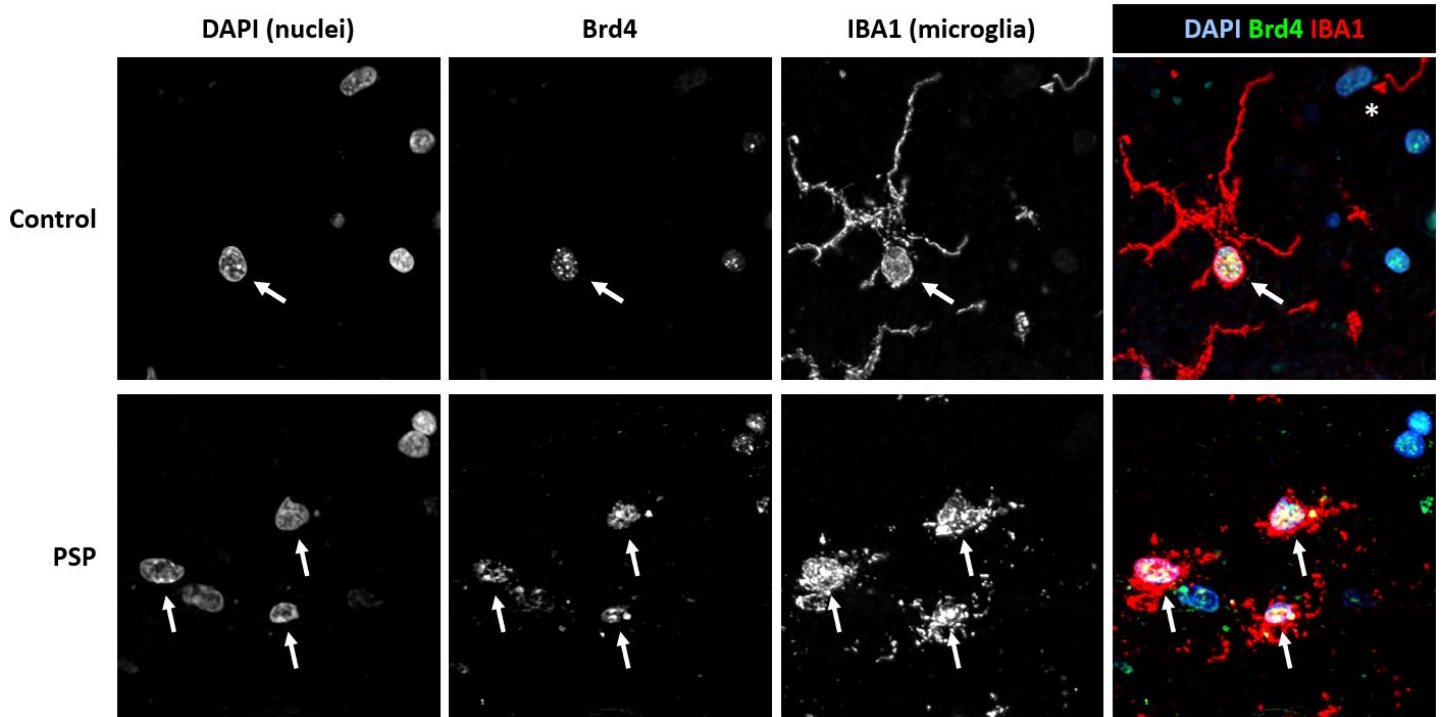
Similar to findings with (+)JQ1 exposure, decreased Brd4 expression did not rescue OKR deficits in the Tau model at the time points evaluated.

Supplementary Figure S40 – Rescue of synaptic puncta in Tau zebrafish with heterozygous *brd4*^{+/-} mutations



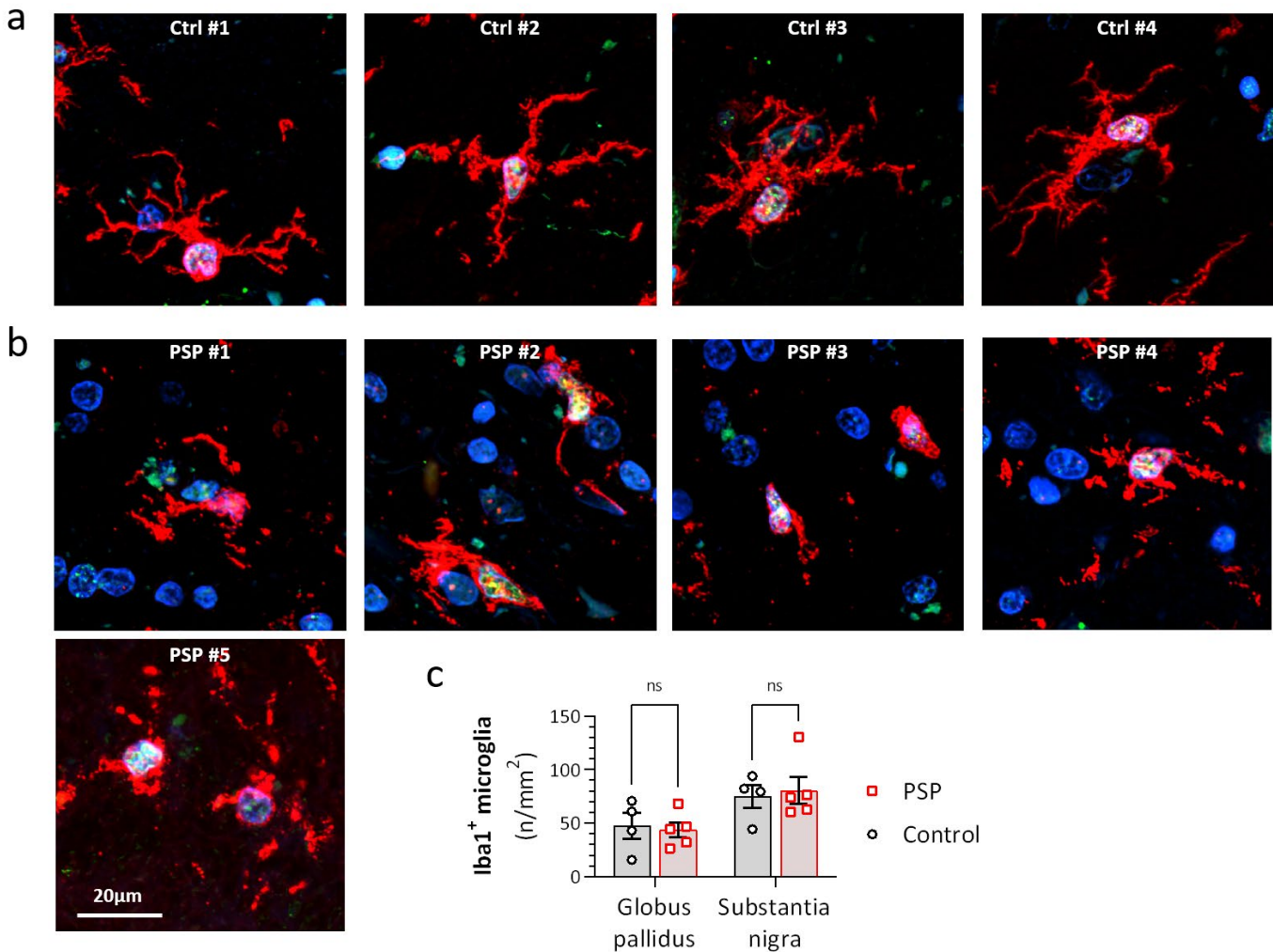
5dpf Tau and Ctrl larvae resulting from [Tg(*elavl3:gal4-vp16*); *brd4*^{+/^{Pt435}}] x [Tg(*UAS:hsa.MAPT-p2a-nls-mCherry*) or Tg(*UAS:p2a-nls-mCherry*)] crosses were genotyped by PCR amplification and *Bam*HI restriction digest for the *brd4*^{Pt435} allele, and then fixed for PSD95 immunofluorescence. These example images are alpha-blended and pseudocolored to show depth within the image stack, and accompany the quantitative analysis shown in Figure 10g – 10h.

Supplementary Figure S41 – Brd4 expression in the nuclei of human substantia nigra microglia



Individual fluorescence channels for the images shown in Figure 10j are separated and shown in monochrome for clarity. Image fields are shown from a control brain (top row) and a PSP brain (bottom row). Individual DAPI labeled nuclei (column 1) that were immunoreactive for Brd4 (column 2) and were located within Iba1-immunoreactive microglia (column 3) are indicated with white arrows in each image of a set. The overlaid pseudocolored images are shown in column 4.

Supplementary Figure S42 – Brd4 expression in microglia from multiple control and PSP cases



Human control and PSP brain sections from two brain regions characteristically affected by PSP pathology – the substantia nigra and globus pallidus – were immunolabeled for Brd4 (green), Iba1 (microglial marker; red) and counter-labeled with DAPI (nuclei; blue). Images were acquired by confocal microscopy.

a: Examples of Brd4⁺, Iba1⁺ microglia are shown from the substantia nigra of each of 4 control brains

b: Examples of Brd4⁺, Iba1⁺ microglia are shown from the substantia nigra of each of 5 PSP brains

c: There was no significant overall increase in the density of Iba1-labeled microglia in either the substantia nigra or the globus pallidus of PSP brains in this small sample, despite the characteristic morphological differences (retracted processes, prominent perinuclear cytoplasm) suggestive of activation seen in the images from PSP brains.

References

1. Van Laar, V.S. et al. α -Synuclein amplifies cytoplasmic peroxide flux and oxidative stress provoked by mitochondrial inhibitors in CNS dopaminergic neurons in vivo. *Redox Biol* **37**, 101695 (2020).
2. Zhou, Y., Cattley, R.T., Cario, C.L., Bai, Q. & Burton, E.A. Quantification of larval zebrafish motor function in multiwell plates using open-source MATLAB applications. *Nat Protoc* **9**, 1533-48 (2014).
3. Cario, C.L., Farrell, T.C., Milanese, C. & Burton, E.A. Automated measurement of zebrafish larval movement. *J Physiol* **589**, 3703-8 (2011).
4. Scheetz, S.D. et al. An open-source method to analyze optokinetic reflex responses in larval zebrafish. *J Neurosci Methods* **293**, 329-337 (2018).
5. Hartnett, K.A. et al. NMDA receptor-mediated neurotoxicity: a paradoxical requirement for extracellular Mg²⁺ in Na⁺/Ca²⁺-free solutions in rat cortical neurons in vitro. *J Neurochem* **68**, 1836-45 (1997).
6. Goshi, N., Morgan, R.K., Lein, P.J. & Seker, E. A primary neural cell culture model to study neuron, astrocyte, and microglia interactions in neuroinflammation. *Journal of Neuroinflammation* **17**, 155 (2020).